Rodríguez, A., van Bergen, M. J. (2017): Superficial alteration mineralogy in active volcanic systems: An example of Poás volcano, Costa Rica. - *Journal of Volcanology and Geothermal Research*, *346*, pp. 54—80.

DOI: http://doi.org/10.1016/j.jvolgeores.2017.04.006

SUPERFICIAL ALTERATION MINERALOGY IN ACTIVE VOLCANIC SYSTEMS: AN EXAMPLE OF POÁS VOLCANO, COSTA RICA

Alejandro Rodríguez[a,1] and Manfred J. van Bergen[a]

[a] Department of Earth Sciences, Utrecht University, Budapestlaan 4, 3508 TA, Utrecht, the Netherlands

[1] Current address: Inorganic and Isotope Geochemistry, GFZ Helmholtz-Zentrum, Telegrafenberg, 14473 Potsdam, Germany (email: arodrigu@gfz-potsdam.de)

Abstract

The alteration mineralogy in the crater area of Poás volcano (Costa Rica) has been studied to constrain acid fluid-rock interaction processes and conditions relevant for the formation of sulphate-bearing mineral assemblages found on the surface of Mars. Individual sub-environments, which include the hyperacid lake (Laguna Caliente), ephemeral hot springs, fumarole vents and areas affected by acid rain and/or spray from the lake, are marked by distinct secondary mineral associations, with sulphates commonly as prevailing component. The sulphates occur in a wide mineralogical diversity comprising gypsum/anhydrite, various polyhydrated Al-sulphates, alunite-jarosite group minerals, halotrichite-, voltaite- and copiapite-group minerals, epsomite and römerite. Depending on the sub-environment, they are variably associated with clay minerals (kaolinite-group and smectite-group), zeolites, SiO_2-polymorphs, Fe-(hydro)oxides, Ti-oxides, native sulphur, sulphides, chlorides, fluorides, phosphates and carbonates. Geochemical modelling was performed to identify mechanisms responsible for the formation of the secondary minerals found in the field, and to predict their possible stability under conditions not seen at the surface. The results indicate that the appearance of amorphous silica, hematite, anhydrite/gypsum, pyrite, anatase and kaolinite is relatively insensitive to the degree of acidity of the local aqueous system. On the other hand, alunite-jarosite group minerals, elemental sulphur and $Al(OH)SO_4$ only form under acidic conditions (pH<4). The presence of polyhydrated Mg- and Fe^{2+}-sulphates is restricted to olivine-bearing rocks exposed to acid rain or brine spray. Modelling suggests that their formation required a repetitive sequence of olivine dissolution and evaporation in an open system involving limited amounts of fluid. The mineral variety in the crater of Poás is remarkably similar to sulphate-bearing assemblages considered to be the product of acid-sulphate alteration on Mars. The analogy suggests that comparable fluid-rock interaction controls operated in Martian volcanic environments.

1. INTRODUCTION

The distribution of hydrous alteration minerals on Mars indicates that the oldest terrains (Noachian) are typically dominated by phyllosilicates, middle-aged terrains (Hesperian) by various sulphates, and the youngest (Amazonian) by ferric oxides (e.g. Bibring et al., 2006). Apart from these apparent global mineralogical changes in the history of the planet, there is increasing evidence that large varieties of alteration phases also formed in close spatial associations in single environments. For example, Thollot et al. (2012) described the occurrence of numerous hydrated minerals including halloysite/kaolinite, Fe-smectite, Si-OH bearing phases and polyhydrated, monohydrated, and hydroxylated Fe-sulphates (including jarosite) in a closed depression in the Noctis Labyrinthus region. The authors attributed the mineral variability to local variations in the pH of altering acid sulphate fluids, which possibly formed from groundwater and magmatic sulphur in a site under the influence of volcanic activity and associated hydrothermalism. Similar examples of mineral diversities at a local scale include depressions elsewhere in the Noctis Labyrinthus region (Weitz et al., 2011), in Valles Marineris (Weitz and Bishop, 2016), and the Columbus crater in the Terra Sirenum region, the latter arguably being a groundwater-fed paleolake (Wray et al., 2011). Evidence for acid fluids as major agents in water-rock interaction processes on Mars also comes from Meridiani Planum and Gusev crater where soils and rocks are not only enriched in sulphur but also in halogens (Klingelhöfer et al., 2004; Squyres et al., 2004; McLennan et al., 2005; Grotzinger et al., 2005; Tosca and McLennan, 2006; Chevrier and Mathé, 2007; Squyres et al., 2007).

Volcanic products cover vast areas of Martian surface (Tanaka et al., 1992; Christensen et al., 2001; Bibring et al., 2005). Even though only a few Noachian volcanic terrains have been preserved, Martian volcanism was most likely intense during the early history of the planet and it gradually decreased over time with episodic periods of higher activity (Werner, 2009; Hauber et al., 2011; Robbins et al., 2011; Xiao et al.,2012). Since the sulphur composition of Martian basalts is relatively high compared to their terrestrial counterparts (Lodders, 1998; McSween et al., 2006; 2008) the emplacement of Martian intrusives and lavas must have released significant amounts of sulphur-rich volatiles. Reaction of volatile sulphur compounds with water in magmatic vapours, ice or groundwater will then inevitably have produced acidic fluids. Due to its ubiquity, acid-

sulphate alteration has been a major feature on Mars´ surface (Ehlmann et al., 2011; Gaillard et al., 2013). Moreover, surface deposits contain high levels of sulphur (SO_3 up to ~37 wt.%, average ~6 wt.%) mostly in the form of sulphates (King and McLennan, 2010).

Terrestrial volcanoes hosting hyperacid lakes are settings where fluid-rock interaction occurs in strong chemical, temperature and redox gradients, leading to a diversity of alteration products on small spatial scales. (e.g. Delmelle and Bernard, 1984; Christenson, 2000; Varekamp et al., 2000; Christenson et al., 2010; van Hinsberg et al., 2010a;b; Christenson et al., 2015; Rouwet et al., 2016). These systems are commonly fed by input fluids, derived from magmatic sources, with a typical acid sulphate-chloride composition. The surface expressions of volcanic-hydrothermal systems on Earth are potentially powerful analogues for interpreting specific Martian settings where a variety of acid alteration products formed in close proximity.

This paper documents the distribution of alteration products in the active crater area of Poás volcano (Costa Rica), where a hyperacid lake, subaerial fumaroles, hot-springs and deposition of acid rain/spray provide a range of conditions potentially suitable for the formation of sulphur- and chlorine-bearing secondary minerals through interaction with solid volcanic materials. Geochemical modelling is applied to test mechanisms and circumstances required for the formation of the mineral assemblages observed at the surface, and to assess conditions under which secondary minerals are stable in the hydrothermal system at depth. Finally, the implications that these findings have for Mars are discussed in terms of sulphate abundances and alteration processes.

2. GEOLOGICAL SETTING

Poás volcano, located in the Central Cordillera of Costa Rica, is a broad basaltic-andesitic stratovolcano with a maximum elevation of 2708 m.a.s.l. (Fig. 1a). The volcanic products mainly consist of calc-alkaline basaltic and andesitic lavas and pyroclastics (Prosser and Carr, 1987; Cigolini et al., 1991; Malavassi, 1991) but the rock composition spans the range from basalts to dacites (Ruiz et al., 2010). The 1.3 km wide active crater, located between Von Frantzius and Botos craters, host an acidic lake known as Laguna Caliente in a 300 m-diameter pit and a ~30 m high composite pyroclastic cone (CPC, Casertano et

al., 1987; Martínez et al., 2000; Martínez, 2008) (Fig. 1b). The CPC was constructed from tephra and lava during the 1953-55 eruption. Lava flows emitted from the base of the CPC flowed towards the lake and formed a terrace (Casertano et al., 1987; Rowe et al., 1992a). Although fumarolic activity has been continuously migrating over the last 25 years around the main crater (Vaselli et al., 2003; Rouwet et al., 2016), the main fumarolic activity nowadays occurs on the northern flank of the CPC. During the last 700 k.a. Poás volcano has been rising over the Central Proto-Cordillera in different episodes of effusive, explosive, phreatic, phreatomagmatic and erosive activity (Ruiz et al., 2010). In the last 200 years, the activity of Poás has been characterized by frequent phreatic explosions and continuous fumarolic activity (Alvarado, 2009). More details about the petrology, geochemistry, age and geographic distribution of the units and formations around Poás volcano can be found in Prosser (1983), Prosser and Carr (1987), Kussmaul (1988), Cigolini et al. (1991), Malavassi (1991), Campos et al. (2004), Gazel and Ruiz (2005), Carr et al. (2007) and Ruiz et al. (2010).

Over the last decades, Laguna Caliente has shown temperatures between 22 and 94°C (OVSICORI-UNA, intern. reps.). As a product of the dissolution magmatic volatiles (SO_2, H_2S, HCl) in meteoric waters, sulphate (3300–285000 mg/kg) and chloride (2500–15000 mg/kg) are the major cations in this lake; additionally, the high acidity of these waters (pH= -0.87-1.75) make them very reactive, easily dissolving the surrounding rocks and incorporating rock-forming elements in solution (Rowe et al.,1992a; 1992b; Rowe and Brantley, 1993; Martínez et al., 2000; Martínez, 2008; OVSICORI-UNA, intern. reps.). Martínez (2008) subdivided the activity of Poás since the early 1970´s into five stages. During Stage I (1972 - August 1980), fumarolic discharges were strong within the lake and were accompanied with occasional phreatic explosions. Stage II (September 1980 – April 1986) was characterized by a relative quiescence in the lake and absence of phreatic activity despite a strong discharge of high-temperature fumaroles through the CPC. In the following Stage III (May 1986 - August 1995), a vigorous subaqueous fumarolic discharge and intense phreatic activity accompanied a strong volume decrease, ultimately leading to a dry out of the lake. Stage IV (September 1995 – February 2005) was a calm period, when the lake re-established and subaerial fumaroles and hot springs appeared in the surrounding crater area (Vaselli et al., 2003; Rymer et al., 2009; Fischer et al., 2015; Rouwet et al., 2016). This stage was followed by an intense fumarolic discharge into the

lake during Stage V (March 2005 – October 2014) together with frequent phreatic eruptions and a steady decrease of the lake volume (Rymer et al., 2009; Fisher et al., 2015; de Moor et al., 2016; Rouwet et al., 2016). Fumarolic activity concentrated at the CPC, occasionally showing incandescence as gas temperatures rose above 600°C (OVSICORI-UNA, intern. reps.).

3. SAMPLING AND ANALYTICAL METHODS

3.1. Sampling techniques

Field work was carried out in April - May 2012. Geographic coordinates and altitude were registered with a handheld GPS at each sampling location. Mineral and rock samples were collected from several sites (Fig. 2) within the crater area and in the "dead zone", an area SW of the lake that is constantly affected by acid rain. Minerals were gathered with a plastic spatula and put into 25 ml plastic Greiner® tubes. Fresh and altered rocks were stored in plastic bags.

A considerable number of samples from Laguna Caliente, hot springs around the lake, fumarole condensates and gases used in this study were collected by OVSICORI-UNA (Observatorio Vulcanológico y Sismológico de Costa Rica, Universidad Nacional). Data for some of these samples are presented by Martínez et al. (2000) and Martínez (2008). Temperature (°C), pH, electrical conductivity (C) and redox potential (Eh) were measured *in situ* in water samples from Laguna Caliente, using an OMEGA® HH2001A K-type thermocouple and a WTW® 3430 portable multimeter. All electrodes were calibrated daily before fieldwork. Calibration of the pH electrode was performed using pH 1, 4 and 7 buffers. The conductivity and Eh electrode was calibrated in a 0.01 M KCl standard and a 420 mV buffer solution, respectively. Water samples for IC (ion-chromatography) and ICP-OES (inductively coupled plasma optical emission spectrometry) analysis were filtered on site through 0.2 μm pore size cellulose acetate membranes with the aid of a hand pump. Samples for IC analyses were collected in 250 ml HDPE bottles. For ICP-OES analyses, 60 ml HDPE bottles were used and samples were treated with 1 ml Suprapur® HNO_3 per 100 ml of sample. For pH determinations at room temperature, unfiltered samples were collected in 20 ml amber glass air-tight bottles.

3.2. Analytical techniques

Minerals, sediments and hydrothermally altered rocks were dried at low temperature (40°C) during several days until a constant weight (<1% mass difference) was measured between two consecutive readings. Then the samples were ground in an agate mortar to a very fine grain size (approximately No.40 mesh). The powders were analysed by X-ray diffraction (XRD) at the Department of Inorganic Chemistry and Catalysis (Utrecht University) with a Bruker® AXS D2 Phaser powder X-ray diffractometer, in Bragg-Brentano mode, equipped with a LYNXEYE® detector. The radiation used was cobalt $K_{\alpha 1,2}$ l = 1.79026 Å, operated at 30kV, 10 mA. The diffraction patterns were processed and interpreted with DIFFRAC.SUITE software. Thin sections of fresh and altered rocks were investigated under a polarizing optical microscope. Some of the samples were selected for electron microprobe analysis (EPMA), which was done on carbon coated samples with a JEOL® 8600 instrument, equipped with an energy-dispersive spectrometer (EDS), at the Department of Earth Sciences, Utrecht University. Operating conditions were 15 kV accelerating voltage, 10 nA bean current and 30 s counting time. PROZA software provided by JEOL® was used for matrix correction.

Conductivity, pH and redox potential of water samples were determined in the laboratory at room temperature (19±1°C) using a WTW® 3430 portable multimeter. Calibration of the pH electrode was performed using pH 1, 4 and 7 buffers. The conductivity and Eh electrode was calibrated in a 0.01 M KCl standard and a 420 mV buffer solution, respectively. The concentrations of F^-, Cl^-, Br^- and SO_4^{2-} in untreated and diluted samples (25 to 500 times, depending on the calibration curve, with deionised water) were determined in a Dionex® ICS-3000 ion chromatograph (IC), equipped with a Dionex®IonPac® AS 19 column at the Department of Earth Sciences of Utrecht University. A gradient elution of 10 – 50 mM KOH was utilized. Concentrations of total sulphur (S_T), Al, B, Ca, Fe, K, Mg, Mn, Na, P, Si, Sr, Ti, V and Zn in diluted samples (10 to 100 times, depending on the calibration curve, with 2% v/v Suprapur® HNO_3) were determined using a Spectro® Ciros® ICP-OES at the Department of Earth Sciences of Utrecht University.

3.3. Geochemical modelling

PHREEQC software, version 3.1 (Parkhust and Appelo, 1999), was used to calculate aqueous species distributions, mineral saturation states and simulations of reaction path, heating and evaporation processes. The Lawrence Livermore National Laboratories thermodynamic database (llnl.dat), expanded with recently available thermodynamic data on sulphates and halides was used for this purpose. In addition, ion interaction parameters from Pitzer and Mayorga (1973) were included for many relevant ion pairs. The pH values of extreme acid fluids (pH<1) were recalculated from charge balance (adding H^+) with PHREEQC because of the strongly reduced linearity of the pH vs. potential (mV) curve of the electrode when pH values are below zero (Nordstrom et al., 2000). Thermodynamic calculations involving equilibria between fumarolic gases, solids and liquids were performed using the SOLVGAS and GASWORKS codes of M.H. Reed (University of Oregon). It must be emphasized that the modelling work presented here assumes thermodynamic equilibrium and ignores any effects of reaction kinetics. Hence, it predicts direct precipitation of a mineral from the solution as soon as it becomes saturated. Obviously, mineral precipitation can be considerably delayed or can completely fail to appear in natural systems if crystal nucleation or growth are the limiting processes (Stumm and Morgan, 1996). Furthermore, the thermodynamic models used are most suitable for closed-system behaviour without mass or energy exchange with the surroundings, which is a simplification of the crater lake settings studied.

4. RESULTS

For convenience, the results will be grouped in different scenarios, arbitrarily based on the relative amounts of solid and fluid (water or gas) involved in reactions at each of the investigated sites within the crater area (Fig. 2): a low rock/water scenario in the crater lake itself, a medium rock/water scenario represented by hot springs, and a high rock/water scenario for areas affected by acid rain or acid brine spray from the lake. We also ranked the active and fossil fumaroles at Poás as a high rock/fluid setting. For each case, the chemical composition of fluids and associated primary and secondary minerals will be described. The geochemical models explore the reaction between primary phases (i.e., rock or mineral) and fluids (liquid or gas), with the secondary phases as a reaction

products. Even though most of the fluids observed at Poás are notably acid, neutral-bicarbonate and neutral sulphate waters with a pH up to 8.0 have been reported by Rowe et al. (1995). Therefore, the models were extended into alkaline pH ranges. The reason for this approach is that the modelling should also have a predictive value together with the descriptive one. Demonstrating that a certain assemblage occurs in alkaline conditions implies that it is less probably to occur at Poás and, eventually on Mars.

In order to facilitate the interpretation of XRD results, the secondary minerals were grouped into 11 categories: 1) kaolinite group, 2) smectite group, 3) zeolites, 4) SiO_2 polymorphs, 5) oxides (Fe and Ti), 6) elemental sulphur, 7) sulphides, 8) fluorides and phosphates, 9) chlorides and borates, 10) carbonates and 11) sulphates. In view of their large diversity and interest for this study, the sulphate minerals were further divided into 9 subcategories: 1) calcium sulphates, 2) aluminium sulphates, 3) alunite group, 4) jarosite group, 5) halotrichite group, 6) voltaite group, 7) copiapite group, 8) magnesium sulphates, and 9) iron sulphates.

4.1. Scenario 1: Laguna Caliente (low rock/water ratios)

4.1.1. Water chemistry

The acid sulphate waters of Laguna Caliente (pH<2) have a SO_4-Cl composition (Fig. 3). The high acidity of these waters is mainly caused by HSO_4^- and $HCl_{(aq)}$, products of the input of magma-derived gases HCl and SO_2 (Giggenbach, 1988; 1991; Truesdell 1991; Giggenbach and Corrales, 1992). The pH is mainly buffered by the HSO_4^-/SO_4^{-2} pair, and an acidy increase is to be expected with a temperature decrease because the dissociation constant of HSO_4^- decreases with temperature (Arnórsson et al., 2007). Other gases such as HF and HBr are minor contributors to the acidy through their aqueous dissociation. The chemical composition of Laguna Caliente water is variable and strongly dependent on the balance between heat and volatile input and dilution with meteoric or groundwater. The evaporation effect seems to be sometimes more important than the volatile input in order to explain salinity increases (Rouwet et al., 2016). From the early 1980s till April 2014, average contents of SO_4, Cl, F were 50000; 21000 and 1800 mg/kg, respectively (Fig. 3), and those of Al, Fe, Ca and Mg were 1400, 1200, 1000 and 600 mg/kg,

266 respectively. Highest concentrations of all of these elements were recorded during
267 periods of intense activity, as was the case in Stages III and V (Rowe et al., 1992b; Martínez
268 et al., 2000; Martínez, 2008; Rouwet et al., 2016). The high percentage of residual acidy
269 (PRA) of Laguna Caliente waters (Varekamp et al., 2000) makes them capable to dissolve
270 important amounts of rocks, consequently incorporating high concentrations of rock-
271 forming elements (Delmelle et al., 2000; Varekamp et al., 2001). The high concentrations
272 of Al, Fe, Ca and Mg in Laguna Caliente water are mainly derived from the dissolution of
273 silicate minerals and glass.
274
275 Because direct redox potential measurements of the water of Laguna Caliente are scarce,
276 the redox state of the system must be estimated for modelling purposes. Since $H_2S_{(g)}$ and
277 $SO_{2(g)}$ are the most abundant gaseous S species that enter the aqueous system of Laguna
278 Caliente, the S^{2-}/S^{6+} couple probably plays an important role in regulating the redox state.
279 Based on occasional determinations of dissolved $H_2S_{(g)}$ and $SO_{2(g)}$ in the lake waters (see
280 Martínez, 2008), a maximum concentration of 0.2 ppm $H_2S_{(g)}$ was adopted. Speciation
281 models in PHREEQC that assume a redox potential control by the S^{2-}/S^{6+} couple yielded
282 results consistent with the field occurrence of secondary minerals, as well as with the fact
283 that most of the dissolved Fe must be in its Fe^{2+} form, given the high acidity of the waters.
284 Similar observations apply to acid mine drainage (AMD) environments (Nordstrom et al.,
285 2000; Fernández-Remolar et al., 2005; Hubbard et al., 2009).
286
287 Representative samples for each of the activity stages (see section 2) were selected, based
288 on the completeness of chemical data and the availability of sufficient material for re-
289 analysis if needed. Two samples representing Stage V, labelled Substage VA and Substage
290 VB, were included to distinguish between different levels of activity during this interval
291 (the former less active than the latter). The labels only indicate a difference in chemical
292 composition (Table 2) and are not intended to introduce new substages in the eruptive
293 history of Poás.
294
295 For geochemical modelling, two compositions were selected from the complete data set
296 available of Laguna Caliente. They were labelled LoALW (Low Activity Lake Water),
297 sampled during Substage IVC (January 31th, 2002) and HiALW (High Activity Lake Water),
298 sampled during Stage VB (May 27th, 2011). These LoALW and HiALW compositions

represent periods of low and high activity in the history of the lake, respectively, and thus represent compositional extremes.

4.1.2. Primary and secondary mineralogy in the field

The XRD analysis of lake sediments exposed on southern and eastern sectors of the crater (sites 4, 10; Figs. 2 and 4; Table 1) and on the western shore of the lake (site 14; Fig. 2; Table 1) revealed the presence of tridymite, cristobalite, quartz, kaolinite, sauconite, cowlesite, phillipsite, greigite, woodhouseite and ralstonite. In addition, sulphates are represented by gypsum, K-alunite, Na-alunite, minamiite, meta-alunogen, halotrichite and magnesiocopiapite.

Two rock samples, collected within lake sediments exposed on the eastern shore of Laguna Caliente (site 10; Figs., 2 and 4; Table 1), were investigated for the effect of alteration by Laguna Caliente water. These samples correspond to lavas that show a vesicular texture, with phenocrysts of plagioclase, pyroxenes and opaques. The plagioclase composition is close to An_{58}, whereas pyroxenes consist of two groups: augite $Wo_{38.8}En_{41.6}Fs_{19.6}$ and enstatite $Wo_{3.9}En_{62.2}Fs_{33.9}$, and opaques range between magnetite $Fe^{2+}Fe^{3+}{}_2O_4$ and ulvöspinel $TiFe^{2+}{}_2O_4$. In the altered parts of the lavas, both plagioclase and pyroxene phenocrysts are intensely silicified. Frequently, the entire crystal structure has been replaced by a SiO_2-rich phase which corresponds to amorphous silica. In general, silicification is less pervasive in the pyroxenes than in the plagioclase. Within the lava vesicles, the most common alteration mineral is an Al_2O_3-SO_3-rich phase, which corresponds to alunite with a composition close to the H-alunite end-member (Figs. 5 and 6). There is also an Al_2O_3-SiO_2-rich phase with a composition close to kaolinite. Pyrite and elemental sulphur globules are present within the vesicles as well. Textures indicate that pyrite and sulphur formed before H-alunite and kaolinite. Temporal relationships between amorphous silica and the other alteration minerals are unclear, but silica probably formed early, considering that it is a residue after the mobile cations (Ca^{2+}, Al^{3+}, Fe^{2+}, Mg^{2+}, Na^{+} and K^{+}) are incorporated into solution (Oelkers, 2001).

4.1.3. Heating model

Heating models (Fig. 7) were ran in PHREEQC to explore changes in the saturation state of representative minerals when temperature increases from those measured in the lake (30 and 62°C) up to 300°C. The heating models only consider a temperature increase, ignore any reaction with surrounding rock, and thus predict changes in the chemical composition of the lake water solely in response to mineral precipitation or dissolution. The heating models provide insight into the saturation state of acid brine water at depth, e.g. in the hydrothermal system below the lake, envisage changes in response to an increased input of heat due to increased volcanic activity, and simulates chemical effects on lake water that circulates back into the deeper parts within volcanic edifice (i.e. Rouwet et al., 2016). Conversely, the runs can also be interpreted in a reverse way as cooling models for deep hot brine water travelling upward and ultimately feeding the lake.

Under surface conditions, Laguna Caliente waters were saturated with elemental sulphur and pyrite, and close to saturation with amorphous silica, anhydrite and gypsum (Fig. 7). A temperature rise will increase the solubility of amorphous silica, pyrite and elemental sulphur, and will decrease the solubility of gypsum, anhydrite, diaspore, kaolinite, K-alunite, Na-alunite, and AlF_3. In aqueous systems, the solubility curves of gypsum and anhydrite intersect at 42°C, with gypsum being the stable phase below and anhydrite the stable phase above this temperature (Braitsch, 1971).

The LoALW composition (T=28°C) formed pyrite up to 100°C, followed by anhydrite, diaspore and AlF_3. While K-alunite was only stable between 100 and 200°C, anhydrite, diaspore and eventually AlF_3 persisted up to 300°C. The pH increased until K-alunite or diaspore appeared, remained more or less constant, then decreased and finally increased at temperatures higher than 250°C. On the other hand, the HiALW composition (T=62°C) was already saturated in elemental sulphur at such temperature and this phase dissolved when the temperature increased.

4.1.4. Water-rock reaction model

Results of PHREEQC water-rock reaction path models, with the same set of water samples and a basaltic-andesite analysed by Cigolini et al. (1991) as reactants, are presented in

Figure 8. In every run, 1 mole of rock (110 g) was reacted with 1 kg of crater lake water. The water-rock reaction path can be visualised as a titration model in which the water sample (acid) is incrementally titrated with small amounts of rock (base). As a rule, the pH of the system will increase due to H^+ consumption by the rock, and at the same time cations will be liberated into solution. It must be noted that the crater lake water used in the interaction models is not a "pristine" liquid end-member, since the samples collected at the surface represent liquids that had previously reacted with surrounding rocks at depth before reaching the crater area. Also, as discussed in the previous section, the fluids that reach Laguna Caliente were probably chemically modified by mineral precipitation due to cooling and boiling. Nevertheless, due to their extreme acidy, the waters are still capable of dissolving large amounts of rock. As the reaction progress proceeds, secondary phases or minerals will be formed and, in some cases, their presence will be transient. Each model was run at a constant temperature, corresponding to the lake water temperature when the sample was taken. Minerals allowed to precipitate were selected according to the assemblages found by XRD and EMP analysis. Finally, for practical purposes, it is assumed that dissolution of primary phases in the rock occurs congruently. This implies that the basaltic andesite is considered to behave as a homogenous phase, similar to a glass, and that all of its components dissolve instantaneously.

The water-rock reaction path models for the LoALW composition showed amorphous silica, hematite and anatase at low reaction-progress values (<0.001 mole rock/kg water). At intermediate values (0.01 – 0.1 mole rock/kg water) K-alunite, $Al(OH)SO_4$, kaolinite, pyrite and fluorite appear. Finally, at high values (>0.1 mole rock/kg water), illite is added to the mineral assemblage. The HiALW composition produced fewer secondary minerals and probably represents the scenario of the most unreacted system due to the low pH values reached at the end of the run. This system is characterized by the formation of anatase and amorphous silica followed by anhydrite and H-jarosite $HFe_3(SO_4)_2(OH)_6$.

In summary, the water-rock interaction models for Laguna Caliente, representing a low rock/water system, demonstrate that during low volcanic activity periods, the secondary mineral assemblage is marked by the presence of amorphous silica, anatase, hematite, $Al(OH)SO_4$, K-alunite, kaolinite, pyrite, fluorite, gypsum and illite. In contrast, during

periods of high activity, the mineral assemblage with be constituted only by amorphous silica, anatase, anhydrite and eventually H-jarosite.

4.1.5. Evaporation model

Water evaporation is a major process in crater lakes (Pasternak and Varekamp, 1997) and induces changes in the chemical composition of the waters such as increasing concentrations of dissolved species until saturation is reached and phases precipitate or evaporate along with the water (Varekamp et al., 2000; Rouwet and Ohba, 2015; de Moor et al., 2016; Rouwet et al., 2016). The rate of evaporation usually fluctuates as it is a function of different parameters that vary with time, of which heat input from magma at depth is an important factor and sealing processes as well. The evaporation process for Laguna Caliente water was simulated by removing small amounts of H_2O from a 1 kg of sample; at a constant temperature corresponding to the one of the lake when the sample was taken (Fig. 9). The run reached 98% of water loss. Beyond this point there were convergence problems with PHREEQC due to the high ionic strength of the solutions that, in the case of the HiALW composition, went up to 37.9 mol/kg H_2O from a starting value of 2.39 mol/kg H_2O. Phases precipitating in the HiALW model are anatase, anhydrite and elemental sulphur. As a consequence of water removal, pH drops drastically and the extreme acidity promotes the formation of hydrogen chloride $HCl_{(g)}$. This gas often forms in Laguna Caliente and as well as in other acidic volcanic lakes (Martínez et al., 2000; Rouwet and Ohba, 2015; Shinohara et al., 2015; Tamburello et al., 2015; Rouwet et al., 2016). The saturation indices of amorphous silica, halite, and iron and magnesium sulphates such as szolmolnokite $FeSO_4 \cdot H_2O$, rozenite $FeSO_4 \cdot 4H_2O$, siderotile $FeSO_4 \cdot 5H_2O$, melanterite $FeSO_4 \cdot 7H_2O$, kieserite $MgSO_4 \cdot H_2O$, and epsomite $MgSO_4 \cdot 7H_2O$ steadily increased until 80% of the water was evaporated and then abruptly decreased. Similar evaporation runs were performed on the LoALW composition at 30°C in order to explore possible temperature effects. In this case, gypsum formed instead of anhydrite, and amorphous silica was present. Anatase was not included in the model since Ti was not analysed in the LoALW sample. The temperature effect was particularly reflected in the type of calcium sulphate present (gypsum or anhydrite) and in the saturation of amorphous silica (Fig. 9).

In summary, the results of models for the low rock/water scenario, applied to the Laguna Caliente waters, demonstrate that the observed secondary mineralogy can be generated by a combination of the simulated processes. Whereas elemental sulphur and pyrite formed by cooling; anhydrite, gypsum, diaspore, K-alunite and AlF_3 became saturated by heating of brine water at depth, without any concomitant rock interaction. On the other hand, the formation of H-jarosite, hematite, $Al(OH)SO_4$, kaolinite, illite and fluorite required rock dissolution.

4.2. Scenario 2: hot springs (medium rock/water ratios).

4.2.1. Water chemistry

Hot springs issuing acidic waters existed at various locations on the eastern terrace of Laguna Caliente from March 1999 till January 2007. Samples from the years 2000, 2001, 2003 and 2006, documented by Martínez (2008) and Vaselli et al. (2003) were included in this study. The hot spring waters were dominantly SO_4-rich steam heated waters with temperatures between 42 and 92°C and pH values between 0.99 and 2.47 (at 20-24°C) (Fig. 3; Table 3). Presumably, hot vapours coming from degassing magma interacted with meteoric waters that may have been derived through subsurface flow from Botos Lake, since it is located topographically higher than the active crater (Sanford et al., 1995). No samples of alteration minerals were collected from sites were the hot springs existed since most were covered by landslide deposits produced by an earthquake on January 8th, 2009 (Alvarado, 2010).

4.2.2. Water-rock reaction model

Water-rock reaction models follow the same approach as the ones described in section 4.1.4, including use of the basaltic andesite described by Cigolini et al. (1991). Each run was carried out at the temperature of the spring (Fig. 10). Two spring samples were selected as end-member examples in terms of initial temperature and pH: White Algae (August 23rd, 2000; T=42°C) and Norte-Este (February 14th, 2003; T=87°C). At low reaction progress values (<0.001 mole rock/kg water), the modelled secondary mineral association for the White Algae composition is represented by anatase, amorphous silica,

hematite, K-alunite and kaolinite. At intermediate reaction progress (0.01 – 0.1 mole rock/kg water), pyrite and illite appear. Diaspore formed at high reaction progress (>0.1 mole rock/kg water). The runs with the Norte-Este spring composition show a dominance of amorphous silica, anatase and hematite at low reaction progress (<0.001 mole rock/kg water), followed by K-alunite, kaolinite, anhydrite, pyrite and illite. Diaspore and magnetite become stable at high reaction progress values (>0.1 mole rock/kg water).

4.3. Scenario 3: fumaroles (high rock/fluid ratios).

This scenario is represented by the active fumarole field on the northern flank of the CPC (site 8; Fig. 2) and fossil fumarole fields on the south-western (sites 1, 3; Figs. 2 and 11), eastern and north-eastern walls of the crater. The fumaroles of the last two groups were particularly active from mid-1999 till 2007 (Martínez, 2008; Vaselli et al., 2003; Fischer et al., 2015). Variable rock/water/gas proportions mark the interactions within fumarole conduits and vents, whereby the liquid water phase corresponds to the gas condensate. Following the description of the alteration mineralogy, modelling results for rock-gas and rock-gas condensate interaction will be treated. For this study, only samples from the CPC were taken into account.

4.3.1. Gas and gas condensate chemistry

The gases of the CPC fumaroles consist mainly of H_2O (up to 95 mol %), followed by CO_2, SO_2, H_2, HCl, HF and H_2S (Vaselli et al., 2003; OVSICORI, 2012, unpublished data; F. Tassi, pers. comm., 2012; Fischer et al., 2015). Since the aqueous solubilities of these gas components are very different, the fumarole composition is extremely variable and dependent on the degree of interaction of deeply derived gas with shallow aquifers. This interaction has been referred to as “scrubbing” by Symonds et al. (2001). These authors demonstrated that low-temperature (<250°C) gas is likely to have experienced “scrubbing” by aquifers in which a considerable amount of the components dissolved in the water (especially HCl, HF and, to a minor extent, SO_2) leaving the gas relatively enriched in the less soluble gaseous components. In any case, magma gases commonly experience processes such as cooling, oxidation and condensation before reaching the atmosphere (Africano and Bernard, 2000).

In order to assess changes in the chemical composition of the Poás fumarolic gases due to cooling, SOLVGAS (Symonds and Reed, 1993) was used. This software is well suited for restoring volcanic gas compositions, modelling the speciation of gas mixtures and computing the saturation indices of potential sublimates. For this modelling, gas samples taken by OVSICORI on June 25th, 2010 (T=763°C), August 16th, 2010 (T=650°C) and March 18th, 2011 (T=250°C) were used (Fig. 3; Table 4). Gas cooling models ran in SOLVGAS from the sampling temperature down to 25°C demonstrated that, at T≤100°C, these gases experience an important total sulphur loss in form of (1) droplets of the following sulphuric acid hydrates: $H_2SO_4 \cdot 2H_2O$, $H_2SO_4 \cdot 3H_2O$, $H_2SO_4 \cdot 4H_2O$, $H_2SO_4 \cdot 6H_2O$, and (2) elemental sulphur. Between 100 and 25°C liquid H_2O and $H_2SO_4 \cdot H_2O$ form.

When high-temperature gases cool down during their rise through the fumarole conduit, atmospheric O_2 ultimately enters the system at very shallow levels, leading to oxidation of the gas phase. At low temperatures (<350°C), elemental sulphur can be produced by the reaction (Mizutani and Sugiura, 1996):

$$SO_2 + 2H_2S \Leftrightarrow 3S^0 + 2H_2O \quad (1)$$

Below 330°C (H_2SO_4 boiling temperature), acidic droplets can form by H_2S oxidation upon increasing f_{O_2} (Symonds, 1990):

$$H_2S_{(g/l)} + 2O_{2\,(g/l)} \Leftrightarrow H_2SO_{4\,(g/l)} \quad (2)$$

In addition, sulphuric acid can also form by SO_2 disproportionation (Kusakabe et al., 2000; Africano and Bernard, 2000):

$$4SO_{2\,(g/l)} + 4H_2O_{(g/l)} \Leftrightarrow 4H_2SO_{3\,(l)} \Leftrightarrow 3H_2SO_{4\,(l)} + H_2S_{(g/l)} \quad (3)$$

The stability of H_2SO_4 together with its hydrated forms mentioned above also depends on the total amount of S in the gases and increases with decreasing temperature. At low temperatures (<200°C) elemental sulphur can be produced as follows (Kusakabe and Komoda, 1992):

$$3SO_{2\,(g/l)} + 3H_2O_{(g/l)} \Leftrightarrow 3H_2SO_{3\,(l)} \Leftrightarrow 2H_2SO_{4\,(l)} + S^0_{(l/s)} + H_2O_{(g/l)} \quad (4)$$

Reactions 2-4 can explain the low pH of volcanic condensates.

4.3.2. Secondary mineralogy in the field

Minerals detected by XRD include SiO_2 polymorphs (cristoballite, quartz and trydimite), anatase, elemental sulphur, calcium sulphates (anhydrite and gypsum) and sulphates of the alunite group, represented by K-alunite, Na-alunite and minamiite (Fig. 2; Table 1). Pervasive alteration observed at sites 1, 3 and 8 (Figs. 2 and 11) completely erased primary minerals and textures, leaving a silicified rock residue of the attack by acid fluids. Hence, these sites present good examples of extreme acid alteration.

4.3.3. Gas-rock reaction model

The reaction between the CPC gases and surrounding rocks was modelled using GASWORKS (Reed, 1982), which is a complementary program to SOLVGAS and computes both gas-solid-liquid equilibria and reaction progress. For the simulations, the gas samples (Table 4) of June 25th, 2010 (T=763°C), August 16th, 2010 (T=650°C) and March 18th, 2011 (T=250°C) were reacted with a basaltic andesite (Cigolini et al., 1991). In each model, one mole of gas sample (~26 g) was cooled and reacted with one mole of basaltic andesite (~110 g) from the corresponding sampling temperature down to 114°C. Below this temperature convergence problems occurred. Nevertheless, it is well representative for the lowest temperatures recorded for the CPC fumaroles. The modelling results in terms of saturation indices and amounts of secondary minerals formed are shown in Figure 12. The predicted secondary mineral assemblages for the samples of June 25th, 2010 (T=763°C) and August 16th, 2010 (T=650°C) are the same and consist of liquid sulphur as the most abundant phase, followed by $MnSO_4 \cdot H_2O$, $Na_2SO_4 \cdot 5H_2O$, K_2SO_4, and finally MgF_2 and anhydrite. Magnesium fluoride was the only phase formed in the model with the sample of March 18th, 2010 (T=250°C). According to the cooling models explained above, the total sulphur content of this sample was probably already considerably depleted. Therefore, sulphur availability for the formation of sulphates or elemental sulphur was limited.

556 *4.3.4. Gas condensate-rock reaction model*

557

558 The reaction between gas condensates of the CPC fumaroles collected on September 8th,
559 2010 (T=760°C) and February 10th, 2012 (T=107°C) (Fig. 3; Table 5) and a basaltic-
560 andesite (Cigolini et al., 1991) were simulated in PHREEQC. In all runs, 1 kg of the gas
561 condensate was titrated with 1 mole of the basaltic-andesite (~110 g) at 95°C (Fig. 13).
562 The high temperature sample (T=760°C) only produced amorphous silica and anatase
563 during low (<0.01 mole rock/kg water) and medium (0.01-0.1 mole rock/kg water)
564 reaction progress values. Hematite, kaolinite and K-alunite, followed by pyrite, illite,
565 fluorite and magnetite became stable at high reaction progress (>0.1 mole rock/kg water).
566 The low temperature composition (T=107°C) resulted in a more complex secondary
567 mineralogy along the reaction path. Amorphous silica, anatase and hematite formed
568 during low reaction progress (<0.01 mole rock/kg water), then K- and Na-alunite,
569 anhydrite and kaolinite at medium reaction progress (0.01-0.1 mole rock/kg water), and
570 finally pyrite, illite, magnetite and diaspore appeared at high reaction progress (>0.1
571 rock/kg water).

572

573 **4.4. Scenario 4: acid rain / acid brine spray (high rock/water ratios).**

574

575 This scenario supposes high rock/water ratios similar to the gas condensate – rock
576 interaction case, but is treated separately because of the spatial extension of the impact
577 of airborne acid deposition and the specific secondary mineralogy produced. Areas
578 around Laguna Caliente receive input from acid rain and brine spray, either continuously
579 or during phreatic eruptions. Due to the prevailing, north-easterly wind direction at the
580 summit of Poás volcano, the impact of acid fluids transported as aerosols particularly
581 affect an area SW of Laguna Caliente, known as the "dead zone", which is approximately 2
582 km^2 large and is characterized by intense rock alteration and absence of vegetation (Figs.
583 2, 3 and 14).

584

585 *4.4.1. Secondary mineralogy in the field*

586

587 XRD analysis of deposits from the 1910 eruption, SW of Laguna Caliente (site 2; Fig. 2;
588 Table 1), revealed the presence of tridymite, cristobalite, quartz and K-alunite. Gypsum

and anhydrite were found on the ceiling of a cave at site 6 (Figs. 2, 14; Table 1), and probably formed from infiltrated acid brine from Laguna Caliente that was expulsed during a phreatic eruption. Material collected from the NE rim of the main crater (sites 28, 31, 32; Fig. 2; Table 1) contained cristobalite, goethite, hematite, magnetite, tennantite, ralstonite, potassium halite, tychite, ankerite, H-jarosite and polyhalite. Lake sediments ejected by a phreatic eruption on April 13th (2012) and collected on the southern plain of the main crater (site 33; Fig. 2; Table 1) contained polyhalite and meta-alunogen. Basaltic-andesitic lava blocks in the "dead zone" close to Cerro Pelón (sites 18, 20, 21; Figs. 2, 15; Table 1), which contain clinopyroxene, orthopyroxene and olivine (up to 5%) as phenocrysts, exhibit a complex secondary mineralogy consisting of halloysite, nontronite, sauconite, montmorillonite, mordenite, phillipsite, chabazite, goethite, hematite, magnetite, carobbiite, kogarkoite, ralstonite, alunogen, meta-alunogen, rostite, K-jarosite, copiapite, magnesiocopiapite, epsomite, tamarugite and sodium alum. A close observation of the alteration pattern of the blocks revealed that their crusts are primarily composed of massive amorphous silica and jarosite void fillings (Figs. 15a and 15b). Smectites and kaolinite were identified in the inner parts of the blocks (Fig. 15c). The most altered primary mineral is olivine, which commonly appears as "ghosts" (Figs. 15c and 15d), whereas fresh olivine is rare (Fig. 15e). Amorphous silica has replaced various primary minerals (Fig. 15f). A lava flow near the east shore of Laguna Caliente with the same composition of these lava blocks shows a similar alteration pattern. Most of the clinopyroxene, orthopyroxene and plagioclase phenocrysts are relatively fresh (Fig. 16a) but olivine is considerably altered or shows a "ghost" texture (Figs. 16b and 16c). Jarosite precipitated in veins that dissected the matrix and some phenocrysts (Figs. 16d to 16e, and 17a to 17f). EMP analysis revealed a K-jarosite composition $(K_{0.68}Na_{0.12}H_{0.21})(Fe_{2.98}Al_{0.13})(SO_4)_{2.10}(OH)_6$, with H^+ and Na^+ substitution up to 50% and 25%, respectively (Fig. 18).

In summary, the alteration mineralogy in samples representing this scenario shows the following systematics: (1) Silica polymorphs and tennantite probably formed at relatively high temperatures. (2) This probably also applies to the fluorides, since modelling showed that MgF_2 is stable in the CPC fumaroles; moreover, ralstonite is a common alteration product of cryolite (AlF_3), which is often found in fumarolic vents, as is carobbiite. (3) Zeolites could be alteration products formed at higher temperatures as it is common in

many hydrothermal systems (Reyes, 1998). (4) Carbonates are probably products of interaction with meteoric water at ambient temperature and near neutral pH conditions; (5) Sulphates such as alunogen, meta-alunogen, rostite and especially copiapite, magnesiocopiapite, jarosite and epsomite reveal water-poor conditions, given the large solubility of these salts; (6) Samples from lava blocks in the "dead zone" and from a lava flow near Laguna Caliente exhibit an alteration mineralogy dominated by amorphous silica, jarosite, kaolinite and smectite; (7) The intense alteration of olivine and its association with jarosite and epsomite, suggest that Fe- and Mg-rich fluids capable of forming Fe- and Mg-sulphates are mainly derived from olivine. In the following section, this evidence will be used in the modelling strategy.

4.4.2. Water-rock reaction model

A sample from Laguna Caliente collected on August 30th, 1994 (Stage III) (Martínez et al., 2000) was titrated by the addition of small amounts of olivine in PHREEQC. A composition of Fo_{75} was adopted, based on an average of EPM analyses of olivine in the basaltic-andesitic blocks of Cerro Pelón (dead zone). Up to 1 mole of this olivine (156.01 g) was reacted in 1000 steps with 1 kg of Laguna Caliente sample at T=24°C. At low reaction progress (<0.01 mole rock/kg water) only amorphous silica formed, which was followed by K-jarosite, goethite and jurbanite $Al(SO_4)(OH)\cdot 5H_2O$ at medium reaction progress (0.01-0.1 mole rock/kg water), and finally by K-alunite, kaolinite Mg-montmorillonite and laumontite at high reaction progress (>0.1 mole rock/kg water) (Fig. 19a). From this run, an aliquot of the solution obtained during step 40, before the formation of K-jarosite, was evaporated in 1000 steps at T=24°C until 97.6% of the initial water was removed. Beyond this point, the run did not converge, mainly due to the high ionic strength of the solution (22.4 mol/kg H_2O). The secondary phases formed where only amorphous silica and gypsum (Fig. 19b). The solution from the last step of the evaporation run was reacted again with 1 mole of Cerro Pelón olivine in 1000 steps. However, the run did not go further than step 320, after 0.320 moles or 49.9 grams of the olivine had reacted with the solution. The secondary phases formed were gypsum and amorphous silica (<0.01 mole rock/kg water), followed by anhydrite, goethite and K-montmorillonite (0.01-0.1 mole rock/kg water), and ultimately elemental sulphur and magnetite (>0.1 mole rock/kg water) (Fig. 19c). Since the concentrations of Fe^{2+} and Mg^{2+} remained high, another evaporation

model was run in which a solution from step 56 of the previous model (after the reaction of 0.052 moles or 8.74 g of olivine) was evaporated at T=24°C. In this second evaporation step, the run did not converge after removal of 41.7% of the initial 24.34 g of water, because of the extremely high ionic strength (43.91 mol/kg H_2O). Nevertheless, amorphous silica and gypsum were present (Fig. 19d). In order to add more Mg^{2+} and Fe^{2+} to the system, a final reaction run was performed in which the solution from step 327 of the previous evaporation run was reacted again with 1 mol of olivine at T=24°C. This time the run was subdivided into 10000 steps in order to track small changes in mineral saturation states. The secondary minerals formed were amorphous silica, gypsum and elemental sulphur (<0.001 mole rock/kg water), and epsomite and ferrohexahydrite (0.001-0.001 mole rock/kg water) (Fig. 19e). This combined sequence of previous runs modelled a hyperacid water-olivine reaction scenario for an open system, in which subsequent cycles of reaction and evaporation were envisaged.

4.5. Summary of geochemical models

The geochemical modelling results presented above are a representative selection of water-rock reaction path and heating models from a more comprehensive set of runs that were performed for each setting. Here, the stability of secondary minerals as a function of pH or temperature is summarized taking all the results into account. As will be discussed below, the initial pH of water is an important variable, even more than temperature, which signals the degree of previous water-rock interaction in the system, excluding the dilution with near-neutral meteoric water. Low-pH compositions can be regarded as a low-reacted system since more rock needs to react with these fluids in order to increase the pH and/or deliver more cations into solution and consequently form secondary minerals. In contrast, high-reacted systems, represented by high-pH samples, may reflect a considerable degree of neutralization due to rock interaction.

A compilation of six heating models for Laguna Caliente water is presented in Figure 20. As explained in section 4.1.3., the heating models simulate a scenario of a fluid circulating in the deeper parts of the hydrothermal system of Poás volcano. Up to 98°C, the only minerals predicted to precipitate from the solutions are elemental sulphur and pyrite. Anhydrite appears at 98°C, followed by diaspore (136°C) and AlF_3 (173°C), and these

phases continue to be stable until 300°C, which was the end-temperature in the models. Potassium alunite only forms between 95° and 164°C.

Water-rock models of Laguna Caliente, as described in 4.1.4., are summarized in Figure 21. Nine runs cover different stages and substages of activity of the lake. Anatase and amorphous silica are the most persistent minerals, present from pH -0.4. In addition, anhydrite (pH ≥ -0.3), hematite (pH ≥ 1.1) and gypsum (pH ≥ 1.3) are also stable over a large range. Hydronium jarosite (pH 1.1 to 1.2) and potassium jarosite (pH 1.2 to 1.3) are present in a narrow pH interval under acidic conditions at the beginning of the water-rock reaction path models, followed by K-alunite (pH 1.7 to 3.8), $Al(OH)SO_4$ (pH 1.7 to 3.7) and Na-alunite (pH 2.6 to 3.0). Finally, at pH >2 the mineral assemblage consists of kaolinite, fluorite, pyrite and illite.

Figure 22 presents a compilation of seven water-rock interaction models for the hot spring compositions (section 4.2.2.), similar to the complete versions shown in Figure 10. These waters have considerable higher pH values than the lake water, suggesting that they may have interacted more extensively with rocks. Also, the $HCl_{(aq)}$ contribution to acidity is much less important. In the water-rock interaction models the hot spring waters are always saturated in anatase (pH ≥ 0.7), amorphous silica (pH ≥ 0.7), hematite (pH ≥ 0.9) and anhydrite (pH ≥ 1.2). Hydronium jarosite (pH 0.8 to 0.9) followed by K-alunite (pH 1.6 to 3.6), Na-Alunite (pH 1.9 to 2.7) and $Al(OH)SO_4$ (pH 2.3 to 2.9) are only stable where low pH conditions still prevail. Kaolinite also appears early, but continues to be saturated over an extended pH range (≥ 2.1). Pyrite and fluorite start to form at higher pH values (≥ 4.1). The most advanced stages of rock interaction (pH ≥ 5) are characterized by the presence of illite, magnetite and finally diaspore.

The gas condensate-rock reaction models for the CPC fumaroles, described in section 4.4.3.4., are summarized in Figure 23. Anatase (pH ≥ 1.3), amorphous silica (pH ≥ 1.3), anhydrite (pH ≥ 2.0) and kaolinite (pH ≥ 2.1) are stable throughout the runs. Only at low pH, elemental sulphur (pH 1.3 to 2.3), K-alunite (pH 1.9 to 3.2) and Na-alunite (pH 2.1 to 2.3) are part of the mineral assemblage. Pyrite also forms under acid conditions (pH 1.3) but continues to be stable until pH 7.3. Fluorite (pH ≥ 4.1) and hematite (pH ≥ 4.4) precipitate at higher pH conditions, followed by illite and brucite (pH ≥ 5.3).

5. DISCUSSION

5.1. Field observation vs. geochemical modelling

In general, there is a good agreement between the secondary minerals predicted in the models and the ones observed in the field. Differences can be attributed to incomplete sampling, analytical issues, assumptions and limitations in modelling as a consequence of the often extreme acidity and salinity of the fluids, and missing phases in the thermodynamic database. Analytical restrictions include the sensitivity of powder XRD analysis, which will usually not detect crystalline phases with a concentration less than 5 volume % (Poppe et al., 2002), and grain sizes that are too small for microprobe analysis or phases that are not stable under the electron beam.

Modelling results suffer from the limitation that the thermodynamic database (llnl.dat) used in PHREEQC only includes pure end-members for solid solutions. Similar to what analysed alunites and jarosites of Poás show, many other sulphates form solid solutions. For example, the halotrichite group consists of monoclinic hydrated sulphates with the general formula $XY_2(SO_4)_4 \cdot 22H_2O$, where X is a divalent (Co^{2+}, Fe^{2+}, Mg^{2+}, Mn^{2+}, Ni^{2+}, Zn^{2+}) cation and Y a trivalent (Al^{3+}, Cr^{3+}, Fe^{3+}) cation. Complete solid solutions between the end-members are expected to exist (Ballirano, 2006). Another example is magnesiocopiapite $MgFe^{3+}{}_4(SO_4)_6(OH)_2 \cdot 20H_2O$ of the copiapite group with general formula $A^{2+}R^{3+}{}_4(SO_4)_6(OH)_2 \cdot 20H_2O$, where R is dominated by Fe^{3+} in all members, which shows a complete substitution by divalent (Mg^{2+}, Fe^{2+}) and trivalent (Fe^{3+}, Al^{3+}) cations on the A-site (Bayliss and Atencio, 1985; Robinson, 1999).

Silica polymorphs (tridymite, cristobalite and quartz), detected by XRD, may have formed at temperatures higher than those considered in the water-rock interaction models (T≤300°C). The only stable SiO_2-phase at the lake-water temperatures (T≤70°C) is amorphous silica. The llnl database used in PHREEQC only includes the zeolites phillipsite and mordenite. In models reacting the LoALW sample with the basaltic andesite reported by Cigolini et al. (1991) at 30°C, mordenite appears at pH ≥ 4.11. By the other hand, the same model at 300°C indicates the presence of phillipsite at pH ≥ 1.65. Consequently, it is

754 probable that phillipsite was formed at deeper levels within the volcanic system. Since
755 zeolites are not very common on Poás surface environments, they were not routinely
756 included in the models. Zinc and phosphorous were not analysed in the lake waters, which
757 explains why neither sauconite nor woodhouseite appeared as secondary phases in the
758 models. Absence of greigite ($Fe^{2+}Fe^{3+}{}_2S_4$) in the models despite its inclusion in the
759 thermodynamic database (llnl.dat), is possibly attributable to an inadequate estimation
760 of the redox state. Hence, the S^{2-}/S^{6+} and Fe^{2+}/Fe^{3+} ratios in Laguna Caliente waters must
761 be better constrained since the models assume that all S^{2-} is consumed by Fe^{2+} to form
762 FeS_2 and there should probably be more Fe^{3+} in the system to produce greigite.
763
764 Other minerals such as ralstonite, H-alunite, minamiite, meta-alunogen, halotrichite and
765 magnesiocopiapite that were detected in the field did not appear in the models since they
766 are not included in the database. According to the speciation results, Al tends to form
767 complexes with F such as AlF^{2+}, $AlF_2{}^+$ and $AlF_3{}^0$, increasing the Al solubility in Laguna
768 Caliente waters and eventually promoting the formation of solid AlF_3. Moreover, $SO_4{}^{2-}$ has
769 also a strong affinity to Al^{3+} and forms complexes such as $AlSO_4{}^+$ and $Al(SO_4)_2{}^-$ that
770 eventually lead to the formation of aluminium-hydroxysulphate minerals. For instance,
771 alunogen $Al_2(SO_4)_3{\cdot}17H_2O$ is the most stable aluminium sulphate under extremely low pH
772 conditions (<0) and probably only forms by efflorescence in capillary films (Nordstrom,
773 1982). Subsequent dehydration of alunogen can yield meta-alunogen (Zhou and Wang,
774 2013). Both meta-alunogen and alunogen have been also reported at Te Kopia geothermal
775 field (Taupo volcanic zone, New Zealand) where they are confined to sheltered and humid
776 microenvironments associated with warm (T=25-50°C) and acid (pH=2.5-3.0) ponds
777 (Martin et al., 1999). Previous XRD analyses of sediments collected from the lake bottom
778 on September 14th (2011) identified rhomboclase $HFe^{3+}(SO_4)_2{\cdot}4H_2O$ and bilinite
779 $Fe^{2+}Fe^{3+}{}_2(SO_4)_4{\cdot}22H_2O$ (Rodríguez and van Bergen, 2015). Their origin is unclear. Both
780 bilinite and rhomboclase have been described in acid mine drainage systems related to
781 oxidized sulphide deposits (Jambor et al., 2000; Hammarstrom et al., 2005). Nordstrom
782 and Alpers (1999) described the formation of rhomboclase stalagmites at Iron Mountain
783 in association with extremely acid water (pH = -3.6). The origin of meta-alunogen,
784 halotrichite and magnesiocopiapite is possibly related to their occurrence in lake
785 sediments, ejected during phreatic eruptions that subsequently dried and were protected
786 from rain.

While all the fluid-rock models in this study included chemical compositions of fluids that are far from being pristine and, rather represent fluids that have previously reacted with the surrounding rocks; this is not the case for the rocks, since the models include a fresh rock as starting material. This might be far from reality considering that around Laguna Caliente most rocks are intensively altered. Therefore, in order to investigate the effect of using an altered rock as starting material in the secondary mineralogy produced, models were run with an altered andesite and its fresh counterpart from Kawah Ijen (van Hinsberg et al., 2010b). These include water-rock reaction path models using Laguna Caliente waters, hot spring waters, fumarole condensates and gas-rock reaction path models with gases from the CPC fumaroles. Only the ones including Laguna Caliente waters are shown here (Figure 24), since these are probably the most representative from Poás. The results indicate that the same secondary minerals appear in the models involving both fresh and altered andesites. The main difference is that in the altered andesite models, the secondary minerals form at latter reaction progress stages compared to the fresh andesite. In other words, more altered rock needs to react with the fluids in order to produce the same secondary mineralogy compared to the fresh rock scenario. This probably explains the lack of secondary minerals observed in the field compared to the predicted in the models. Nevertheless, the models using fresh rock offer a good approximation of the processes occurring at Poás volcano.

5.2. Buffers and chemical changes as a product of water-rock interaction in the waters of Poás volcano

Water-rock interaction promotes neutralization in acid SO_4-Cl waters and causes liberation of cations from solid rocks and minerals. Following the principle of electric charge balance, any lack of cations in acid waters is thought to be compensated by H^+. Varekamp et al. (2000) defined the "degree of neutralization" (DON) as an indication of the amount of acid consumption through rock dissolution, estimated by the residual acidy (%). If the effects from dilution with near-neutral meteoric waters can be ignored, a system could be dominated by rock dissolution (low residual acidity) or magmatic volatiles (high residual acidity). In such cases, pH would be a good indicator of how evolved a fluid is by reaction with surrounding rocks. From the water-rock reaction models it can be inferred that, of all the secondary phases, jarosites, followed by alunites

820 are typically indicative for low pH conditions that are mostly associated with intermediate
821 reaction progress values (<0.1 mole/kg water). Nevertheless, if the initial pH is extremely
822 low (e.g., pH~0), both jarosites and alunites remain stable until high reaction progress
823 values (>0.1 mole rock/kg water) are reached. The obvious reason is that aqueous
824 systems with higher H^+ concentration need more rock to become neutralized. Hence, a
825 meaningful comparison between modelling results for different compositions concerning
826 the stability of secondary mineral should be based on pH rather than reaction progress.
827 According to Marini et al. (2003), several buffers operate in acidic volcanic waters at
828 different pH intervals (pH 0.5-1.5 and pH 3.5-5). The pH curves in the water-rock models
829 of Laguna Caliente, hot springs and fumarole condensates suggest the following buffers:
830
831 The first operates at pH -0.8 to 2.0 and is controlled by the HCl/Cl^- and/or the HSO_4^-/SO_4^{2-}
832 couple. The second buffer (pH 1.5) is not always active and involves either K-jarosite or
833 H-jarosite consumption to produce $Al(OH)SO_4$ and hematite:

$$KFe_3(SO_4)_2(OH)_6 + Al^{3+} = K^+ + Fe^{3+} + SO_4^{2-} + Fe_2O_3 + Al(OH)SO_4 + 2H_2O + H^+ \quad (5)$$

$$HFe_3(SO_4)_2(OH)_6 + Al^{3+} = Fe^{3+} + SO_4^{2-} + Fe_2O_3 + Al(OH)SO_4 + 2H_2O + 2H^+ \quad (6)$$

834
835 The third buffer is transient, occurs at pH values slightly lower than 3, and is controlled
836 by $Al(OH)SO_4$ and K-alunite:

$$Al(OH)SO_4 + K^+ + 3H_2O = KAl_3(SO_4)_2(OH)_6 + SO_4^{2-} + 3H^+ \quad (7)$$

837
838 A fourth and more stable buffer (pH 2.5 to 3.5) involves $Al(OH)SO_4$ and kaolinite:

$$2Al(OH)SO_4 + 2SiO_{2_{am}} + 3H_2O = Al_2Si_2O_5(OH)_4 + 2SO_4^{2-} + 4H^+ \quad (8)$$

839
840 If $Al(OH)SO_4$ is absent as secondary phase, particularly in the hot springs and fumaroles
841 condensates, K-alunite or Na-alunite can also buffer the solutions:

$$KAl_3(SO_4)_2(OH)_6 + 3SiO_{2_{am}} + {}^3/_2\, H_2O = {}^3/_2\, Al_2Si_2O_5(OH)_4 + 2SO_4^{2-} + K^+ + 3H^+ \quad (9)$$

$$NaAl_3(SO_4)_2(OH)_6 + 3SiO_{2_{am}} + {}^3/_2\, H_2O = {}^3/_2\, Al_2Si_2O_5(OH)_4 + 2SO_4^{2-} + Na^+ + 3H^+ \quad (11)$$

Finally, a fifth buffer (pH 9.8 to 10.3) is controlled by illite formation:

$$Al_2Si_2O_5(OH)_4 + 0.3Al^{3+} + 0.6K^+ + 0.25Mg^{2+} + 1.5SiO_{2_{am}} = K_{0.6}Mg_{0.25}Al_{1.8}Al_{0.5}Si_{3.5}O_{10}(OH)_8 + 2SO_4^{2-} + 2H^+ \quad (12)$$

However, since kaolinite is still being formed rather than consumed at these high pH values, the following reaction is probably more important:

$$2.3Al^{3+} + 0.6K^+ + 0.25Mg^{2+} + 3.5SiO_{2_{am}} + 5H_2O = K_{0.6}Mg_{0.25}Al_{1.8}Al_{0.5}Si_{3.5}O_{10}(OH)_8 + 8H^+ \quad (13)$$

In the CPC gas condensates, pyrite oxidation brings extra acidy in the solution, preventing a rapid pH increase as a result of rock dissolution; this is reflected by a flattening of the curve around pH 7:

$$2FeS_2 + {}^{15}/_2\, O_{2_{(g)}} + 4H_2O = Fe_2O_3 + 4SO_4^{2-} + 8H^+ \quad (14)$$

The role of CO_2 as buffer in the aqueous systems in the summit area of Poás volcano is insignificant. Even though CO_2 is the second most abundant gas after H_2O in the CPC fumaroles (Table 4), its contribution to acidity when fumarole gas interact with water is minimal, due to its presence as $CO_{2_{(g)}}$ and eventually also in the undissociated $H_2CO_{3_{(aq)}}$ form. Moreover, with exception of tychite and ankerite at Site 28 (Fig. 2, Table 1), carbonates are absent in the crater area, indicating that CO_2 is unimportant in the formation of secondary minerals.

In summary, the mineral alteration assemblages in Laguna Caliente, hot springs and CPC fumaroles predicted by the water-rock interaction models is characterized by the stability of H- and K-jarosite under highly acidic conditions (pH 0.7 to 1.3) conditions, followed by K-Na-alunite, $Al(OH)SO_4$ and elemental sulphur (pH 1.3 to 3.8). Secondary phases associated with relatively high pH conditions (≥5.0) include illite, brucite, magnetite and diaspore. The acid conditions required for the formation of aluminium and iron sulphates are associated with poorly reacted systems. In these cases, fluids interacted with much less rock than in neutral or high-pH aqueous systems, where phyllosilicates, iron and aluminium oxides usually prevail.

5.3. Presence of Fe-, Mg- and Al-sulphates and formation conditions

869 Evidence from the geochemical models indicates that the presence of jarosite is transient
870 and requires extremely low pH conditions. Nevertheless, the mineral was not found in
871 samples of the Laguna Caliente sediments. The only locations XRD and EPM analysis
872 confirmed the occurrence of jarosites are: (1) a lava flow on the eastern margin of Laguna
873 Caliente (site 35; Figs. 2, 16 o 18; Table 1), and (2) the "dead zone" (sites 21, 28; Figs. 2
874 and 15; Table 1). Previously, jarosite together with alunite were also identified by powder
875 XRD in the hot springs that were active from March 1999 to January 2007 (Martínez,
876 2008). It is conceivable that some of the hematite occurrences in the field indicate the
877 former presence of jarosite, since olivine dissolution experiments with H_2SO_4 solutions
878 suggest that H- and Na-jarosites can be precursors of hematite (King et al., 2011). Iron
879 sulphates, together with minerals from the copiapite, voltaite and halotrichite groups
880 were also identified in the Río Agrio hot spring (site 34, Fig. 2, Table 1) by XRD. Epsomite
881 was found at site 20 (Fig. 2, Table 1).
882
883 Furthermore, the formation of Fe- and Mg-sulphates at Poás seems associated with the
884 abundance of sulphate in combination the presence of olivine in lavas such as those
885 outcropping around Cerro Pelón (Fo_{75}) and on the eastern margin of Laguna Caliente
886 (Fo_{65}). At both locations, commonly only olivine ghosts were observed, indicating
887 complete dissolution of this mineral, while other primary phases such as clinopyroxene,
888 orthopyroxene and plagioclase are considerably less altered or, in many cases, completely
889 intact (Figs. 15 to 17). This observation is in agreement with the almost congruent
890 dissolution of olivine in contact with highly acidic solutions (Tosca et al., 2004), which is
891 kinetically favoured over glass, pyroxene or plagioclase dissolution (Hausrath et al.,
892 2008). An overall order of mineral dissolution under acidic conditions is phosphates >
893 olivine > pyroxene ≥ Fe-Ti oxides ≥ mafic silicate glass ≥ felsic silicate glass (Nesbitt and
894 Young, 1984; Nesbitt and Wilson, 1992; Wolff-Boenisch et al., 2004).
895
896 The Poás sites where Fe- and Mg-sulphates were found have medium to high rock/water
897 ratios in common. In the high rock/water locations, the chemical alteration of rock occurs
898 mainly via acid rain and/or brine spray. The models of Figure 19 predict that K-jarosite,
899 jurbanite, K-alunite, followed by epsomite and ferrohexahydrite could form here in a
900 repetitive sequence of olivine dissolution and evaporation in an open system involving
901 limited water amounts. Although römerite was the only simple (iron) sulphate identified

by XRD in the "dead zone" (Fig. 2), these models for combined water-rock interaction and evaporation illustrate that these conditions and processes would be favourable for the formation of other sulphates as well. Their absence in the materials studied might be attributable to their transient stability under changing conditions (e.g., following heavy rainfall), since re-dissolution is expected to be a function of time, pH, temperature and solution chemistry (Miller et al., 2016 and references therein).

Experimental constraints on the formation of Fe- and Mg-sulphates have been discussed by Tosca et al. (2004), Golden et al. (2005) and Hausrath et al. (2013). In the acid weathering experiments of Tosca et al. (2004), involving reaction and evaporation steps, hexahydrite ($MgSO_4 \cdot 6H_2O$) did not form upon pyroxene dissolution, apparently because this mineral did to release enough Mg^{2+} to produce appreciable amounts of Mg-sulphate. Through geochemical modelling of acid dissolution of synthetic basalts and evaporation of the resulting weathering solutions, Tosca et al. (2005) confirmed that the presence of olivine is required instead. Aluminium sulphates such as alunogen and tamarugite $NaAl(SO_4)_2 \cdot 6H_2O$ formed as a result of glass dissolution (Tosca et al., 2004). As the authors pointed out, the glass releases more Al^{3+} than plagioclase because of its faster dissolution rate.

Golden et al. (2005) performed laboratory experiments at 145°C to simulate weathering of volcanic rock by acid fog and acid leaching. Interaction of H_2SO_4 with basaltic sand and tephra from Hawaii resulted in the formation of hexahydrite, $MgSO_4 \cdot nH_2O$, K- and H-jarosite, voltaite, $Fe_2(SO_4)_3$, anhydrite, gypsum and amorphous silica. The Mg-sulphates where more abundant in experiments with the basalt, which had 6 times higher MgO content than the tephra. Jarosites only formed in open-system leaching experiments. Experimental interaction between H_2SO_4 vapour and basaltic glass and San Carlos olivine at T=150-155°C (Hausrath et al., 2013) resulted in the formation of Mg-sulphates (hexahydrite and kieserite) as the most common alteration products in the case of olivine, and Ca- and Al- sulphates in the case of basaltic glass.

5.4. Implications for Mars

5.4.1. Alteration processes - Poás volcano vs. Mars

An environment with high rock/water ratios and limited water availability (rocks exposed to acid rain and/or hyperacid brine spray) that is essential for the formation of Fe- and Mg-sulphates at Poás volcano is consistent with the required conditions inferred for the origin of these minerals on Mars. Similarly, the water-rock interaction models for Poás also revealed that: (1) olivine is the primary mineral that preferentially gives rise to Fe- and Mg-rich solutions, and (2) the most effective way to form both Fe- and Mg-sulphates is through cycles of reaction and evaporation in an open system. In particular, Fe-sulphates point to rather oxidizing and acidic (pH<4) environmental conditions (Nordstrom and Alpers, 1999; Bigham and Nordstrom, 2000; Nordstrom et al., 2000). In the geochemical models presented here, oxidation of Fe^{2+} to Fe^{3+} by atmospheric O_2 was ignored. This does not seriously affect the comparison since the current Martian atmosphere is extremely oxygen-depleted compared to its terrestrial counterpart; P_{O_2}= $7.9x10^{-6}$ bar vs. P_{O_2}= 0.21 bar, respectively (Owen, 1992). Moreover, during active volcanism on early Mars, its atmosphere may have been even more anoxic than today, so that the kinetics of Fe-oxidation by $O_{2(g)}$ were probably orders of magnitude slower than in currently active acidic environments at the Earth´s surface (Burns, 1993; Catling and Moore, 2003).

A direct consequence of high rock/water ratios is that mineral phases with slow dissolution rates such as pyroxene and plagioclase do not contribute substantially to secondary mineral assemblages. Hence, under low H_2O-availability conditions Al-mobilization into alteration phases will be limited (Hurowitz and McLennan, 2007). The larger availability of water at Poás and the fact that its rocks are less mafic (mainly andesites and basaltic andesites) compared to their Martian counterparts (mainly basalts), explain to some extent why at Poás Ca- and Al-sulphates are more common than Fe- and Mg-sulphates. On Mars, Mg-, Fe- and Ca-sulphates and accompanying phases such as amorphous silica seem to dominate the mineralogy of evaporites (Tosca and McLennan, 2006), whereas Ca-sulphates usually prevail and are associated with carbonates and chlorides in terrestrial evaporate deposits. Exceptions are the vast gypsum deposits in the Martian northern polar regions. It is conceivable that they precipitated from acidic fluids comparable to Laguna Caliente, given that gypsum abundantly forms in the lake as the only sulphate.

The presence of alunite and jarosite in the crater area of Poás confirms that the occurrence of these minerals on Mars is an indicator of past aqueous systems. In addition, the Poás setting attests to the acidic, oxidizing, sulphur and aluminium-rich conditions that are also required for their stability. Finally, since on Mars the rise of extensive volcanism during the Hesperian may have been responsible for the acidic environments, following alkaline conditions that prevailed earlier during the Noachian (Bibring et al., 2006; Milliken et al., 2010), the use of the magmatic-hydrothermal system of Poás as analogue for Martian alunite and jarosite-forming processes seems well justified. From dissolution experiments, Miller et al. (2016) proposed that alunite is better preserved in less acidic and warmer aqueous conditions than jarosite, and that alunite is expected to be preserved longer when solutions are dilute, especially under alkaline and high-temperatures conditions. The authors further noted that in high salinity brine environments both minerals would dissolve slower and are expected to be equally preserved. The field observations and models for Poás are consistent since the geochemical models suggest that K-alunite should be present in deeper and hotter sections at Poás (95 to 164°C) and that both K- and Na-alunite are present at higher pH values (1.6 to 3.8) than H- and K-jarosite (0.8 to 1.2).

6. CONCLUSIONS

Field evidence and geochemical modelling have been used to demonstrate that acid fluids of Poás volcano are capable of producing complex mineral assemblages, including Ca-, Al-, Fe- and Mg-sulphates, and to investigate the role of temperature changes, interactions with rocks and minerals, and evaporation. At a macroscopic scale, the models indicate that the formation of amorphous silica, hematite, anhydrite/gypsum, pyrite, anatase and kaolinite is fairly insensitive to the degree of acidity of the aqueous system studied. On the other hand, Fe-sulphates (H- and K-jarosite) followed by elemental sulphur and Al-sulphates such as K-, Na-alunite and $Al(OH)SO_4$ only form in this setting under acidic conditions (pH<4). Finally, the modelling evidence shows that minerals such as fluorite, illite, brucite, magnetite and diaspore require relatively high pH values (pH>4) and/or temperatures to form, which explains their absence at the surface of the crater area.

To a significant extent, local variations in secondary mineralogy within the crater area reflect differences in the relative proportions of rock and acidic fluid during interaction, which is particularly relevant for Mg-, Fe- and Al-sulphates. In general, the Fe- and Mg-sulphates require the highest rock-water ratios to form. A further key factor for their occurrence is probably the presence of olivine as a source of Mg and Fe. For these reasons, the presence of Fe- and Mg-sulphates was found to be restricted to surfaces of olivine-bearing rocks affected by acid rain or acid brine spray. The modelling results rule out a simple interaction mechanism but suggest an open-system scenario where a fluid evolved in a repetitive sequence of interaction with olivine and evaporation. Conversely, the Al-sulphates can also stabilize where brine water is more abundant, and pH and/or temperature are higher.

The secondary mineral assemblages at Poás are strongly reminiscent of sulphate-bearing mineral associations detected on the surface of Mars. The conditions and mechanisms inferred for their formation in the crater area of Poás can therefore be considered to approximate Martian geological environments wherein these minerals formed, particularly in settings with a large mineralogical diversity at small spatial scales. Volcanic activity, acid alteration and low water availability are required to produce Fe- and Mg-sulphates at Poás, conditions that presumably also marked Hesperian times on Mars when similar assemblages could originate. Differences in rock compositions and atmospheric chemistry poses limits to this comparison, in particular when considering the less mafic rock types and oxidizing environment of the crater lake setting studied here. Nevertheless, the results of this work demonstrate that active volcanic-hydrothermal systems on Earth can be regarded as excellent analogues to study processes responsible for the formation of sulphates and associated alteration throughout the early history of Mars.

ACKNOWLEDGEMENTS

The reviews of Dimitri Rouwet and Franco Tassi were quite valuable and helped to improve this manuscript. We also thank Gino González, Yemerith Alpízar and Raúl Mora (RSN-ICE), Erick Fernández, Jorge Brenes, Geoffroy Avard and María Martínez (OVSICORI-UNA) for their support during the fieldwork campaign in Costa Rica. Mark Reed and Jim

Palandri (Oregon University) kindly provided a copy of SOLVGAS and GASWORKS software and helped with using it on the samples included in this paper. Our thanks go to Alfredo Fernández also, for his valuable assistance in GIS. This work was funded by NWO (Netherlands Organization for Scientific Research), project ALW-GO-PL/10-03.

REFERENCES

Africano F. and Bernard A., 2000. Acid alteration of the fumarolic environment of Usu volcano, Hokkaido, Japan. J. Volcanol. Geotherm. Res. 97, 475-495.

Alvarado G.E., 2009. Los volcanes de Costa Rica: geología, historia, riqueza natural y su gente. Third edition. EUNED, San José, Costa Rica, 355 p.

Alvarado G.E., 2010. Aspectos geohidrogeológicos y sedimentológicos de los flujos de lodo asociados al terremoto de Cinchona (M_w 6.2) del 8 de enero del 2009, Costa Rica. Rev. Geol. Am. Centr. 43, 67-96.

Arnórsson S, Stefánsson, A. and Bjarnasson J.Ö. Fluid-Fluid Interactions in Geothermal systems. In: A. Liebscher and C. Heinrich(eds.), Fluid-Fluid Interactions. Rev. Min. Geochem. 65, 259-312.

Ballirano P., 2006. Crystal chemistry of the halotrichite group $XAl_2(SO_4)_4 \cdot 22H_2O$: the X = Fe-Mg-Mn-Zn compositional tetrahedron. Eur. J. Mineral. 18, 463-469.

Bayliss P. and Atencio D., 1985. X-ray power diffraction data and cell parameters for copiapite-group minerals. Can. Mineral. 23, 53-56.

Bibring J., Langevin Y., Gendrin A., Gondet B., Poulet F., Berthe M., Soufflot A., Arvidson R., Mangold N., Mustard J., Drossart P., and OMEGA Team, 2005. Mars surface diversity as revealed by the OMEGA/Mars Express observations. Science 307, 1576-1581.

Bibring J., Langevin, Y., Mustard, J., Poulet, F., Arvidson, R., Gendrin, A., Gondet, B., Mangold, N., Pinet, P., Forget, F. and OMEGA team, 2006. Global mineralogical and aqueous Mars history derived from OMEGA/Mars express data. Science 312, 400-404.

Bigham J.M. and Nordstrom D.K., 2000. Iron and aluminium hydroxysulfates from acid sulfate waters. In: Alpers C.N., Jambor J.L. and Nordstrom D.K. (eds.), Sulfate minerals, crystallography, geochemistry and environmental significance. Rev. Min. Geochem. 40, pp. 391-404.

Bishop J.L., Parente M., Weitz C.M., Dobre, E.Z.N., Roach L.H., Murchie S.L., McGuire P.C., McKeown N.K., Rossi C.M., Brown A.J., Calvin W.M., Milliken R. and Mustard J.F., 2009. Mineralogy of Juventae Chasma: Sulfates in the light-toned mounds, mafic minerals in the bedrock, and hydrated silica and hydroxylated ferric sulfate on the plateau. J. Geophys. Res. 114, E00D09, doi: 10.1029/2009JE003352.

Braitsch O., 1971. Salt deposits, their origin and composition. Springer-Verlag, New York, 297 p.

Burns R.G., 1993. Rates and mechanisms of chemical weathering of ferromagnesian silicate minerals on Mars. Geochim. Cosmochim. Acta 57, 4555-4574.

Campos L.A., Castro L., Gazel E., Montes N., Murillo S., Ramírez S., Ruiz P. and Sequiera M., 2004. Geología, geomorfología, amenazas naturales del Cantón de Poás, Alajuela. Informe de Campaña Geológica, Universidad de Costa Rica, 60 p.

Carr M.J., Saginor I., Alvarado G.E., Bolge L.L., Lindsay F.N., Milidakis K., Turrin B.D., Feigenson M.D. and Swisher C.C. III, 2007. Element fluxes from the volcanic front of Nicaragua and Costa Rica. Geochem. Geophys. Geosyst. 8, Q06001, doi: 10.1029/2006GC001396.

Casertano L., Borgia A., Cigolini C., Morales L.D., Montero W., Gómez M. and Fernández, J.F., 1987. An integrated dynamic model for the volcanic activity at Poás volcano, Costa Rica. Bull. Volcanol. 49, 588-598.

Catling D.C. and Moore J.M., 2003. The nature of coarse-grained crystalline hematite and its

implications for the early environment of Mars. Icarus 165, 277-300.
Chevrier V. and Mathé P.E., 2007. Mineralogy and evolution of the surface of Mars: a review. Planet. Space Sci. 55, 289-314.
Chevrier V., Mathé P.E., Rochette P., Grauby O., Bourrie G. and Trolard F., 2006. Iron weathering products in a CO_2+(H_2O or H_2O_2) atmosphere: implications for weathering processes on the surface of Mars. Geochim. Cosmochim. Acta 70, 4295-4317.
Chevrier V., Rochette P., Mathé P. and Grauby O., 2004. Weathering of iron-rich phases in simulated Martian atmospheres. Geology 32, 1033-1036.
Christensen P., Bandfield J., Hamilton V., Ruff S., Kieffer H., Titus T., Malin M., Morris R., Lane M., Clark R., Jakosky B., Mellon M., Pearl J., Conrath B., Smith M., Clancy R., Kuzmin R., Roush T., Mehall G., Gorelick N., Bender K., Murray K., Dason S., Greene E., Silverman S. and Greenfield M., 2001. Mars Global Surveyor Thermal Emission Spectrometer experiment: investigation description and surface science results. J. Geophys. Res. 106, 23823-23871.
Christenson, B.W., 2000. Geochemistry of fluids associated with the 1995-1996 eruption of Mt. Ruapehu, New Zealand: signatures and processes in the magmatic-hydrothermal reservoir. J. Volcanol. Geotherm. Res. 97, 1-30.
Christenson B.W., Reyes A.G., Young R., Moebis A., Sherburn S., Cole-Baker J. and Britten K., 2010. Cyclic processes and factors leading to phreatic eruption events: Insights from the 25 September 2007 eruption through Ruapehu Crater Lake, New Zealand. J. Volcanol. Geotherm. Res. 191, 15-32.
Christenson B., Németh K., Rouwet D., Tassi F., Vandemeulebrouck J. and Varekamp J.C., 2015. Volcanic Lakes. In: D. Rouwet, B. Christenson, F. Tassi and J. Vandemeulebrouck (eds.), Volcanic Lakes, Advances in Volcanology. Springer-Verlag, pp. 1-21.
Cigolini C., Kudo A.M., Brookins D.G. and Ward D., 1991. The petrology of Poás volcano lavas: basalt-andesite relationship and their petrogenesis within the magmatic arc of Costa Rica. J. Volcanol. Geotherm. Res. 48, 367-384.
de Moor J.M., Aiuppa A., Pacheco J., Avard G., Kern C., Liuzzo M., Martínez M., Giudice G. and Fischer T.P., 2016. Short-period volcanic gas precursors to phreatic eruptions: Insights from Poás Volcano, Costa Rica. EPSL 442, 218-227.
Delmelle P., Bernard A., Kusakabe M., Fischer T.P. and Takano B., 2000. Geochemistry of the magmatic-hydrothermal system of Kawah Ijen volcano, East Java, Indonesia. J. Volcanol. Geotherm. Res. 97, 31-53.
Ehlmann B.L., Mustard J.F., Murchie S.L., Bibring J., Meunier A., Fraeman A.A. and Langevin Y., 2011. Subsurface water and clay mineral formation during the early history of Mars. Nature 479, 53-60.
Elwood-Madden M.E., Madden A.S. and Rimstidt J., 2009. How long was Meridiani Planum wet? Applying a jarosite stopwatch to determine the duration of aqueous diagenesis. Geology 37, 635-638.
Fairén A., Fernández-Remolar D., Dohm J., Baker V. and Amils R., 2004. Inhibition of carbonate synthesis in acidic oceans on early Mars. Nature 431, 423-426.
Fernández-Remolar D., Morris R., Gruener J., Amils R. and Knoll, A., 2005. The Río Tinto basin, Spain: mineralogy, sedimentary geobiology, and implications for interpretation of outcrop rocks at Meridiani Planum, Mars. EPSL 240, 149-167.
Fischer T.P., Ramírez C., Mora-Amador R.A., Hilton D.R., Barnes J.D., Sharp Z.D., Le Brun M., de Moor J.M., Barry P.H., Füri E. and Shaw A.M., 2015. Temporal variations in fumarole gas chemistry at Poás volcano, Costa Rica. J. Volcanol. Geotherm. Res. 294, 56-70.
Fishbaugh K.E., Poulet F., Chevrier V., Langevin Y. and Bibring J., 2007. On the origin of gypsum in the Mars north polar region. J. Geophys. Res. 112, E07002, doi: 10.1029/2006JE002862.
Fueten F., Racher H., Stesky R., MacKinnon P., Hauber E., McGuire P.C., Zegers T. and Gwinner K., 2010. Structural analysis of interior layered deposits in Northern Coprates Chasma, Mars. EPSL, 294, 343-356. http://dx.doi.org/10.1016/j.epsl.2009.11.004.
Fueten F., Flahaut J., Stesky R., Hauber E. & Rossi A.P., 2014. Stratigraphy and mineralogy of

1138 Candor Mensa, West Candor Chasma, Mars: Insights into the geologic history of Valles
1139 Marineris. J. Geophys. Res. 119, 331–354, doi: 10.1002/2013JE004557.
1140 Gaillard F., Michalski J., Berger G., McLennan S.M. and Scaillet B., 2013. Geochemical Reservoirs
1141 and Timing of Sulfur Cycling on Mars. Space Science Reviews 174, 251-300.
1142 Gazel E. and Ruiz P., 2005. Los conos piroclásticos de Sabana Redonda: componente
1143 magmático enriquecido del volcán Poás. Rev. Geol. Amér. Cent. 33, 45-60.
1144 Giggenbach W.F., 1988. Geothermal solute equilibria. Derivation of N-K-Mg-Ca geoindicators.
1145 Geochim. Cosmochim. Acta 52, 2749-2765.
1146 Giggenbach W.F., 1991. Chemical techniques in geothermal exploration. In: D´Amore F. (ed.).
1147 Application of Geochemistry in Geothermal Reservoir Development. UNITAR/UNDP
1148 Centre on Small Energy Resources, pp. 119-144.
1149 Giggenbach W.F. and Corrales R., 1992. Isotopic and Chemical-Composition of Water and
1150 Steam Discharges from Volcanic Magmatic Hydrothermal Systems of the Guanacaste
1151 Geothermal Province, Costa-Rica. Appl. Geochem. 7, 309-332.
1152 Golden D., Ming D., Morris R. and Mertzman S., 2005. Laboratory-simulated acid-sulfate
1153 weathering of basaltic materials: Implications for formation of sulfates at Meridiani
1154 Planum and Gusev crater, Mars. J. Geophys. Res. 110, E12S07, doi:
1155 10.1029/2005JE002451.
1156 Grindrod P.M. and Balme M.R., 2010. Groundwater processes in Hebes Chasma, Mars.
1157 Geophys. Res. Lett. 37, L13202, doi: 10.1029/2010GL044122.
1158 Grotzinger J., Arvidson R., Bell J., Calvin W., Clark B., Fike D., Golombek M., Greeley R.,
1159 Haldemann A., Herkenhoff K., Jolliff B., Knoll A., Malin M., McLennan S., Parker T.,
1160 Soderblom L., Sohl-Dickstein J., Squyres S., Tosca N. and Watters W., 2005. Stratigraphy
1161 and sedimentology of a dry to wet eolian depositional system, Burns formation,
1162 Meridiani Planum, Mars. EPSL 240, 11-72.
1163 Hammarstrom J.M., Seal R.R.I., Meier A.L. and Kornfeld J.M., 2005. Secondary sulfate minerals
1164 associated with acid drainage in the eastern US: recycling of metals and acidity in
1165 surficial environments. Chemical Geology 215, 407-431.
1166 Hauber E., Broz P., Jagert F., Jodlowski P. and Platz T., 2011. Very recent and wide-spread
1167 basaltic volcanism on Mars. Geophys. Res. Lett. 38, L10201, doi:
1168 10.1029/2011GL047310.
1169 Hausrath E.M., Golden, D.C., Morris R.V., Agresti D.G. and Ming D.W., 2013. Acid sulfate
1170 alteration of fluorapatite , basaltic glass and olivine by hydrothermal vapors and fluids:
1171 Implications for fumarolic activity and secondary phosphate phases in sulfate-rich Paso
1172 Robles soil at Gusev Crater, Mars. J. Geophys. Res. 118, 1-13, doi:
1173 10.1029/2012JE004246.
1174 Hausrath E.M., Navarre-Sitchler A.K., Sak P.B., Steefel C.I. and Brantley S.L., 2008. Basalt
1175 weathering rates on Earth and the duration of liquid water on the plains of Gusev Crater,
1176 Mars. Geology 36, 67-70.
1177 Hubbard C.G., Black S. and Coleman M.L., 2009. Aqueous geochemistry and oxygen isotope
1178 compositions of acid mine drainage from the Rio Tinto, SW Spain, highlight
1179 inconsistencies in current models. Chem. Geol. 265, 321-334.
1180 Hurowitz J.A. and McLennan S.M., 2007. A similar to 3.5 Ga record of water-limited, acidic
1181 weathering conditions on Mars. EPSL 260, 432-443.
1182 Jambor J.L., Nordstrom D.K. and Alpers C.N., 2000. Metal-sulfate salts from sulfide mineral
1183 oxidation. In: Alpers C.N., Jambor J.L. and Nordstrom D.K. (eds.), Sulfate minerals,
1184 crystallography, geochemistry and environmental significance. Rev. Min. Geochem. 40,
1185 pp. 305-350.
1186 King H.E., Plümper O., Geisler T. and Putnis A., 2011. Experimental investigations into the
1187 silicification of olivine: Implications for the reaction mechanism and acid neutralization.
1188 Am. Mineral. 96, 1503-1511.
1189 King P.L. and McLennan S.M., 2010. Sulfur on Mars. Elements 6, 107-112.
1190 Klingelhöfer G., Morris R.V., Bernhardt B., Schroder C., Rodionov D.S., de Souza P.A., Yen A.,
1191 Gellert R., Evlanov E.N., Zubkov B., Foh J., Bonnes U., Kankeleit E., Gutlich P., Ming D.W.,

1192 Renz F., Wdowiak T., Squyres S.W. and Arvidson R.E., 2004. Jarosite and hematite at
1193 Meridiani Planum from Opportunity's Mossbauer spectrometer. Science 306, 1740-
1194 1745.
1195 Kusakabe M. and Komoda Y., 1992. Sulfur isotopic effects in the disproportionated reaction of
1196 sulfur dioxide at hydrothermal temperatures. Rep. Geol. Surv. Jpn. 279, 93-96.
1197 Kusakabe M., Komoda Y., Takano B. and Abiko T., 2000. Sulfur isotopic effects in the
1198 disproportionation reaction of sulfur dioxide in hydrothermal fluids: implications for
1199 the delta S-34 variations of dissolved bisulfate and elemental sulfur from active crater
1200 lakes. J. Volcanol. Geotherm. Res. 97, 287-307.
1201 Kussmaul S., 1988. Comparación petrológica entre el piso del Valle Central y la Cordillera
1202 Central de Costa Rica. Ciencia y Tecnología 12, 109-116.
1203 Langevin Y., Poulet F., Bibring J. and Gondet B., 2005. Sulfates in the north polar region of Mars
1204 detected by OMEGA/Mars express. Science 307, 1584-1586.
1205 Lodders K., 1998. A survey of shergottite, nakhlite and chassigny meteorites whole-rock
1206 compositions. Meteor. Planet. Sci. 33, A183-A190.
1207 Malavassi E., 1991. Magma sources and crustal processes at the terminous of the Central
1208 American Volcanic Front. PhD Thesis, University of California, Santa Cruz, USA, 435 p.
1209 Marini L., Vetuschi-Zuccolini M. and Saldi G., 2003. The bimodal pH distribution of volcanic
1210 lake waters. J. Volcanol. Geotherm. Res. 121, 83-98.
1211 Martin R., Rodgers K.A. and Browne P.R.L., 1999. The nature and significance of sulphate-rich,
1212 aluminous efflorescences from the Te Kopia geothermal field, Taupo Volcanic Zone, New
1213 Zealand. Mineral. Magazine 63, 413-419.
1214 Martínez M., Fernández E., Valdés J., Barboza V., van der Laat R., Duarte E., Malavassi E.,
1215 Sandoval L., Barquero J. and Marino P. 2000. Chemical evolution and volcanic activity of
1216 the active crater lake of Poás volcano, Costa Rica, 1993-1997. J. Volcanol. Geotherm. Res.
1217 97, 127-141.
1218 Martínez, M., 2008. Geochemical evolution of the acid crater lake of Poás volcano (Costa Rica):
1219 Insights into volcanic-hydrothermal processes. Ph.D. thesis, Utrecht University, 161 p.
1220 Massé M., Bourgeois O., Le Mouélic S., Verpoorter C., Le Deit L. and Bibring J.P., 2010 Martian
1221 polar and circum-polar sulfate-bearing deposits: Sublimation tills derived from the
1222 North Polar Cap. Icarus 209, 434-451.
1223 McLennan S.M., Bell J.F., Calvin W.M., Christensen P.R., Clark B.C., de Souza P.A., Farmer J.,
1224 Farrand W.H., Fike D.A., Gellert R., Ghosh A., Glotch T.D., Grotzinger J.P., Hahn B.,
1225 Herkenhoff K.E., Hurowitz J.A., Johnson J.R., Johnson S.S., Jolliff B., Klingelhöfer G., Knoll
1226 A.H., Learner Z., Malin M.C., McSween H.Y., Pocock J., Ruff S.W., Soderblom L.A., Squyres
1227 S.W., Tosca N.J., Watters W.A., Wyatt M.B. and Yen A., 2005. Provenance and diagenesis
1228 of the evaporite-bearing Burns formation, Meridiani Planum, Mars. EPSL 240, 95-121.
1229 McSween H.Y., Ruff S.W., Morris R.V., Gellert R., Klingelhöfer G., Christensen P.R., McCoy T.J.,
1230 Ghosh A., Moersch J.M., Cohen B.A., Rogers A.D., Schroeder C., Squyres S.W., Crisp J. and
1231 Yen A., 2008. Mineralogy of volcanic rocks in Gusev Crater, Mars: reconciling Mossbauer,
1232 Alpha Particle X-ray Spectrometer, and Miniature Thermal Emission Spectrometer
1233 spectra. J. Geophys. Res. 113, E06S04, doi: 10.1029/2007JE002970.
1234 McSween H., Wyatt M., Gellert R., Bell J., Morris R., Herkenhoff K., Crumpler L., Milam K.,
1235 Stockstill K., Tornabene L., Arvidson R., Bartlett P., Blaney D., Cabrol N., Christensen P.,
1236 Clark B., Crisp J., Des Marais D., Economou T., Farmer J., Farrand W., Ghosh A., Golombek
1237 M., Gorevan S., Greeley R., Hamilton V., Johnson J., Joliff B., Klingelhöfer G., Knudson A.,
1238 McLennan S., Ming D., Moersch J., Rieder R., Ruff S., Schroder C., de Souza P., Squyres S.,
1239 Wanke H., Wang A., Yen A. and Zipfel J., 2006. Characterization and petrologic
1240 interpretation of olivine-rich basalts at Gusev Crater, Mars. J. Geophys. Res. 111, E02S10,
1241 doi: 10.1029/2005JE002477.
1242 Miller J.L., Elwood-Madden A.S., Phillips-Lander C.M., Pritchett B.N. and Elwood-Madden M.E.,
1243 2016. Alunite dissolution rates: Dissolution mechanisms and implications for Mars.
1244 Geochim. Cosmochim. Acta 172, 93-106.
1245 Milliken R.E., Grotzinger J.P. and Thomson B.J., 2010. Paleoclimate of Mars as captured by the

1246 stratigraphic record in Gale Crater. Gephys. Res. Lett. 37, L04201.
1247 Milliken R.E., Swayze G.A., Arvidson R.E., Bishop J.L., Clark R.N., Ehlmann B.L., Green R.O.,
1248 Grotzinger J.P., Morris R.V., Murchie S.L., Mustard J.F. and Weitz C. 2008. Opaline silica
1249 in young deposits on Mars. Geology 36, 847-850.
1250 Mizutani Y. and Sugiura T., 1996. The chemical equilibrium of the SO_2+2H_2S↔3S+2H_2O
1251 reaction in solfataras of the Nasudake Volcano. Bull. Chem. Soc. Jpn. 39, 2411-2414.
1252 Nesbitt H.W. and Wilson R.E., 1992. Recent chemical weathering of basalts. Am. J. Sci. 292,
1253 740-777.
1254 Nesbitt H.W. and Young G.M., 1984. Prediction of some weathering trends of plutonic and
1255 volcanic-rocks based on thermodynamic and kinetic considerations. Geochim.
1256 Cosmochim. Acta 48, 1523-1534.
1257 Niles P.B. and Michalski J., 2009. Meridiani Planum sediments on Mars formed through
1258 weathering in massive ice deposits. Nat. Geosci. 2, 215-220.
1259 Niles, P.B. and Michalski, J.R., 2011. Evolution of CO2 and H2O on Mars: A cold early
1260 history? 42nd Lunar Planet. Sci. Conf., 2471.
1261 Nordstrom D.K., 1982. The effect of sulfate on aluminium concentrations in natural waters:
1262 some stability relations in the system Al_2O_3-SO_3-H_2O at 298 K. Geochim. Cosmochim.
1263 Acta 46, 681-692.
1264 Nordstrom D.K. and Alpers C., 1999. Negative pH, efflorescent mineralogy, and consequences
1265 for environmental restoration at the Iron Mountain Superfund site, California. Proc.
1266 Natl. Acad. Sci. USA 96, 3455-3462.
1267 Nordstrom D.K, Alpers C., Ptacek C. and Blowes D., 2000. Negative pH and extremely acidic
1268 mine waters from Iron Mountain, California. Environ. Sci. Technol. 34, 254-258.
1269 Oelkers E.H., 2001. General kinetic description of multioxide silicate mineral and glass
1270 dissolution. Geochim. Cosmochim. Acta 65, 3703-3719.
1271 Owen T., 1992. The composition and early history of the atmosphere of Mars. In: Kieffer, H.H.,
1272 Jakosky, B.M., Snyder, C.W. and Matthews, M.S. (eds.), Mars. University of Arizona Press,
1273 Tucson, pp. 818-834.
1274 Parkhurst D.L. and Appelo C.A.J., 1999. User's guide to PHREEQC (Version 2), A computer
1275 program for speciation, batch-reaction, one-dimensional transport, and inverse
1276 geochemical calculations. USGS Report 99-4259, 312 p.
1277 Pasternack G.B. and Varekamp J.C., 1997. Volcanic lake systematic 1. Physical constraints. Bull.
1278 Volcanol. 58, 528-538.
1279 Pitzer K.S. and Mayorga G., 1973. Thermodynamics of electrolytes II. Activity and osmotic
1280 coefficients for strong electrolytes with one or both ions univalent. J. Phys. Chem. 77,
1281 2300-2308.
1282 Poppe L.J., Paskevich V.F., Hathaway J.C. and Blackwood D.S., 2002. A Laboratory Manual for
1283 X-Ray Powder Diffraction. USGS Report 01-041 http://pubs.usgs.gov/of/2001/of01-
1284 041/index.htm
1285 Prosser J.T., 1983. The Geology of Poás Volcano, Costa Rica. MSc. thesis, Dartmouth College,
1286 Virginia, USA, 165 p.
1287 Prosser J.T. and Carr M.J., 1987. Poás volcano, Costa Rica: Geology of the summit region and
1288 spatial and temporal variations among the most recent lavas. J. Volcanol. Geotherm. Res.
1289 33, 131-146.
1290 Reed M.H., 1982. Calculation of Multicomponent Chemical-Equilibria and Reaction Processes
1291 in Systems Involving Minerals, Gases and an Aqueous Phase. Geochim. Cosmochim. Acta
1292 46, 513-528.
1293 Reyes, A., 1998. Petrology and mineral alteration in hydrothermal systems: from diagenesis
1294 to volcanic catastrophes. UNU-GTP Report 118, 77 p.
1295 Robbins S.J., Achille G.D. and Hynek B.M., 2011. The volcanic history of Mars: High-resolution
1296 crater-based studies of the calderas of 20 volcanoes. Icarus 211, 1179-1203.
1297 Robinson C., 1999. The role of jarosite and copiapite in the chemical evolution of acid drainage
1298 waters, Richmond mine, Iron Mountain, California. Queen´s University, Ontario, Canada,
1299 205 p.

1300 Rodríguez A. and van Bergen M.J., 2015. Volcanic hydrothermal systems as potential
1301 analogues of Martian sulphate-rich terrains. Nederlands Journal of Geosciences, doi:
1302 http://dx.doi.org/10.1017/njg.2015.12.
1303 Rouwet D. and Ohba T., 2015. Isotope fractionation and HCl partitioning during evaporative
1304 degassing from active crater lakes. In: Rouwet D., Tassi F., Christenson B. and
1305 Vandemeulebrouck J. (eds.), Volcanic Lakes, Advances in Volcanology. Springer-Verlag,
1306 pp. 179-200.
1307 Rouwet D., Mora-Amador R., Ramírez-Umaña C.J., González G. and Inguaggiato S., 2016.
1308 Dynamic fluid recycling at Laguna Caliente (Poás, Costa Rica) before and during the
1309 2006–ongoing phreatic eruption cycle (2005–10). In: T. Ohba, B. Capaccioni and C.
1310 Caudron (eds.), Geochemistry and Geophysics of Active Volcanic Lakes. Geological
1311 Society of London, Special Publications, 437, http:doi.org/10.1144/SP437.11.
1312 Rowe G.L. Jr, and Brantley S.L., 1993. Estimation of the dissolution rates of andesitic glass,
1313 plagioclase and pyroxene in a flank aquifer of Poás Volcano, Costa Rica. Chem. Geol. 105,
1314 71-87.
1315 Rowe G.L. Jr, Brantley S.L., Fernández M., Fernández J.F., Borgia A. and Barquero J., 1992. Fluid-
1316 volcano interaction in an active stratovolcano: the crater lake system of Poás volcano,
1317 Costa Rica. J. Volcanol. Geotherm. Res. 49, 23-51.
1318 Rowe G.L. Jr., Ohsawa S., Takano B., Brantley S.L., Fernández J.F. and Barquero J., 1992. Using
1319 crater lake chemistry to predict volcanic activity at Poás Volcano, Costa Rica. Bull.
1320 Volcanol. 54, 494-503.
1321 Ruiz P., Gazel E., Alvarado G.E., Carr M.J. and Soto G.J., 2010. Geochemical and petrographical
1322 characterization of the geological units of Poás volcano massif, Costa Rica (in Spanish).
1323 In: Mora R. and Alvarado R. (eds.) Volumen especial: Volcán Poás. Rev. Geol. Amér. Cent.
1324 43, 37-66.
1325 Rymer H., Locke C.A., Borgia A., Martínez M., Brenes J., Van der Laat R. and Williams-Jones G.,
1326 2009. Long-term fluctuations in volcanic activity: implications for future environmental
1327 impact. Terra Nova 21, 304-309.
1328 Sanford W.E., Konikow L.F., Rowe G.L. Jr. and Brantley S.L., 1995. Groundwater transport of
1329 crater-lake brine at Poás Volcano, Costa Rica. J. Volcanol. Geotherm. Res. 64, 269-293.
1330 Sefton-Nash E., Catling D.C., Wood S.E., Grindrod P.M. and Teanby N.A., 2012. Topographic,
1331 spectral and thermal inertia analysis of interior layered deposits in Iani Chaos, Mars.
1332 Icarus 221, 20-42.
1333 Shinohara H., Yoshikawa S. and Y. Miyabuchi, Y., 2015. Degassing activity of a volcanic crater
1334 lake: Volcanic plume measurements at the Yudamari crater lake, Aso Volcano, Japan. In:
1335 Rouwet D., Tassi F., Christenson B. and Vandemeulebrouck J. (eds.), Volcanic Lakes,
1336 Advances in Volcanology. Springer-Verlag, pp. 201-217.
1337 Squyres S.W., Aharonson O., Clark B.C., Cohen B.A., Crumpler L., de Souza P.A., Farrand W.H.,
1338 Gellert R., Grant J., Grotzinger J.P., Haldemann A.F.C., Johnson J.R., Klingelhöfer G., Lewis
1339 K.W., Li R., McCoy T., McEwen A.S., McSween H.Y., Ming D.W., Moore J.M., Morris R.V.,
1340 Parker T.J., Rice J.W. Jr., Ruff S., Schmidt M., Schroeder C., Soderblom L.A. and Yen A.,
1341 2007. Pyroclastic activity at Home Plate in Gusev Crater, Mars. Science 316, 738-742.
1342 Squyres S.W., Grotzinger J.P., Arvidson R.E., Bell J.F., Calvin W., Christensen P.R., Clark B.C.,
1343 Crisp J.A., Farrand W.H., Herkenhoff K.E., Johnson J.R., Klingelhöfer G., Knoll A.H.,
1344 McLennan S.M., McSween H.Y., Morris R.V., Rice J.W., Rieder R. and Soderblom L.A., 2004.
1345 In situ evidence for an ancient aqueous environment at Meridiani Planum, Mars. Science
1346 306, 1709-1714.
1347 Squyres S.W. and Knoll A.H., 2005. Sedimentary rocks at Meridiani Planum: Origin, diagenesis,
1348 and implications for life on Mars. EPSL 240, 1-10.
1349 Stumm W. and Morgan J.J., 1996. Aquatic chemistry: chemical equilibria and rates in natural
1350 waters, 3rd ed. John Wiley & Sons, Inc., USA, 1042 p.
1351 Symonds R.B., 1990. Applications of multicomponent chemical equilibria to volcanic gases at
1352 Augustine volcano, volcanic halogen emissions, and volcanological studies of gas-phase
1353 transport. Ph.D. thesis, Michigan Technological University, USA, 512 p.

1354 Symonds R.B. and Reed M.H., 1993. Calculation of multicomponent chemical equilibria in gas-
1355 solid-liquid systems: calculation methods, thermochemical data and applications to
1356 studies of high-temperature volcanic gases with examples from Mount St. Helens. Am. J.
1357 Sci. 293, 758-864.
1358 Symonds R.B., Gerlach T.M. and Reed M.H., 2001. Magmatic gas scrubbing: implications for
1359 volcano monitoring. J. Volcanol. Geotherm. Res. 108, 303-341.
1360 Tamburello G., Agusto M., Caselli A., Tassi F., Vaselli O., Calabrese S., Rouwet D., Capaccioni B.,
1361 Di Napoli R., Cardellini C., Chiodini G., Bitetto M., Brusca L., Bellomo S. and Aiuppa A. ,
1362 2015. Intense magmatic degassing through the lake of Copahue volcano, 2013–2014. J.
1363 Geophys. Res. 120, 6071-6084.
1364 Tanaka K.L., Scott D.H. and Greeley R., 1992. Global Stratigraphy. In: Kieffer H.H., Jakosky B.M.,
1365 Synder C.W. and Matthews M.S. (eds). University of Arizona Press (Tucson), pp. 345-
1366 382.
1367 Thollot P., Mangold N., Ansan V., Le Mouelic S., Milliken R.E., Bishop J.L., Weitz C.M., Roach L.H.,
1368 Mustard J.F. and Murchie S.L., 2012. Most Mars minerals in a nutshell: Various alteration
1369 phases formed in a single environment in Noctis Labyrinthus. J. Geophys. Res. 117,
1370 E00J06, doi: 10.1029/2011JE004028.
1371 Tosca N.J., McLennan S.M., Clark B.C., Grotzinger J.P., Hurowitz J.A., Knoll A.H., Schroder C. and
1372 Squyres S.W., 2005. Geochemical modeling of evaporation processes on Mars: Insight
1373 from the sedimentary record at Meridiani Planum. EPSL 240, 122-148.
1374 Tosca N.J., McLennan S.M., Lindsley D.H. and Schoonen M.A.A., 2004. Acid-sulfate weathering
1375 of synthetic Martian basalt: The acid fog model revisited. J. Geophys. Res. 109, doi:
1376 10.1029/2003JE002218.
1377 Tosca N.J. and McLennan S.M., 2006. Chemical divides and evaporite assemblages on Mars.
1378 EPSL 241, 21-31.
1379 Truesdell A., 1991. Origins of acid fluids in geothermal reservoirs. Geothermal Research
1380 Council Trans. 15, 289-296.
1381 van Hinsberg V., Berlo K., van Bergen M. and Williams-Jones, A., 2010a. Extreme alteration by
1382 hyperacid brines at Kawah Ijen volcano, East Java, Indonesia: I Textural and mineral
1383 imprint. J. Volcanol. Geotherm. Res 198, 253-184.
1384 van Hinsberg V., Berlo K., Sumarti S., van Bergen M. and Williams-Jones, A., 2010b. Extreme
1385 alteration by hyperacid brines at Kawah Ijen volcano, East Java, Indonesia: II
1386 Metasomatic imprint and element fluxes. J. Volcanol. Geotherm. Res 196, 169-184.
1387 Varekamp J.C., Pasternack G.B. and Rowe G.L., 2000. Volcanic lake systematics II. Chemical
1388 constraints. J. Volcanol. Geotherm. Res. 97, 161-179.
1389 Varekamp J.C., Ouimette A., Herman S., Bermúdez A. and Delpino D., 2001. Hydrothermal
1390 element fluxes from Copahue, Argentina: A "beehive" volcano in turmoil. Geology 29,
1391 1059-1062.
1392 Vaselli O., Tassi F., Minissale A., Montegrossi G., Duarte E., Fernández E. and Bergamaschi F.,
1393 2003. Fumarole migration and fluid geochemistry at Poás volcano (Costa Rica) from
1394 1998 to 2001. In: Oppenheimer C., Pyle D.M. and Barkley J. (eds), Volcanic Degassing.
1395 The Geological Society, London. pp. 247-262.
1396 Weitz C.M., and J.L. Bishop, 2016. Stratigraphy and formation of clays, sulfates, and hydrated
1397 silica within a depression in Coprates Catena, Mars, J. Geophys. Res. 121, 805–835,
1398 doi:10.1002/2015JE004954.
1399 Weitz C.M., Milliken R.E., Grant J.A., McEwen A.S., Williams R.M.E., Bishop J.L. and Thomson
1400 B.J., 2010. Mars Reconnaissance Orbiter observations of light-toned layered deposits
1401 and associated fluvial landforms on the plateaus adjacent to Valles Marineris. Icarus
1402 205, 73-102.
1403 Weitz C.M., Bishop J.L., Thollot P., Mangold N. and Roach L.H., 2011. Diverse mineralogies in
1404 two troughs of Noctis Labyrinthus, Mars. Geology 39, 899-902.
1405 Wendt L., Gross, C., Kneissl T., Sowe M., Combe J., LeDeit L., McGuire P.C. and Neukum G., 2011.
1406 Sulfates and iron oxides in Ophir Chasma, Mars, based on OMEGA and CRISM
1407 observations. Icarus 213, 86-103.

Werner S.C., 2009. The global Martian volcanic evolutionary history. Icarus 201, 44-68.
Wolff-Boenisch D., Gíslason S.R., Oelkers E.H. and Putnis C.V., 2004. The dissolution rates of natural glasses as a function of their composition at pH 4 and 10.6, and temperatures from 25 to 74°C. Geochim, Cosmochim. Acta 68, 4843-4858.
Wray J.J., Milliken R.E., Dundas C.M., Swayze G.A., Andrews-Hanna J.C., Baldridge A.M., Chojnacki M., Bishop J.L., Ehlmann B.L., Murchie S.L., Clark R.N., Seelos F.P., Tornabene L.L. and Squyres S.W., 2011. Columbus crater and other possible groundwater-fed paleolakes of Terra Sirenum, Mars. J. Geophys. Res. 116, E01001, doi:10.1029/2010JE003694.
Xiao L., Huang J., Christensen P.R., Greeley R., Williams D.A., Zhao J. and He Q., 2012. Ancient volcanism and its implication for thermal evolution of Mars. EPSL 323, 9-18.
Zhou Y. and Wang A., 2013. A comparison of dehydration processes of Al-, Fe^{2+}- and Mg-sulfates under Mars relevant pressures and three temperatures. 44th Lunar Planet. Sci. Conf.

FIGURE AND TABLE CAPTIONS

Figure 1. (a) Location of Poás volcano (Costa Rica). (b) Photograph of Laguna Caliente and the composite pyroclastic cone (CPC), taken from the NE rim of the main crater on May 11th, 2012.

Figure 2. Secondary mineralogy at Poás volcano in different settings according to their rock/water/gas ratios. Minerals were identified by powder XRD technique, except for Site 35, in which EMPA was used.

Figure 3. S_T-10xF-Cl molar (%) composition of fluids from Poás volcano. The composition range is illustrated for: Laguna Caliente (green), main crater´s hot springs (yellow), CPC gases (red), CPC gas condensates (orange) and acid rain from Cerro Pelón (2003-2006; OVSICORI, unpublished data) (light blue). The points, except from the acid rain, correspond to the samples from Tables 2-5.

Figure 4. Ancient Laguna Caliente sediments on site 4 (a) and site 10 (b) to (d); see Figure 2. Tabular (a, b) and convolute bedding (c). Within the sediments, elemental sulphur is commonly present (d).

Figure 5. EMP images of a lava within ancient Laguna Caliente sediments (site 10; Figs., 2 and 4). Primary minerals: pyroxene (Px) and orthopyroxene (Opx). Secondary minerals: amorphous silica (SiO_2 am.), elemental sulphur (S), pyrite (Py), alunite (Al) and kaolinite (Kl).

Figure 6. (a) EMP analyses (Fe_2O_3-Al_2O_3-SO_3; wt.%) of some of the secondary minerals present in a lava within the ancient Laguna Caliente´s sediments (site 10; Figs. 2, 4 and 5). Alunite and an Al_2O_3-rich phase are the most abundant secondary minerals in the vesicules. The following minerals are also shown: basaluminite $Al_4(OH)_{10}SO_4 \cdot 5H_2O$, aluminite $Al_2(OH)_4SO_4 \cdot 7H_2O$, jurbanite $Al(OH)SO_4 \cdot 5H_2O$, alunogen $Al_2(SO_4)_3 \cdot 17H_2O$) and K-alum $KAl(SO_4)_2 \cdot 12H_2O$. (b) Compositionally, the alunites from site 10 are close to the alunite H-end-member $HAl_3(SO_4)_2(OH)_6$ and between the K- and Na-end-members $KAl_3(SO_4)_2(OH)_6$ and $NaAl_3(SO_4)_2(OH)_6$, respectively). For comparison purposes, a sample of recent bottom sediments from Laguna Caliente was included, collected by OVSICORI personnel on November 27th, 2011.

Figure 7. Heating models of Laguna Caliente´s waters from lake temperature till 300°C. (a) LoALW: low-activity lake water (T=30°C). (b) HiALW: high-activity lake water (T=62°C). Both high- and low-activity attributes refer to the volcanic activity of Laguna Caliente in terms of input of heat and magmatic volatiles.

Figure 8. Water-rock reaction path models between Laguna Caliente´s waters and a basaltic-andesite analysed by Cigollini et al. (1991). T_r refers to the temperature of the run, which corresponds to the temperature of Laguna Caliente. In every run 1 mole of rock (110 g) was reacted with 1 kg of crater lake water. (a) LoALW: low-activity lake water (T=30°C). (b) HiALW: high-activity lake water (T=62°C). Both high- and low-activity attributes refer to the volcanic activity of Laguna Caliente in terms of input of heat and magmatic volatiles.

Figure 9. Evaporation models of Laguna Caliente´s waters showing both the saturation indices of some minerals and the moles of secondary minerals formed upon evaporation. In every model the starting amount of crater lake water is 1 kg. T_r refers to the temperature of the run, which corresponds to the lake temperature. (a), (b) LoALW: low-activity lake water (T=30°C). (c), (d) HiALW: high-activity lake water (T=62°C). Both high- and low-activity attributes refer to the volcanic activity of Laguna Caliente in terms of input of heat and magmatic volatiles.

Figure 10. Water-rock reaction path models between the waters from the hot springs, active during the years 2003-2006, located inside the main crater and a basaltic-andesite reported by Cigollini et al. (1991). T_s is the temperature of the hot spring. In every run, 1 mole of rock (110 g) was reacted with 1 kg of hot spring water.

Figure 11. Fossil fumaroles on Site 1: note the pervasive acid alteration that has leached the rock and left a residue of cristobalite α, quartz, tridymite, anatase and K-alunite (a), (b); accompanied with elemental sulphur deposition (c), (d). A similar alteration style is observed on site 3 (e), (f); where K- and Na-alunite together with minamiite are present.

Figure 12. Gas-rock reaction path model. One mole of a gas sample (26 g) collected from the CPC was cooled from T_f =763°C to 114°C and reacted with 1 mole (110 g) of a basaltic-andesite reported by Cigollini et al. (1991). T_f refers to the fumarole temperature. During the reaction path the solids formed were successively excluded (fractionated) from the residual fluid. From (a) and (b) it can be observed that the secondary minerals start forming at T<250°C.

Figure 13. Water-rock reaction path models between fumarole gas condensates from the CPC and a basaltic-andesite reported by Cigollini et al. (1991). T_f and T_s refer to the temperature of the fumarole and the one at which the reaction path was ran, respectively. In every run 1 mole of rock (110 g) was reacted with 1 kg of gas condensate.

Figure 14. Examples where rocks have been exposed to the action of acid rain/acid brine spray (high rock/fluid ratios). (a), (b) Site 6, acid brine expelled from Laguna Caliente, due to phreatic eruptions, produced gypsum and anhydrite efflorescences observed on the ceiling of a cave. (c) View from the "dead zone" from the southern rim of the main crater. (d), (e), (f) The lavas in this zone show white patinas mainly composed of amorphous silica, followed a few centimetres deeper by Al- and Mg-sulphates together with minerals from the jarosite and copiapite group (see Fig. 2).

Figure 15. EMP images of a basaltic andesite from site 21, close to Cerro Pelón (see Fig. 2). (a), (b) Amorphous silica (SiO_2 am.) crusts and jarosite (Jar) fillings in the patinas of the lavas. (c), (d) Olivine (Ol) ghost textures, iron oxides (FeOx), kaolinite (Kl), smectites (Sm) and orthopiroxene (Opx). (e), (f) Less altered sections containing plagioclase (Plg), olivine, clinopyroxene (Cpx), iron oxides and silicified phases.

Figure 16. EMP images of a basaltic andesite from site 35, altered mostly by acid brines from Laguna Caliente (see Fig. 2). (a), (b), (c) Olivine (Ol) is completely altered while orthopyroxene (Opx) and clinopyroxene (Cpx) are relatively fresh. (d), (e) The reaction between olivine and acid

brine lead to solutions oversaturated in jarosite (Jar) that eventually precipitated in fractures crossing the plagioclase phenocrysts (Plg).

Figure 17. (a) to (f) EMP images of a basaltic andesite from site 35, altered mostly by acid brines from Laguna Caliente (see Figs. 2 and 16) and showing textural relations between jarosite (Jar) and primary minerals such as plagioclase (Plg) and pyroxene (Px). Plagioclase shows commonly an advance degree of silicification (SiO_2 am.) and jarosite precipitates afterwards within fractures or voids.

Figure 18. Compositions of the jarosites found on the basaltic andesite from site 35 (see Figs. 2, 16 and 17) from EMP analyses (n=30). On average, they present the following composition: $(K_{0.68}Na_{0.12}H_{0.21})(Fe_{2.98}Al_{0.13})(SO_4)_{2.10}(OH)_6$.

Figure 19. Combination of water-rock reaction path and evaporation models between Cerro Pelón olivine (Fo_{75}) and Laguna Caliente water. One mole of this olivine (156 g) was reacted with 1 kg of water. Before the precipitation of any Fe-bearing minerals, an aliquot was taken and evaporated. Towards the end of the evaporation run, the remaining solution was reacted again with the olivine. This was repeated in cycles of reaction (a), (c), (e) and evaporation (b), (d); mimicking and open system at T=24°C.

Figure 20. Laguna Caliente: secondary minerals vs. temperature. Compilation of 6 heating models. The runs went from lake temperatures (28-62°C) to 300°C and included representative lake samples from both active and quiet periods of Laguna Caliente in terms of volcanic activity. The secondary minerals are oversaturated at the following temperature ranges: pyrite (28-98°C), S (44-79°C), anhydrite (98-300°C), K-alunite (95-164°C), diaspore (136-300°C) and AlF_3 (173-300°C).

Figure 21. Laguna Caliente: secondary minerals vs. pH. Compilation of 9 water-rock reaction path models, in which 1 mole (110 g) of a basaltic-andesite reported by Cigollini et al. (1991) was reacted with 1 kg of water from Laguna Caliente at constant temperature. The water samples represent both active and quiet periods of Laguna Caliente in terms of volcanic activity, with temperatures between 28 and 62°C. The secondary minerals are oversaturated at the following pH ranges: anatase (-0.4 to 11.2), SiO_2 am. (-0.4 to 11.2), anhydrite (-0.3 to 9.6), hematite (1.1 to 11.2), H-jarosite (1.1 to 1.2), K-jarosite (1.2 to 1.3), gypsum (1.3 to 10.3), K-alunite (1.7 to 3.8), $Al(OH)SO_4$ (1.7 to 3.7), Na-alunite (2.6 to 3.0), kaolinite (2.6 to 11.2), fluorite (3.9 to 11.2), pyrite (4.6 to 11.2) and illite (5.9 to 11.2).

Figure 22. Crater´s hot springs: secondary minerals vs. pH. Compilation of 7 water-rock reaction path models, in which 1 mole (110 g) of a basaltic-andesite reported by Cigollini et al. (1991) was reacted with 1 kg of water from the hot springs located in the main crater that were active during the years 2003-2006 (T=42-92°C). The secondary minerals are oversaturated at the following pH ranges: anatase (0.7 to 11.0), SiO_2 am. (0.7 to 10.2), H-jarosite (0.8 to 0.9), hematite (0.9 to 11.0), anhydrite (1.2 to 10.3), K-alunite (1.6 to 3.6), Na-alunite (1.9 to 2.7), kaolinite (2.1 to 11.0), $Al(OH)SO_4$ (2.3 to 2.9), pyrite (4.1 to 11.0), fluorite (4.3 to 10.7), illite (5.9 to 11.2), magnetite (9.9 to 10.2) and diaspore (10.2 to 11.2).

Figure 23. CPC´s fumarole gas condensates: secondary minerals vs. pH. Compilation of 3 gas condensate-rock reaction path models, in which 1 mole (110 g) of a basaltic-andesite reported by Cigollini et al. (1991) was reacted with 1 kg of gas condensate from the fumaroles located on the CPC (T=250, 650 and 763°C). The runs were carried out at constant temperature (T=95°C). The secondary minerals are oversaturated at the following pH ranges: anatase (1.3 to 9.7), S (1.3 to 2.3), pyrite (1.3 to 7.3), SiO_2 am. (1.3 to 9.7), K-alunite (1.9 to 3.2), anhydrite (2.0 to 9.7), Na-alunite

(2.1 to 2.3), kaolinite (2.1 to 9.7), fluorite (4.1 to 9.7), hematite (4.4 to 9.7), illite (5.3 to 9.7) and brucite (7.5 to 9.7).

Figure 24. Reaction path models between Laguna Caliente waters and fresh (KV99-844b) and altered (KV99-802a) andesites from Kawah Ijen. Rock compositions taken from van Hinsberg et al. (2010b). T_r is the temperature of the lake.

Table 1. Mineral determinations by XRD and EMP analysis (see Fig. 2).

Table 2. Chemical analysis of waters from Laguna Caliente, Poás volcano. Concentrations in mg/kg. Conductivity (mS/cm) and pH were measured in the laboratory at T=19±1°C.

Table 3. Chemical analysis of waters from the hot springs in the main crater. Concentrations in mg/kg.

Table 4. Chemical analysis of gases from the CPC. Concentrations in molar percentages.

Table 5. Chemical analysis of gas condensates from the fumaroles of the CPC. Concentrations in mg/kg.

1. KAOLINITE		Kaolinite $Al_2Si_2O_5(OH)_4$ Halloysite $Al_2Si_2O_5(OH)_4$
2. SMECTITES		Montmorillonite $(Na,Ca)_{0.3}(Al,Mg)_2Si_4O_{10}(OH)_2 \bullet nH_2O$ Sauconite $Na_{0.3}Zn_3(Si,Al)_4O_{10}(OH)_2 \bullet 4H_2O$
3. ZEOLITES		Cowlesite $CaAl_2Si_3O_{10} \bullet 5\text{-}6(H_2O)$ Phillipsite $(K,Na)_2(Si,Al)_8O_{16} \bullet 4H_2O$ Mordenite $(Ca,Na_2,K_2)Al_2Si_{10}O_{24} \bullet 7H_2O$ Chabazite $(Ca,Na_2,K_2,Mg)Al_2Si_4O_{12} \bullet 6H_2O$ Ca-chabazite $(Ca_{0.5},Na,K)_4Al_4Si_8O_{24} \bullet 12H_2O$ K-chabazite $(K_2,Ca,Na_2,Mg)Al_2Si_4O_{12} \bullet 6H_2O$ Sr-brewsterite $(Sr,Ba)Al_4Si_{12}O_{32} \bullet 10(H_2O)$
4. SiO_2 POLYMORPHS		Trydimite SiO_2 Cristobalite α SiO_2 Quartz SiO_2
5. Fe AND Ti OXIDES		Goethite $FeO(OH)$ Hematite Fe_2O_3 Magnetite $Fe^{2+}Fe^{3+}{}_2O_4$ Magnesioferrite $MgFe_2O_4$ Rutile TiO_2 Titanomagnetite $Fe^{2+}Fe^{3+}{}_2Ti_2O_4$ Anatase TiO_2
6. SULPHUR		S
7. SULPHIDES		Greigite $Fe^{2+}Fe^{3+}{}_2S_4$ Wurtzite $(Zn,Fe)S$ Tenantite $Cu_{12}As_4S_{13}$
8. FLUORIDES AND PHOSPHATES		Carobbiite KF $MnNaF_4$ Woodhouseite $CaAl_3(PO_4)(SO_4)(OH)_6$ Kogarkoite Na_3FSO_4 Ralstonite $Na_{0.5}Mg_{0.5}Al_{1.5}F_4(OH) \bullet H_2O$
9. CHLORIDES		Potassium halite $K_{0.2}Na_{0.8}Cl$ Sophiite $Zn_2(SeO_3)Cl_2$
10. CARBONATES		Tychite $Mg_2Na_6(CO_3)_4SO_4$ Ankerite $Ca(Fe^{2+},Mg)(CO_3)_2$
11. SULPHATES	**11.1 CALCIUM**	Gypsum $CaSO_4 \bullet 2H_2O$ Anhydrite $CaSO_4$
	11.2 ALUMINIUM	Alunogen $Al_2(SO_4)_3 \bullet 17H_2O$ Meta-alunogen $Al_4(SO_4)_6 \bullet 27H_2O$ Khademite $Al(SO_4)F \bullet 7H_2O$ Rostite $Al(SO_4)(OH,F) \bullet 5H_2O$
	11.3 ALUNITE	K-alunite $KAl_3(SO_4)_2(OH)_6$ Na-alunite $KAl_3(SO_4)_2(OH)_6$ Minamiite $(Na_{0.6}K_{0.1}Ca_{0.3})Al_3(SO_4)_2(OH)_6$ Huangite $Ca_{0.5}Al_3(SO_4)_4(OH)_2$
	11.4 JAROSITE	K-jarosite $KFe_3(SO_4)_2(OH)_6$ H-jarosite $HFe_3(SO_4)_2(OH)_6$
	11.5 HALOTRICHITE	Halotrichite $FeAl_2(SO_4)_4 \bullet 22H_2O$ Pickeringite $MgAl_2(SO_4)_4 \bullet 22H_2O$ Apjohnite $MnAl_2(SO_4)_4 \bullet 22H_2O$
	11.6 VOLTAITE	Voltaite $K_2Fe^{2+}{}_5Fe^{3+}{}_3Al(SO_4)_{12} \bullet 18H_2O$ Pertlikite $K_2(Fe^{2+},Mg)_2(Mg,Fe^{3+})_4Fe^{3+}{}_2Al(SO_4)_{12} \bullet 18H_2O$
	11.7 COPIAPITE	Copiapite $Fe^{2+}Fe^{3+}{}_4(SO_4)_6(OH)_2 \bullet 20H_2O$ Magnesiocopiapite $MgFe^{3+}{}_4(SO_4)_6(OH)_2 \bullet 20H_2O$
	11.8 MAGNESIUM	Epsomite $MgSO_4 \bullet 7H_2O$
	11.9 IRON	Römerite $Fe^{2+}{}_{0.97}Fe^{3+}{}_{2.02}(SO_4)_{3.98} \bullet 13.81H_2O$

Stage/ Substage	Date	$T_{sampling}$ (°C)	$pH_{19±1°C}$	$Cond._{19±1°C}$ (mS/cm)	SO_4	S_T[a]	F	Cl	Br	Al	B	Fe	Ca	Mg	Na	K	Si	Mn	Sr	Ti	V	Zn	TDS	Data source
II	29-Nov-85	45	0.3	390	63000	21000	1090	23400	57	2380	20	1260	880	650	610	240	35	31	18	5.6	6.2	2.6	82800	(1)
III	10-Jan-87	58	-0.01	n.d.[b]	64400	n.d.	1590	30400	61	2070	n.d.	1020	2340	550	520	250	88	25	n.d.	n.d.	n.d.	n.d.	107000	(2,3)
III	30-Aug-94	60	0.54	n.d.	19200	5200	1019	10100	305	1830	n.d.	1570	1020	570	470	145	35	30	n.d.	n.d.	n.d.	n.d.	36000	(2,4)
IVA	20-Oct-95	30	1.21	41	6230	3100	190	4200	19	470	5	540	710	530	410	66	72	28	5	n.d.	b.d.l.[c]	1.1	13000	(1)
IVB	17-Apr-98	37	0.68	87	10900	4430	460	8870	17	1000	n.d.	950	1300	630	560	83	77	31	n.d.	n.d.	n.d.	n.d.	24900	(5)
IVC	31-Jan-02	30	1.51	22	3590	1470	52	2540	5	360	n.d.	330	620	230	190	39	110	11	3	n.d.	n.d.	0.9	12600	(1,5)
IVD	12-Aug-03	33	0.61	142	8860	5290	720	18200	n.d.	1410	n.d.	780	1340	490	400	110	32	21	n.d.	n.d.	n.d.	n.d.	35000	(5)
IVE	25-May-04	28	1.31	30	3940	1880	30	5380	8	680	n.d.	420	750	340	280	48	120	14	n.d.	n.d.	n.d.	n.d.	12000	(1,5)
VA	30-Nov-05	54	0.64	134	13600	7530	920	11600	n.d.	1630	n.d.	670	1440	360	450	130	119	15	n.d.	n.d.	n.d.	n.d.	34000	(5)
VB	27-May-11	62	-0.25	571	101500	34900	1170	26700	68	2030	16	1030	660	400	430	240	52	19	13	12.9	5.6	2.4	n.d.	(1)

Notes: (a) total sulfur (ICP-OES); (b) n.d. = not determined; (c) b.l.d = below detection limit. Sources: (1) this study; (2) OVSICORI-UNA; (3) Rowe et al., (1992b); (4) Martínez et al. (2000); (5) Martínez (2008).

Hot spring	Date	$T_{sampling}$ (°C)	pH 20-24±2°C	SO_4	F	Cl	Al	Fe	Ca	Mg	Na	K	Si	Mn	TDS	Source
Este	Feb-00	89	0.12	12200	16	25	520	1000	550	350	180	13	n.d.[a]	13	14900	(6)
	21-Nov-00	91	2.1	2800	1.4	29	42	350	380	33	170	b.l.d.[b]	n.d.	4.3	3800	(4)
	16-Jun-05	92	0.99	16780	33	3885	n.d.	n.d.	n.d.	n.d.	n.d.	n.d.	n.d.	n.d.	n.d.	(4)
White Algae	23-Aug-00	42	2.47	2220	3.0	0.40	82	55	570	19	45	3.7	93	0.90	3090	(6)
	21-Sep-01	52	1.55	6680	10	813	480	570	310	81	130	19	220	3.5	9300	(4)
Norte-Este	23-Aug-00	89	1.51	2890	0.6	22	2.0	470	330	180	260	24	220	8.1	5887	(4)
	14-Feb-03	87	1.95	2530	b.d.l	33	n.d.	n.d.	n.d.	n.d.	n.d.	n.d.	n.d.	n.d.	n.d.	(4)

Notes: (a) n.d. = not determined; (b) b.l.d = below detection limit. Sources: (4) Martínez et al. (2000); (6) Vaselli et al. (2003).

Date	$T_{sampling}$ (°C)	CO_2	HCl	HF	SO_2	H_2S	S	H_2O	N_2	CH_4	Ar	O_2	H_2	CO	Total	Source
25-Jun-10	763	15.84	0.78	0.35	9.17	0.08	0.00	72.45	0.06	0.00	0.00	0.00	1.08	0.10	99.92	(2,6)
16-Aug-10	650	14.84	0.71	0.30	8.76	0.14	0.00	74.10	0.06	0.00	0.00	0.00	0.94	0.09	99.94	(2,6)
18-Mar-11	250	15.84	0.65	0.21	7.60	0.12	0.00	74.57	0.07	0.00	0.00	0.00	0.85	0.07	99.98	(2,6)

Sources: (2) OVSICORI-UNA; (6) Tassi (2012; pers. com.).

Date	$T_{sampling}$ (°C)	pH 19±1°C	Cond. 19±1°C (mS/cm)	SO_4	F	Cl	Br	Data source
19-Jan-10	650	0.09	231	1180	72	21900	51	(1,2)
07-Apr-10	566	2.02	2.5	2770	104	5440	6	(1,2)
08-Sep-10	760	0.09	231	654	14	21400	14	(1,2)
22-Oct-10	590	0.58	73.8	2910	130	4220	8	(1,2)
18-Mar-11	250	-0.27	465	68	86	47000	78	(1,2)
10-Feb-12	107	0.46	103	5480	4	39	n.d.	(1,2)
20-Jul-12	301	0.84	n.d.	4000	30	103	n.d.	(1,2)

Sources: (1) This study; (2) OVSICORI-UNA.

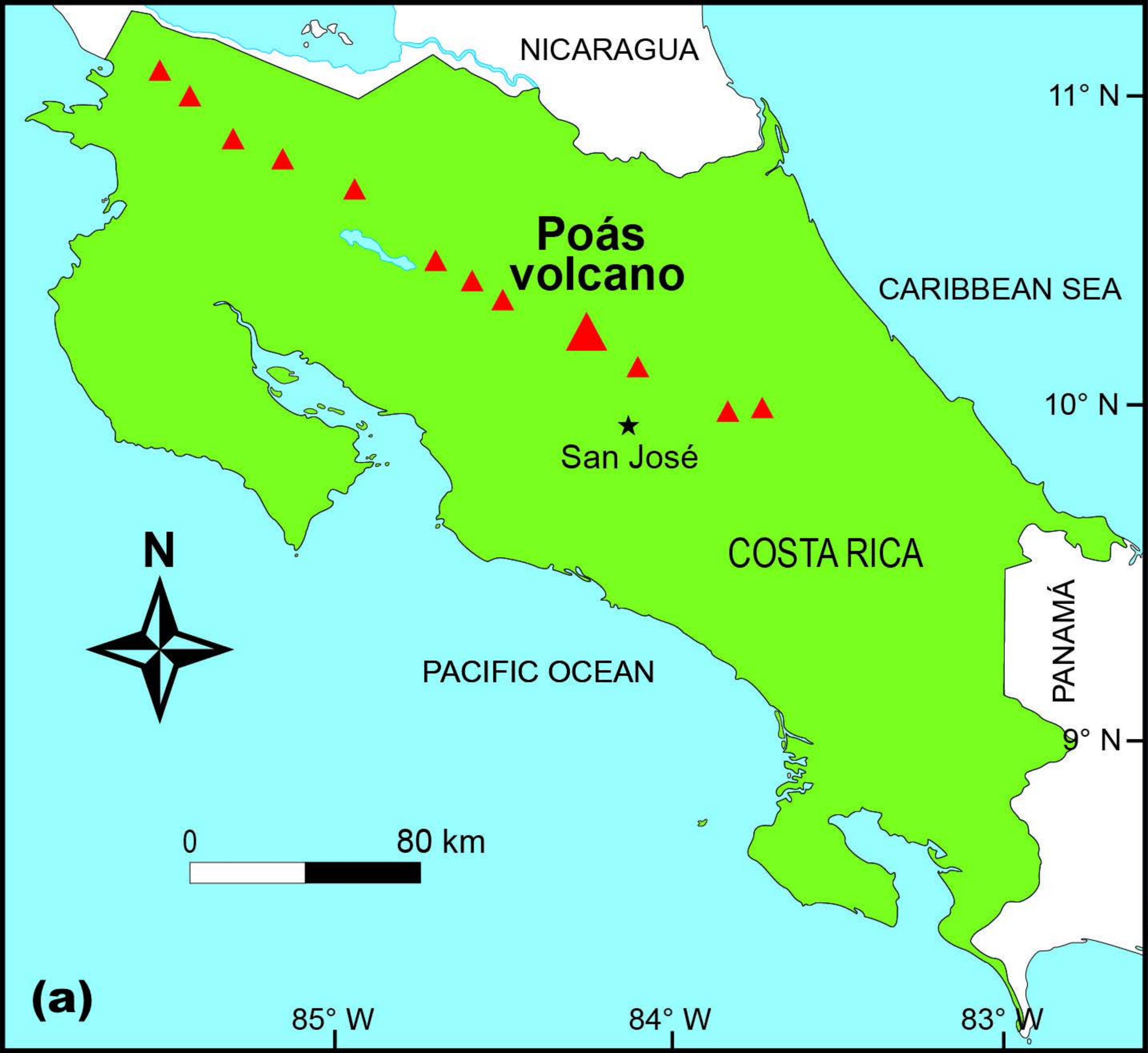
NICARAGUA
11° N
Poás
volcano
CARIBBEAN SEA
10° N
San José
COSTA RICA
PANAMÁ
N
PACIFIC OCEAN
9° N
0
80 km
(a)
85° W
84° W
83° W


(b)
CPC
Laguna Caliente

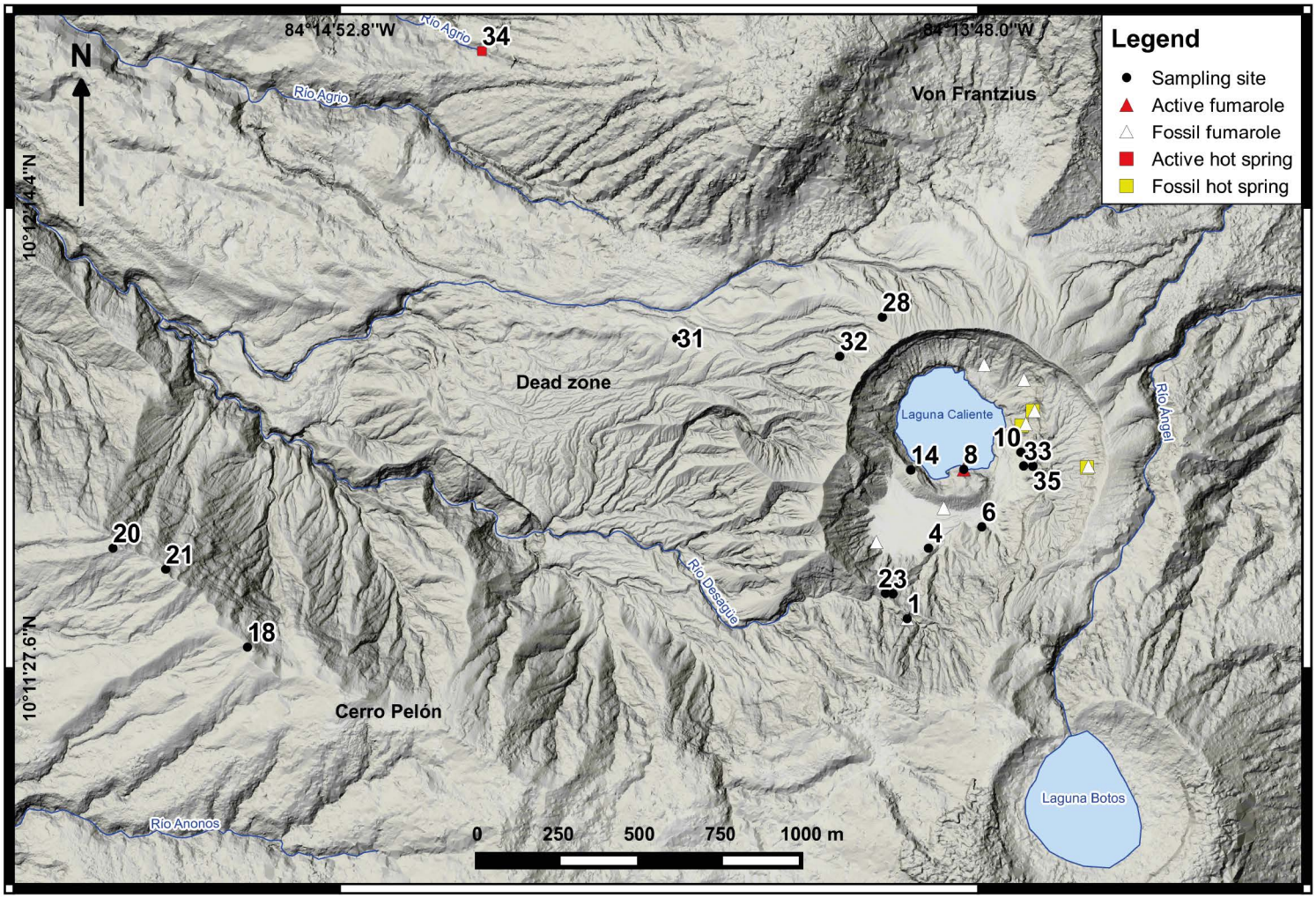

ALL MINERALS

1. Laguna Caliente (low rock/water ratios)

Site 4 | Site 14 | Site 10 | Site 33

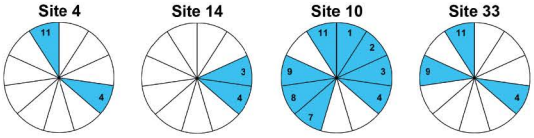

2. Hot springs (medium rock/water ratios)

Site 34

3. Fumaroles (high rock/water/gas ratios)

Site 1 | Site 3 | Site 8

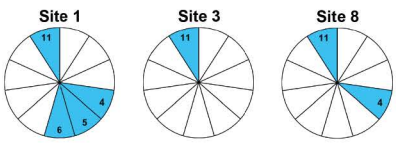

4. Acid rain / acid brine spray (high rock/water ratios)

Site 2 | Site 6 | Site 18 | Site 20 | Site 21

Site 28 | Site 31 | Site 32 | Site 35

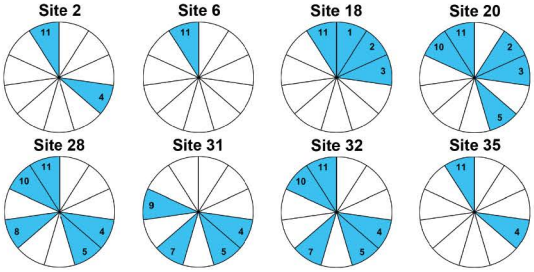

Legend

1. Kaolinite group
2. Smectite group
3. Zeolites
4. SiO_2 polymorphs
5. Oxides (Fe and Ti)
6. Sulphur
7. Sulphides
8. Fluorides and phosphates
9. Chlorides and borates
10. Carbonates
11. Sulphates

SULPHATES

1. Laguna Caliente (low rock/water ratios)

Site 4 | Site 14 | Site 10 | Site 33

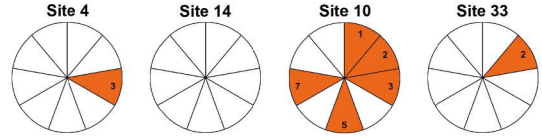

2. Hot springs (medium rock/water ratios)

Site 34

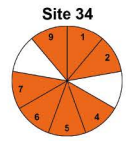

3. Fumaroles (high rock/water/gas ratios)

Site 1 | Site 3 | Site 8

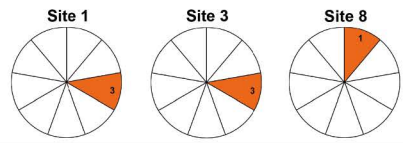

4. Acid rain / acid brine spray (high rock/water ratios)

Site 2 | Site 6 | Site 18 | Site 20 | Site 21

Site 28 | Site 31 | Site 32 | Site 35

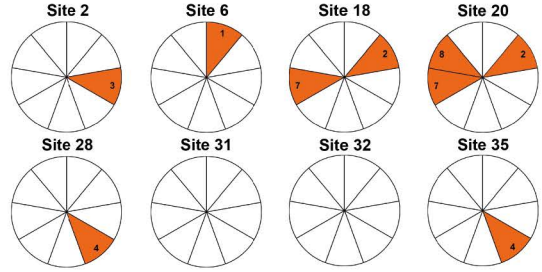

Legend

1. Ca sulphates
2. Al sulphates
3. Alunite group
4. Jarosite group
5. Halotrichite group
6. Voltaite group
7. Copiapite group
8. Mg sulphates
9. Fe sulphates

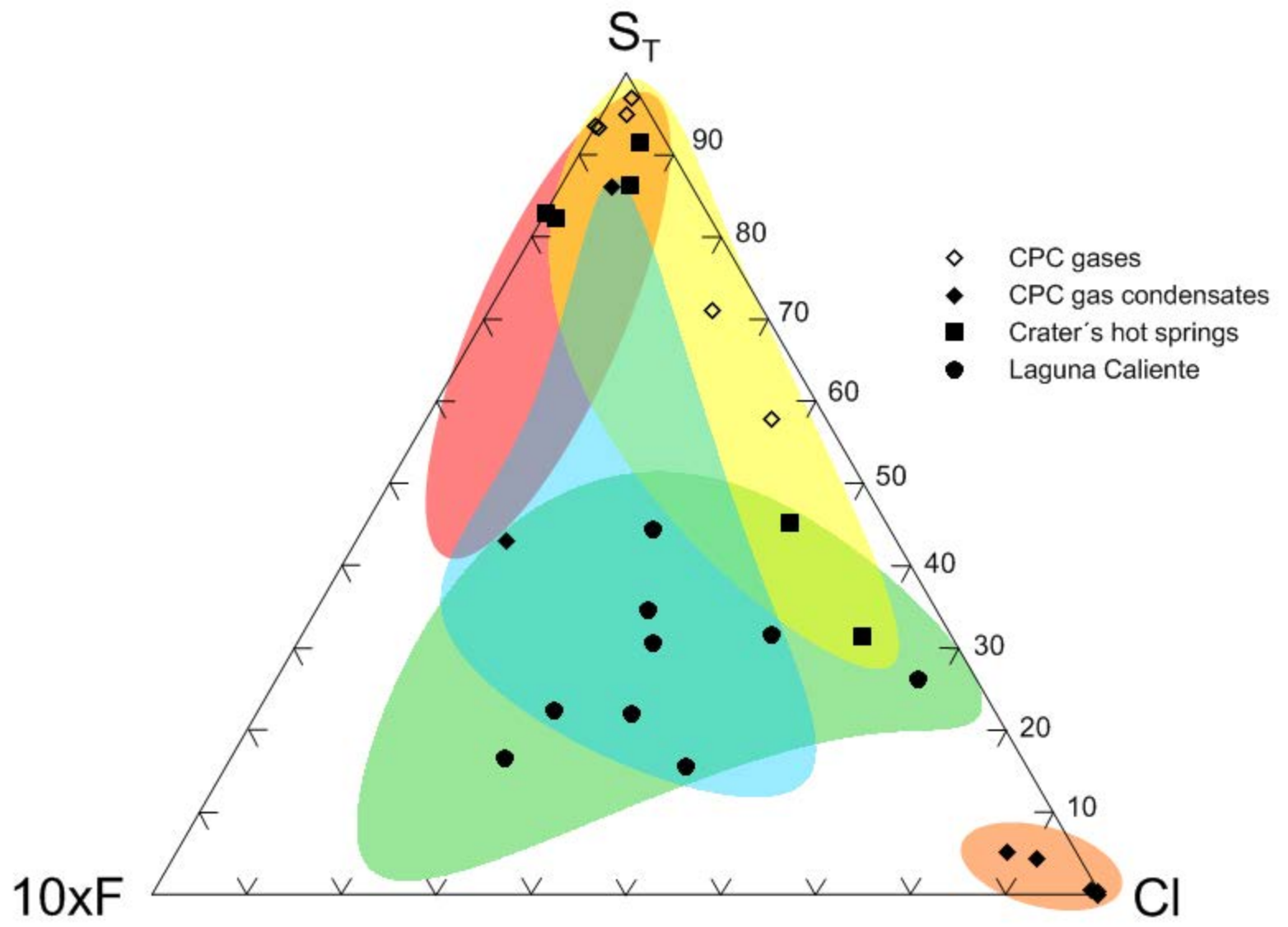
S_T
90
80
70
60
50
40
30
20
10
10xF
Cl
CPC gases
CPC gas condensates
Crater´s hot springs
Laguna Caliente


(a)


(b)


(c)


(d)

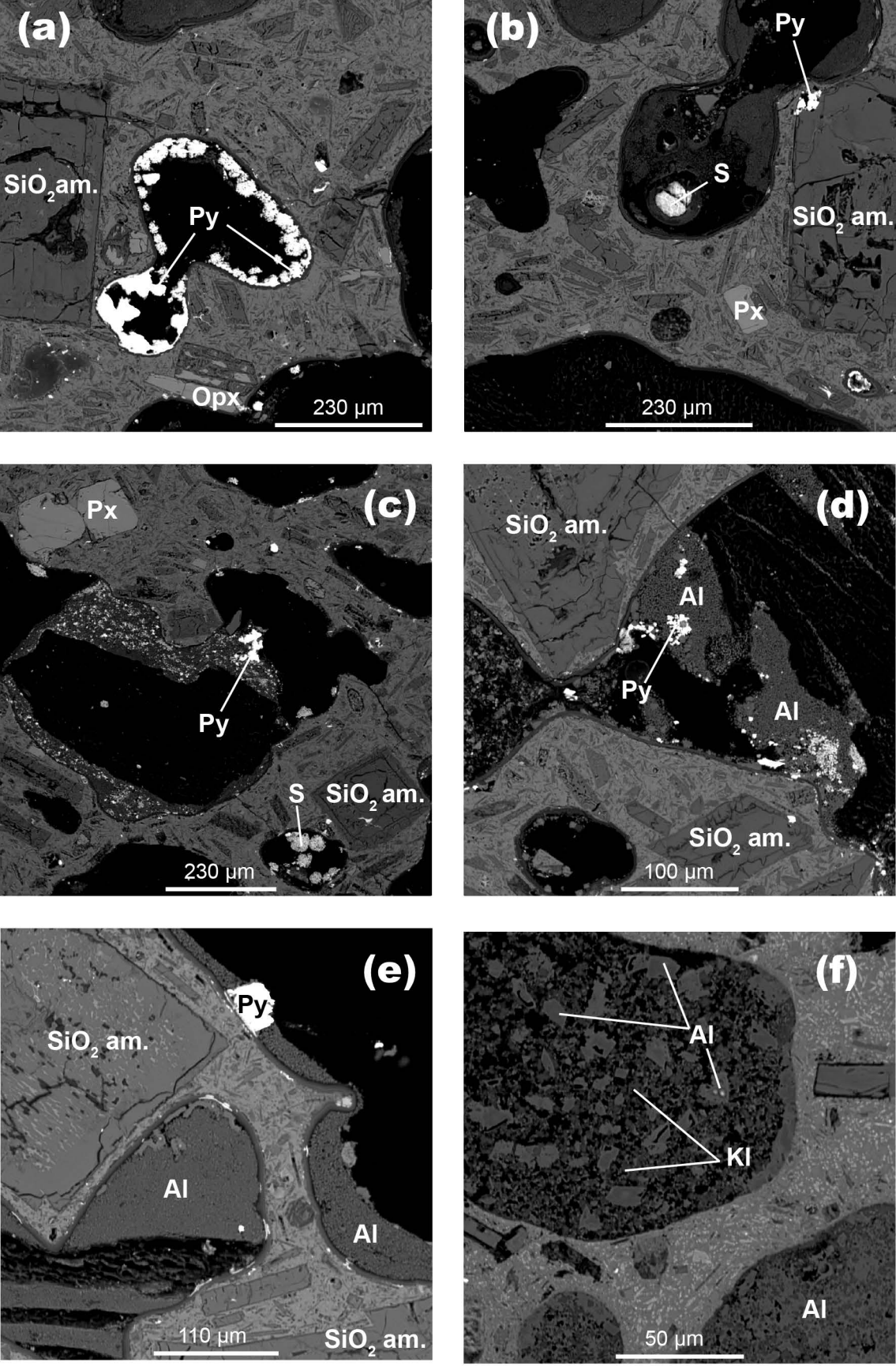
(a)
SiO2am.
Py
Opx
230 µm
(b)
Py
S
SiO2 am.
Px
230 µm
(c)
Px
Py
S
SiO2 am.
230 µm
(d)
SiO2 am.
Al
Py
Al
SiO2 am.
100 µm
(e)
Py
SiO2 am.
Al
Al
110 µm
SiO2 am.
(f)
Al
Kl
Al
50 µm

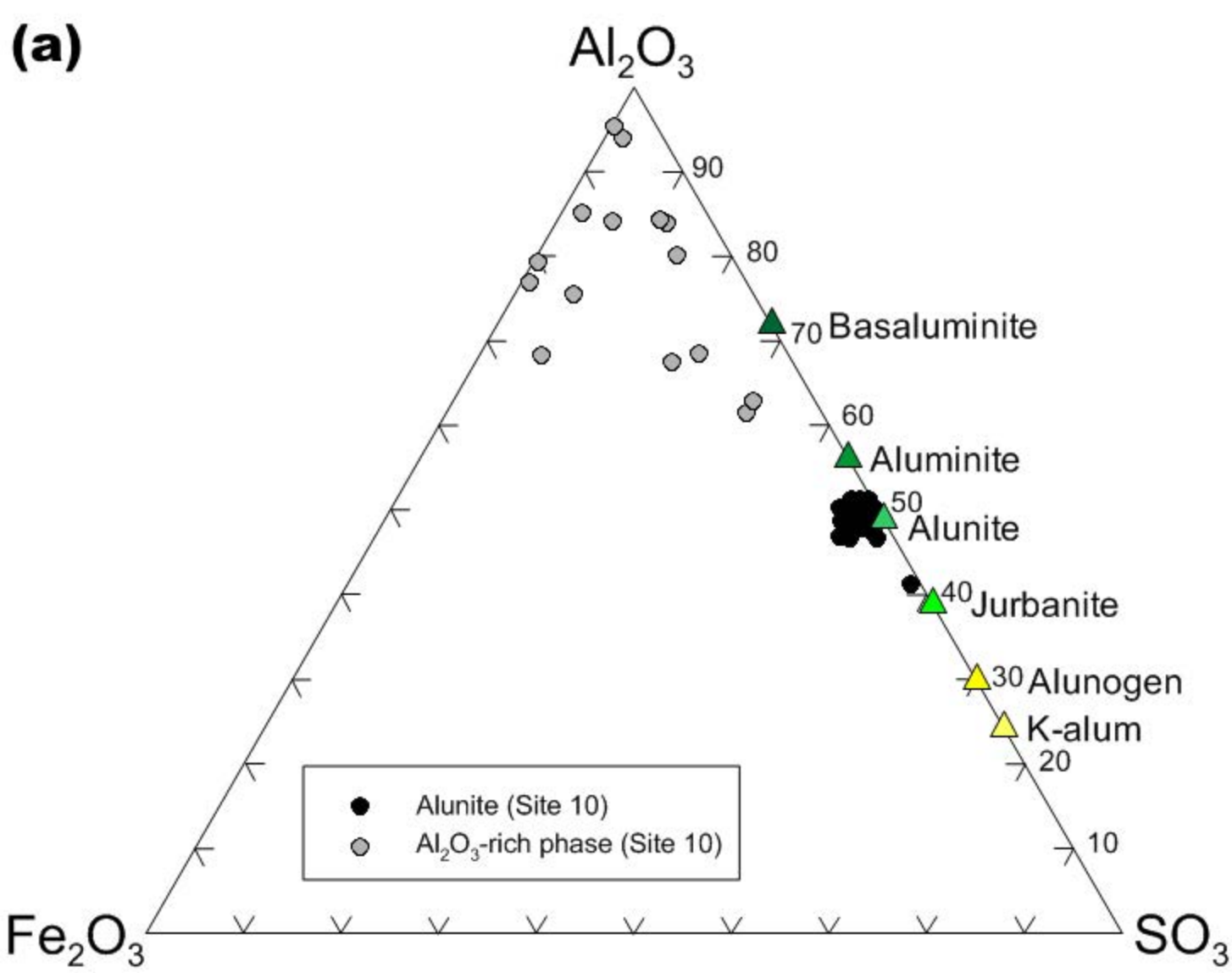
(a)
Al2O3
90
80
70
Basaluminite
60
Aluminite
50
Alunite
40
Jurbanite
30
Alunogen
K-alum
20
10
Alunite (Site 10)
Al2O3-rich phase (Site 10)
Fe2O3
SO3

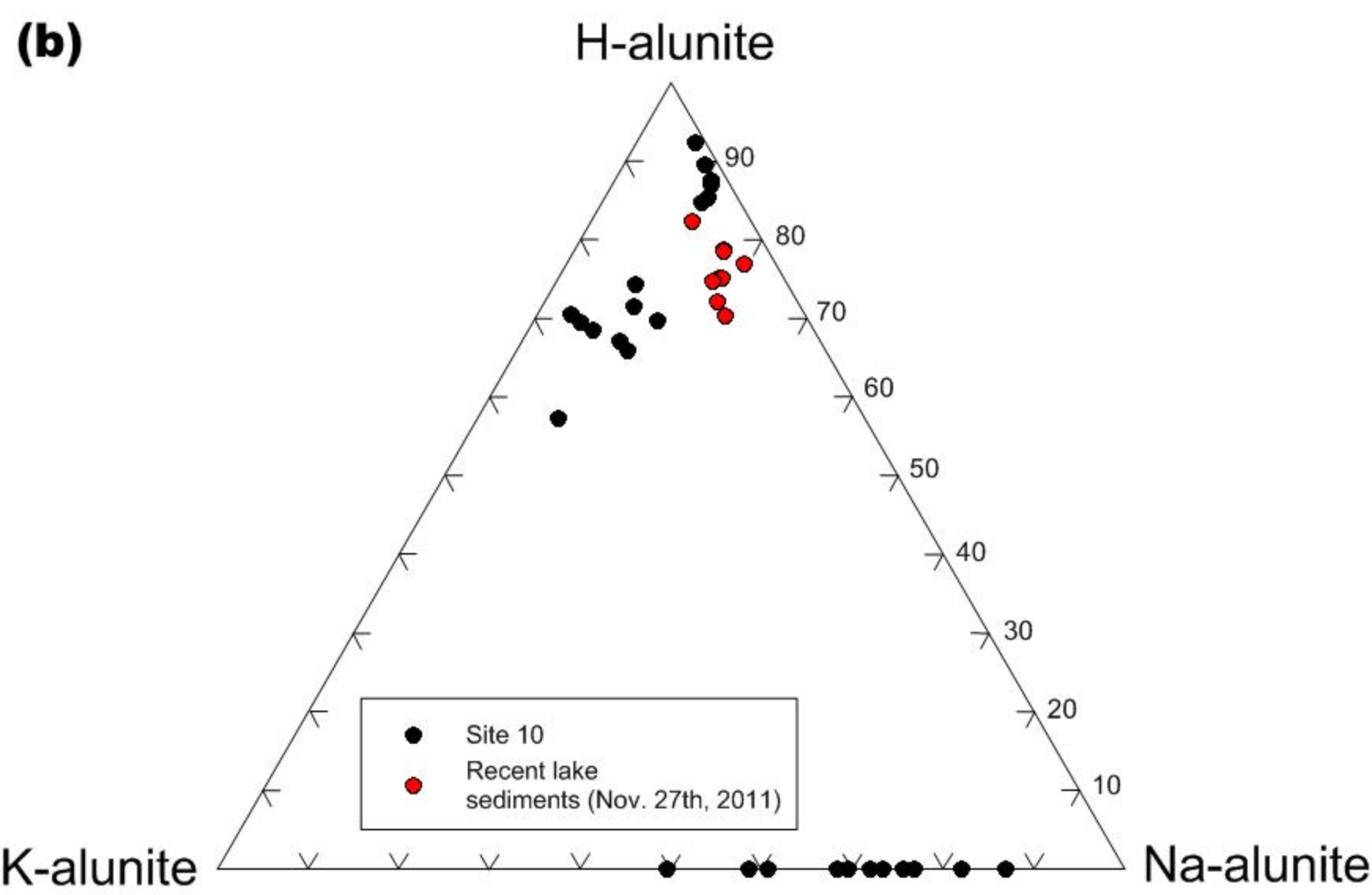
(b)
H-alunite
90
80
70
60
50
40
30
20
10
Site 10
Recent lake
sediments (Nov. 27th, 2011)
K-alunite
Na-alunite

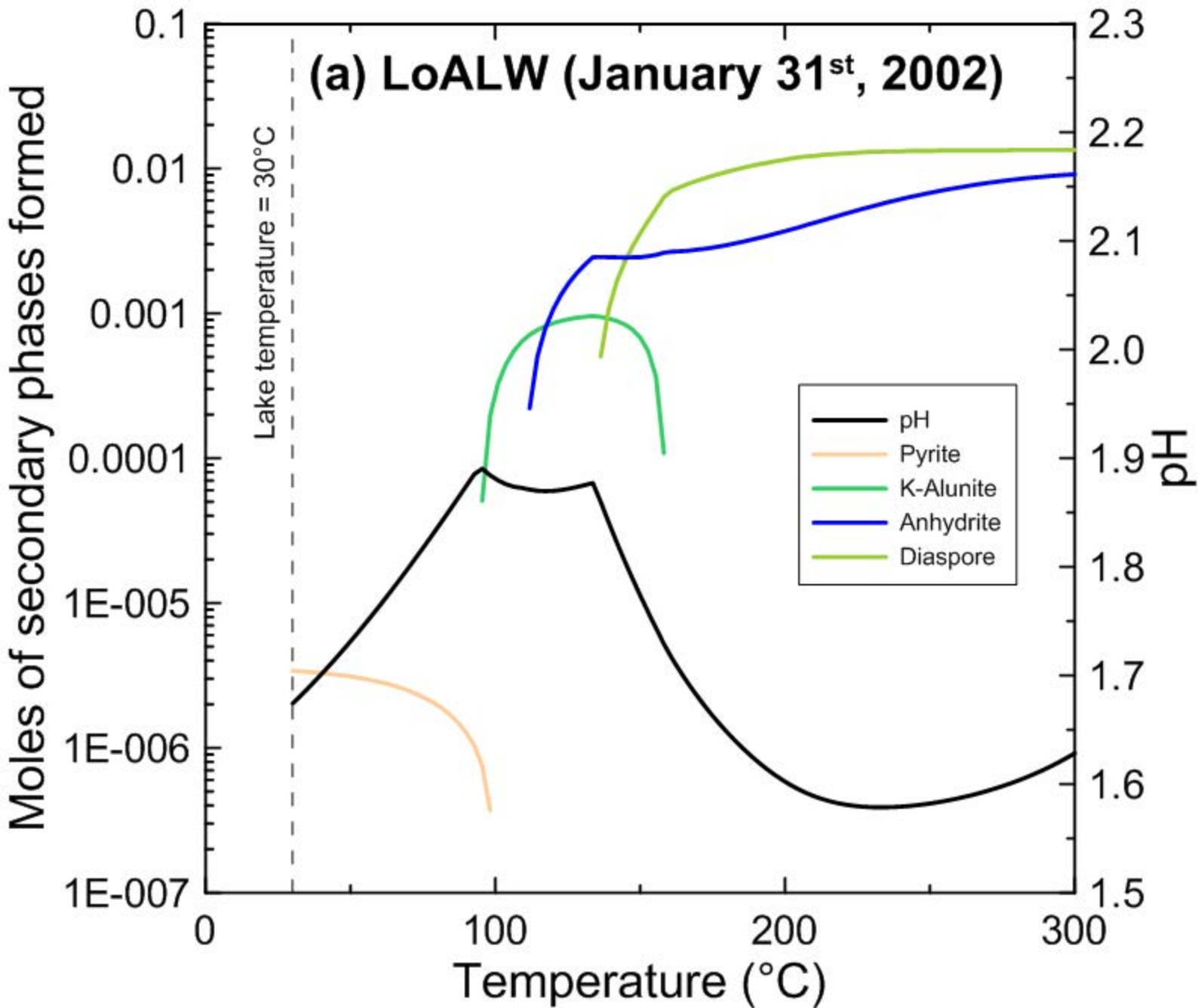
(a) LoALW (January 31st, 2002)
Lake temperature = 30°C
Moles of secondary phases formed
pH
Temperature (°C)
0.1
0.01
0.001
0.0001
1E-005
1E-006
1E-007
2.3
2.2
2.1
2.0
1.9
1.8
1.7
1.6
1.5
0
100
200
300
pH
Pyrite
K-Alunite
Anhydrite
Diaspore

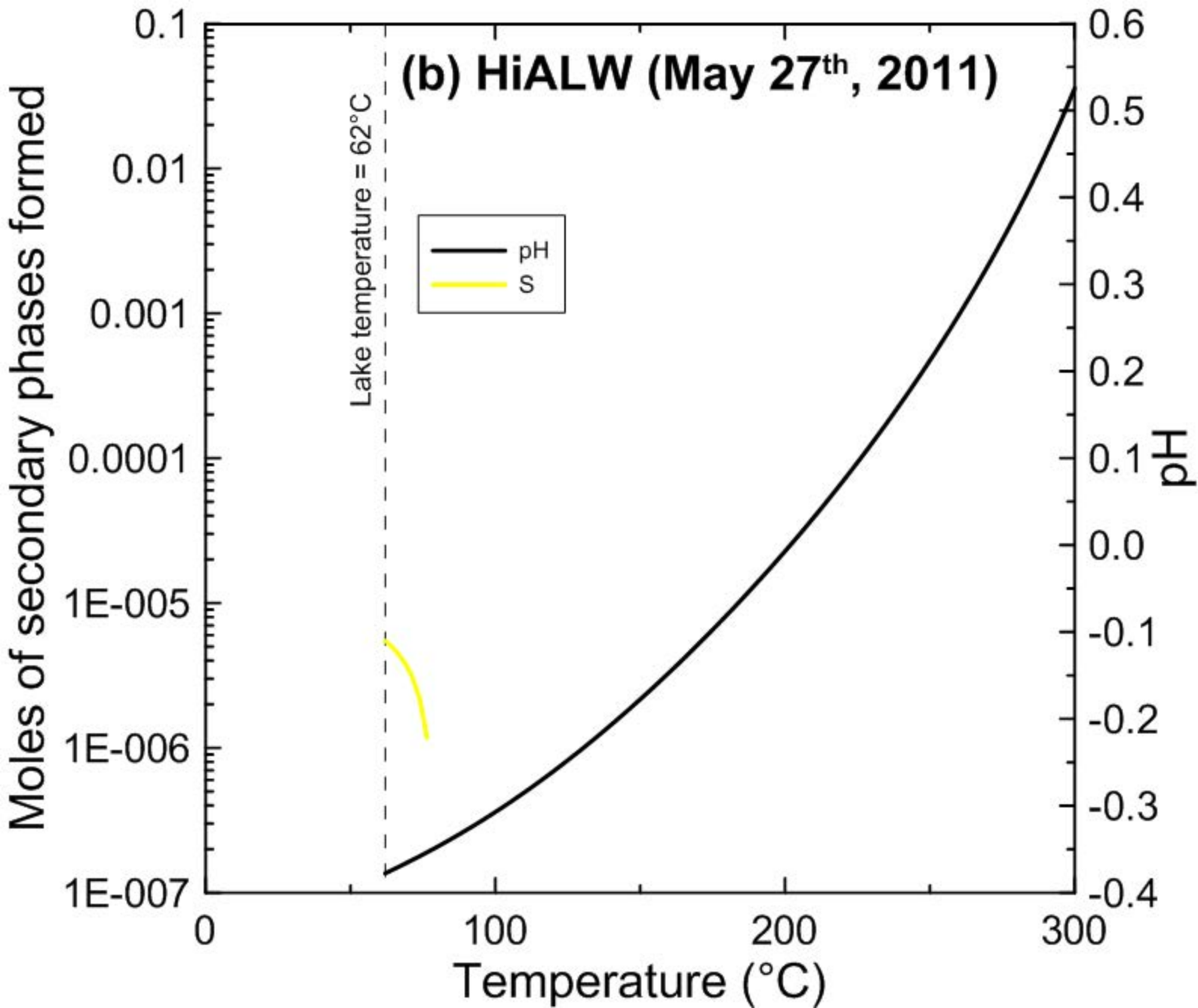
(b) HiALW (May 27th, 2011)
Lake temperature = 62°C
pH
S
Moles of secondary phases formed
pH
Temperature (°C)
0.1
0.01
0.001
0.0001
1E-005
1E-006
1E-007
0.6
0.5
0.4
0.3
0.2
0.1
0.0
-0.1
-0.2
-0.3
-0.4
0
100
200
300

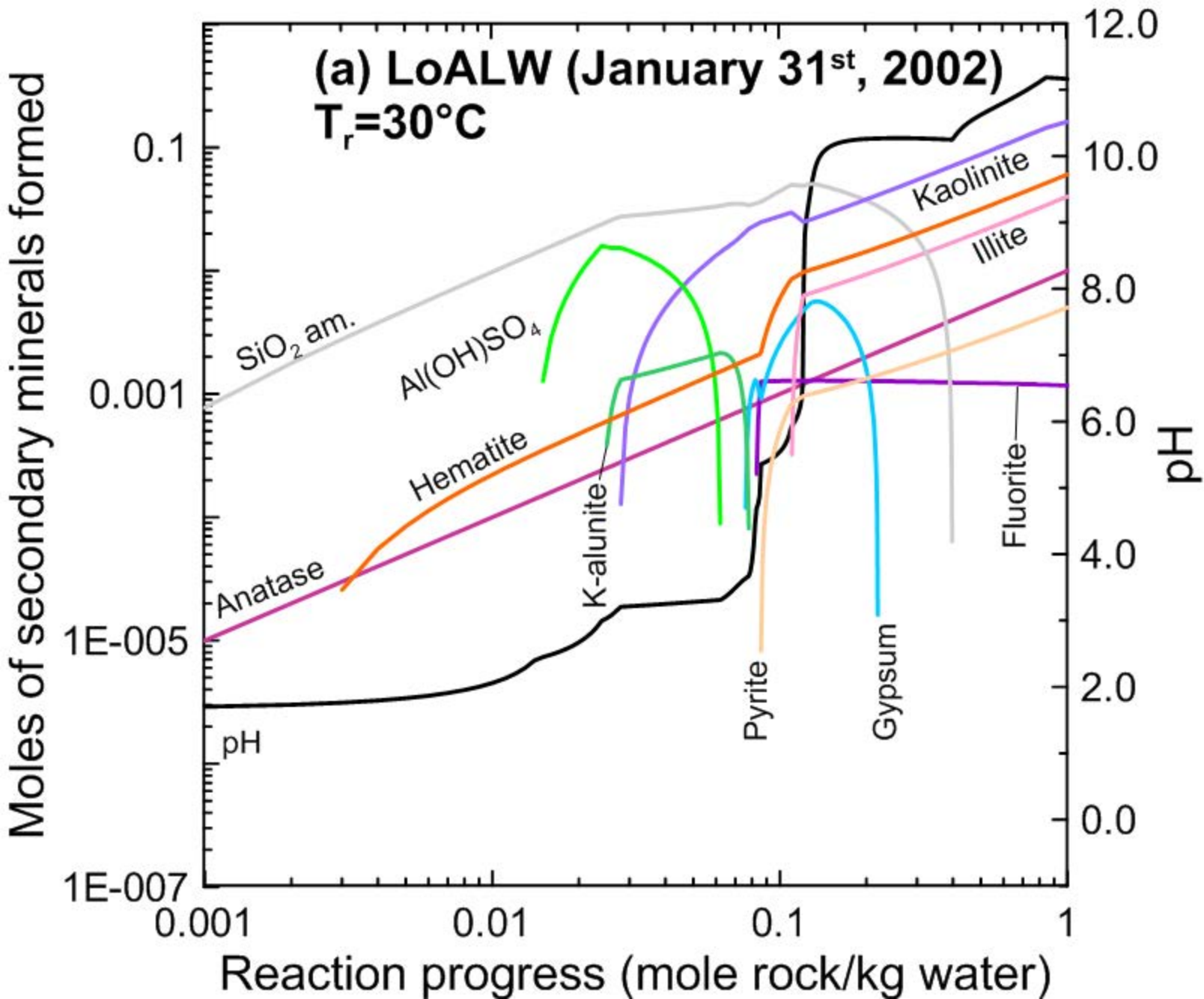
(a) LoALW (January 31st, 2002)
Tr=30°C
Moles of secondary minerals formed
pH
Reaction progress (mole rock/kg water)
0.1
0.001
1E-005
1E-007
0.001
0.01
0.1
1
12.0
10.0
8.0
6.0
4.0
2.0
0.0
SiO2 am.
Al(OH)SO4
Hematite
Anatase
K-alunite
Kaolinite
Illite
Fluorite
Pyrite
Gypsum
pH

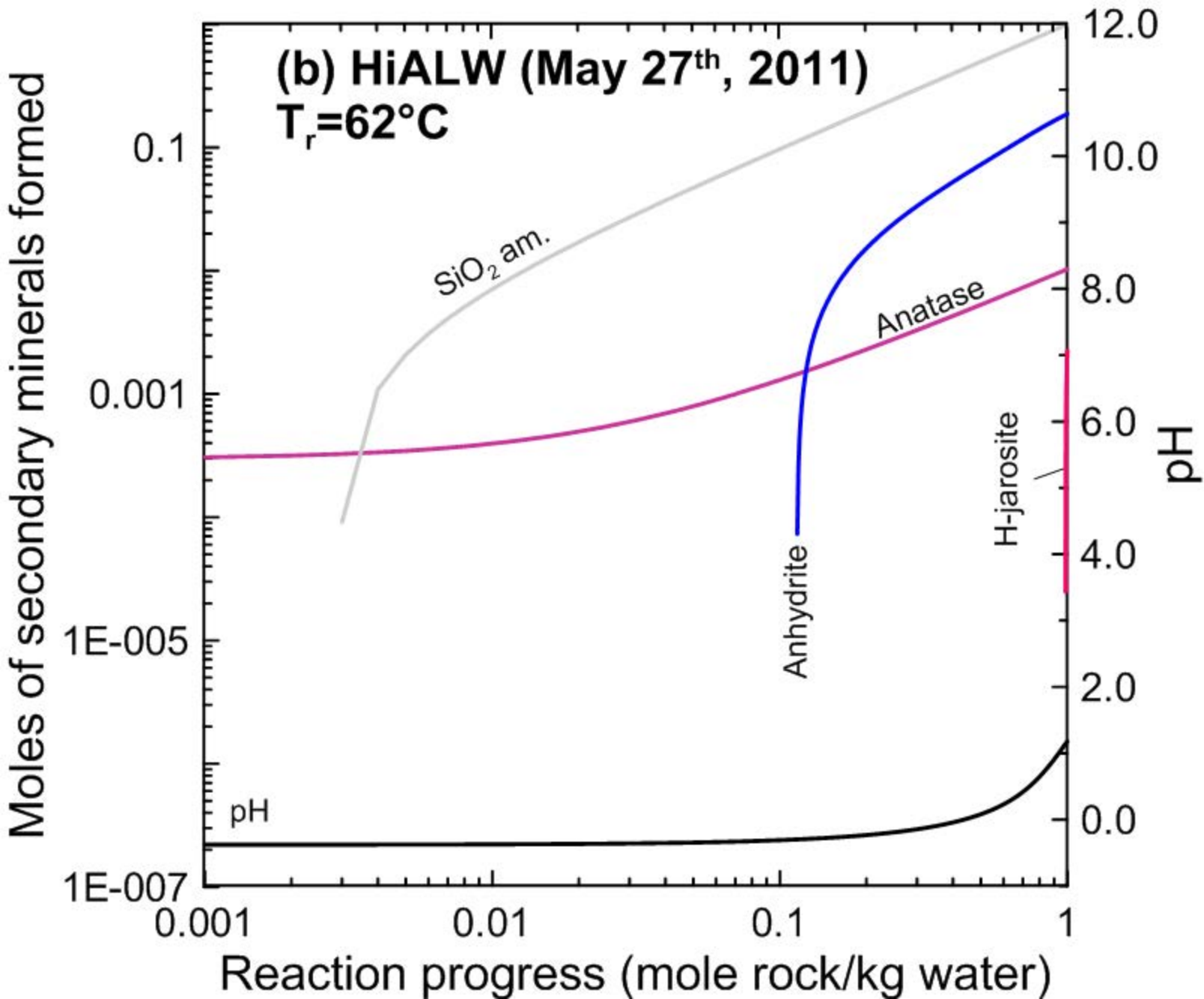
(b) HiALW (May 27th, 2011)
Tr=62°C
SiO2 am.
Anatase
Anhydrite
H-jarosite
pH
Moles of secondary minerals formed
Reaction progress (mole rock/kg water)
0.1
0.001
1E-005
1E-007
0.001
0.01
0.1
1
12.0
10.0
8.0
6.0
4.0
2.0
0.0
pH

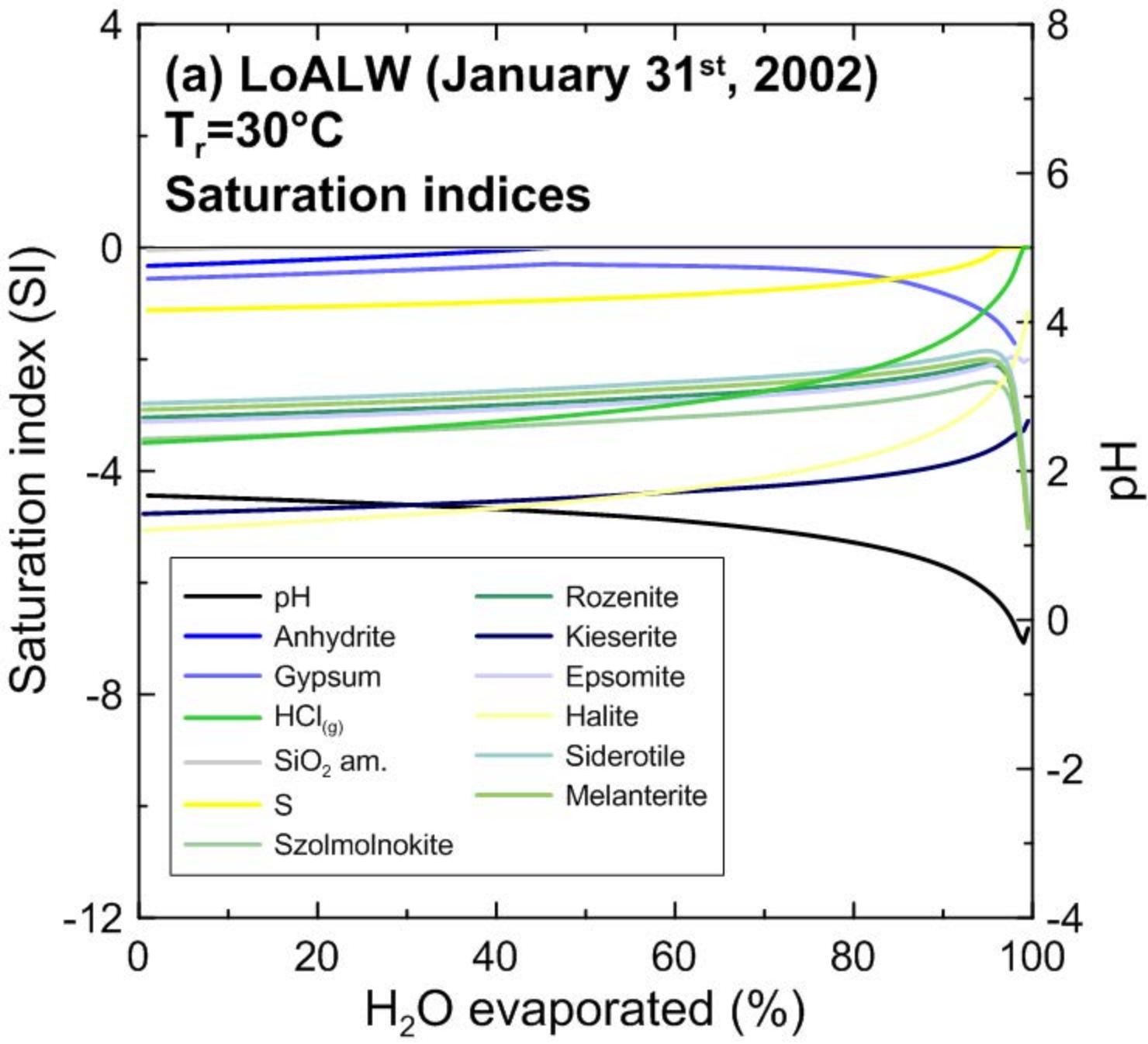
(a) LoALW (January 31st, 2002)
T_r=30°C
Saturation indices
Saturation index (SI)
pH
H2O evaporated (%)
4
0
-4
-8
-12
8
6
4
2
0
-2
-4
0
20
40
60
80
100
pH
Anhydrite
Gypsum
HCl(g)
SiO2 am.
S
Szolmolnokite
Rozenite
Kieserite
Epsomite
Halite
Siderotile
Melanterite

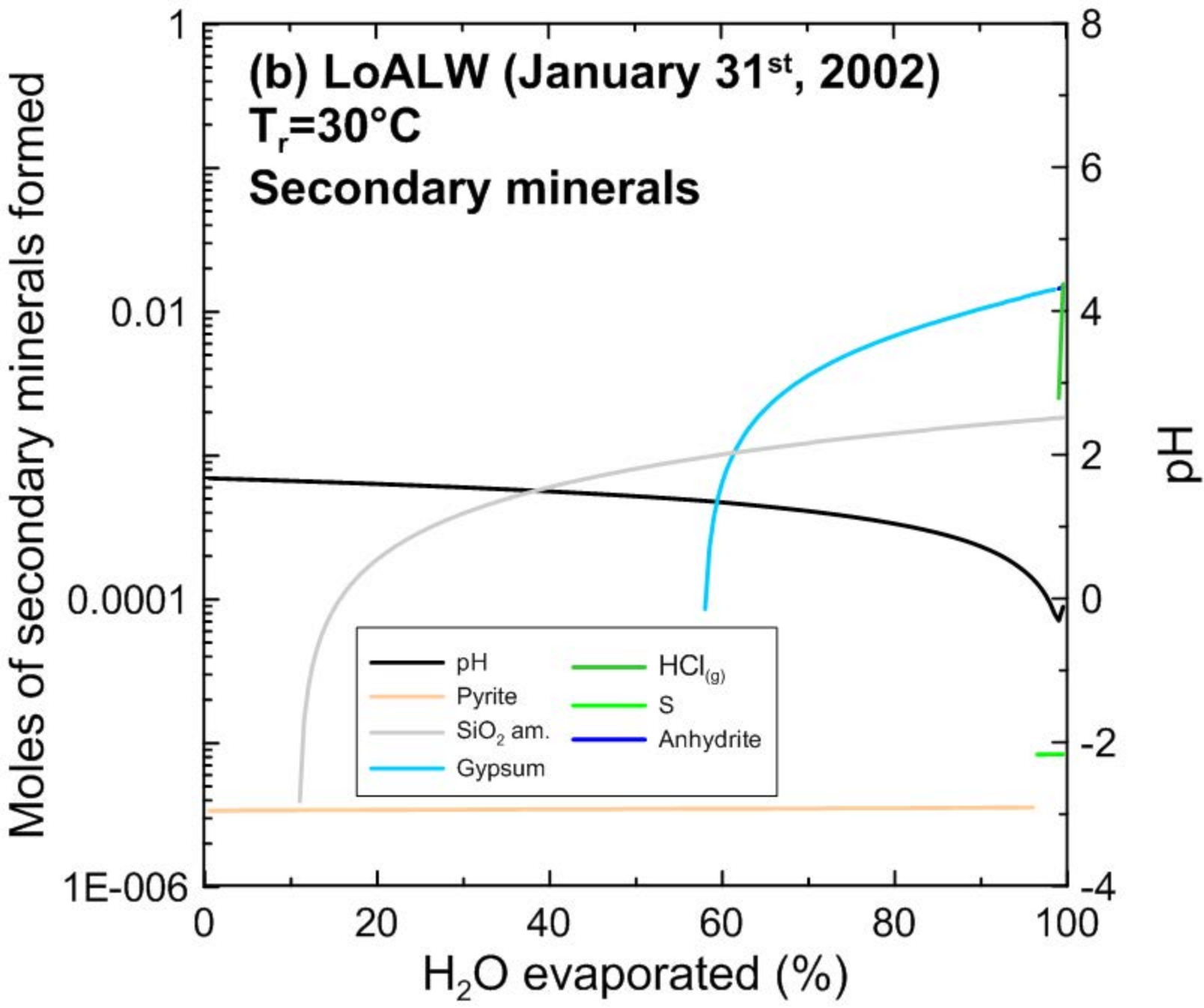
(b) LoALW (January 31st, 2002)
T_r=30°C
Secondary minerals
Moles of secondary minerals formed
pH
H2O evaporated (%)
1
0.01
0.0001
1E-006
8
6
4
2
0
-2
-4
0
20
40
60
80
100
pH
Pyrite
SiO2 am.
Gypsum
HCl(g)
S
Anhydrite

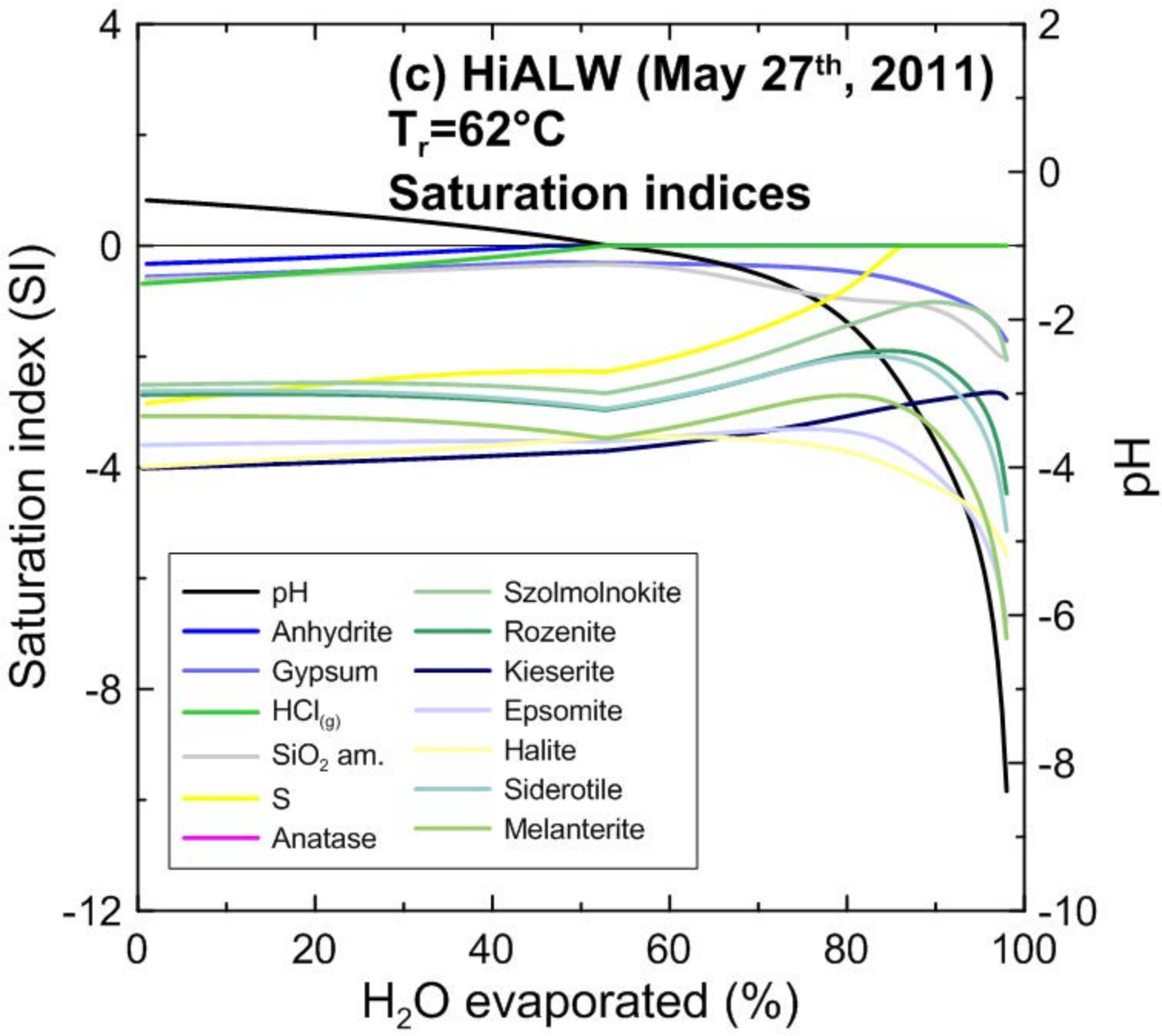
(c) HiALW (May 27th, 2011)
Tr=62°C
Saturation indices
Saturation index (SI)
pH
H2O evaporated (%)
4
0
-4
-8
-12
2
0
-2
-4
-6
-8
-10
0
20
40
60
80
100
pH
Anhydrite
Gypsum
HCl(g)
SiO2 am.
S
Anatase
Szolmolnokite
Rozenite
Kieserite
Epsomite
Halite
Siderotile
Melanterite

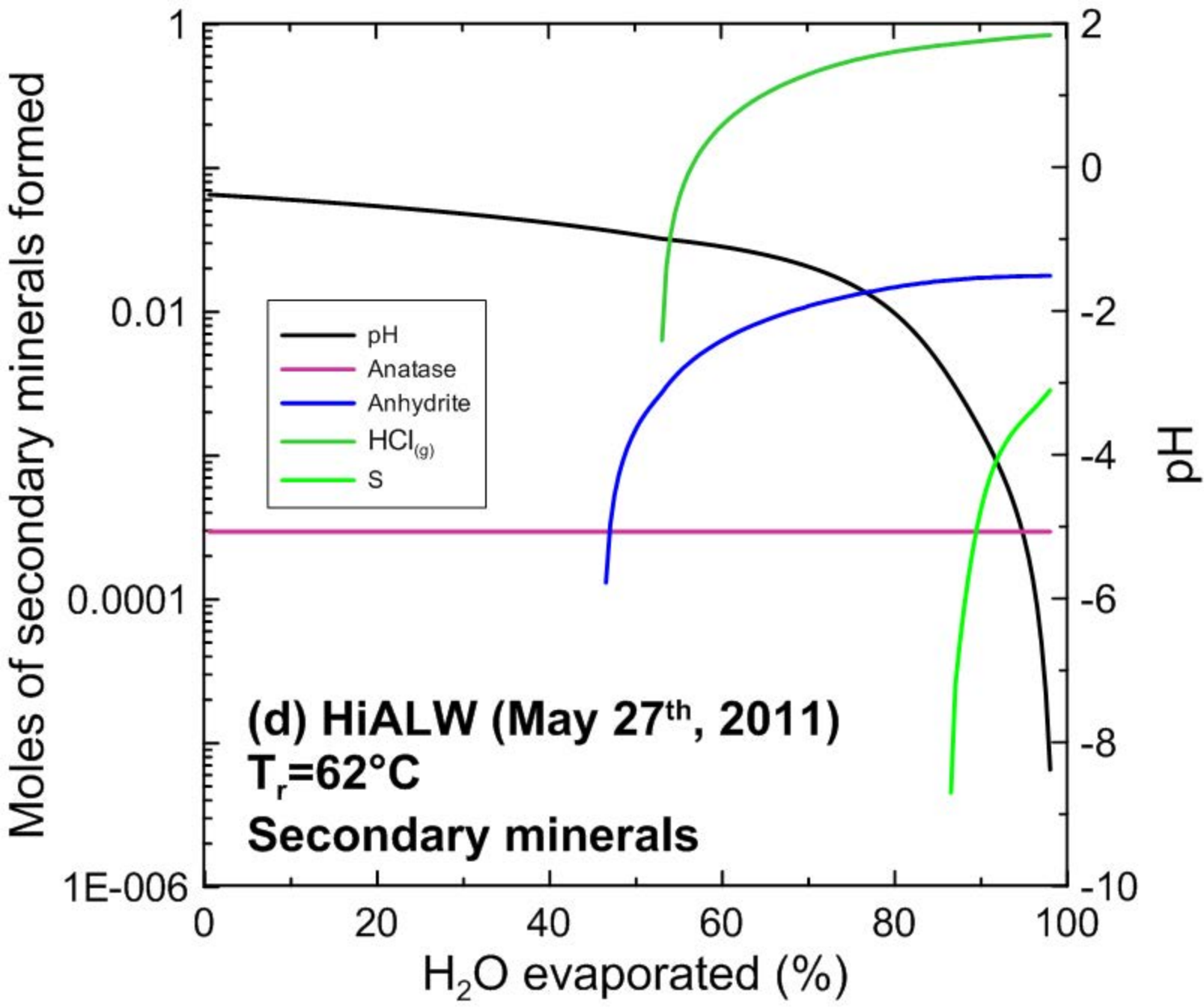
Moles of secondary minerals formed
1
0.01
0.0001
1E-006
pH
2
0
-2
-4
-6
-8
-10
0
20
40
60
80
100
H2O evaporated (%)
pH
Anatase
Anhydrite
HCl(g)
S
(d) HiALW (May 27th, 2011)
Tr=62°C
Secondary minerals

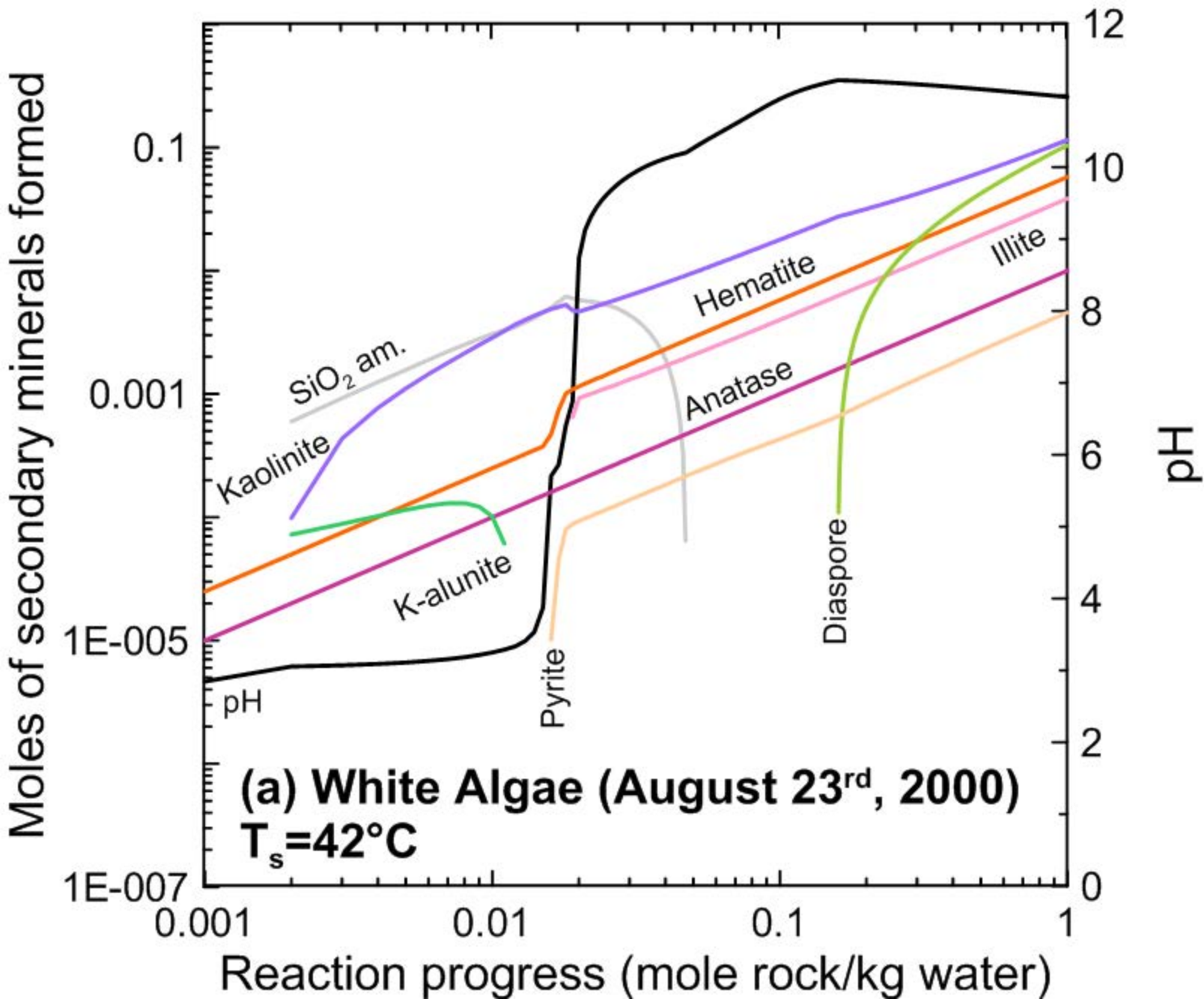
Moles of secondary minerals formed
0.1
0.001
1E-005
1E-007
pH
12
10
8
6
4
2
0
0.001
0.01
0.1
1
Reaction progress (mole rock/kg water)
SiO2 am.
Kaolinite
Hematite
Illite
Anatase
K-alunite
Pyrite
Diaspore
pH
(a) White Algae (August 23rd, 2000)
Ts=42°C

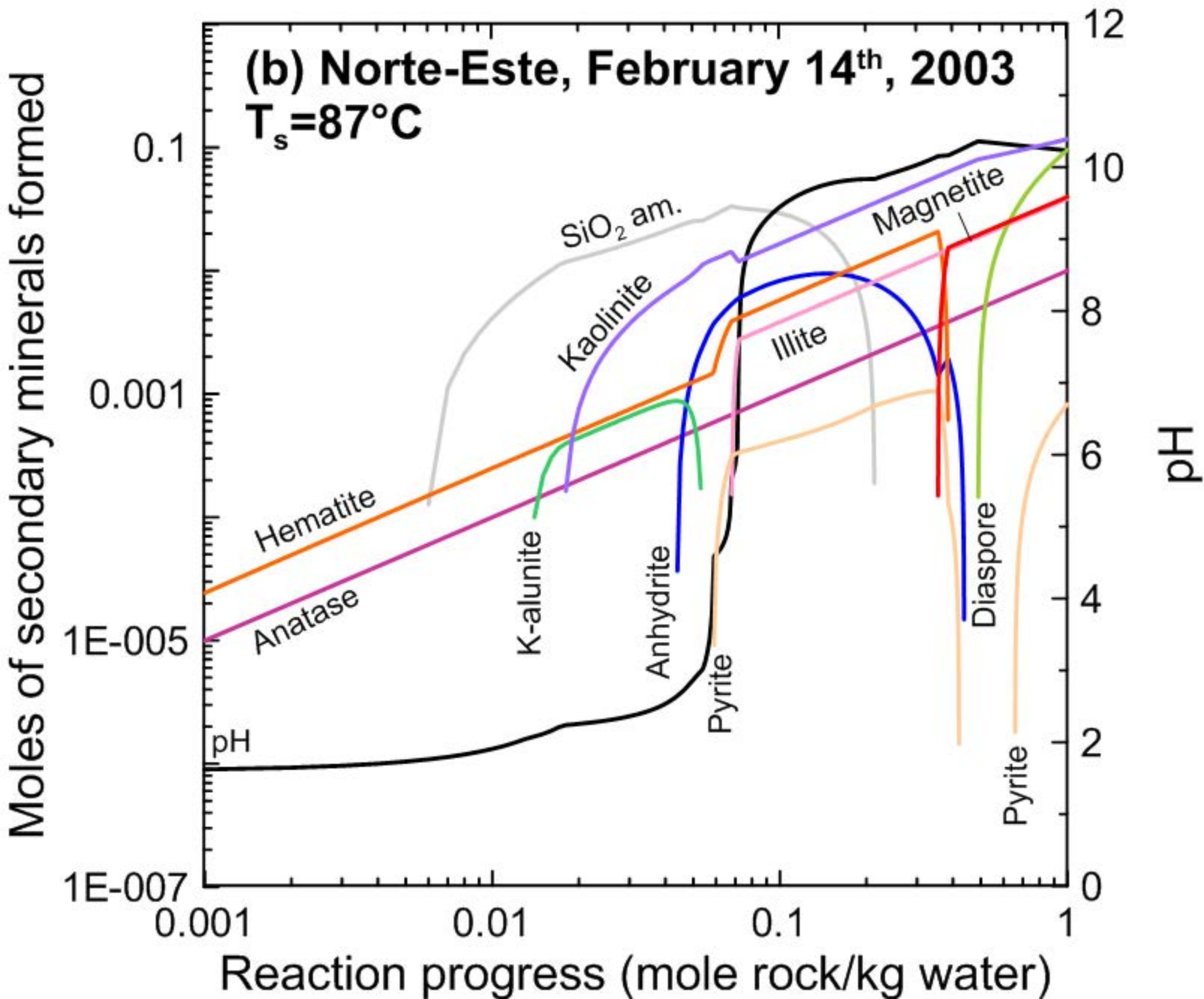
(b) Norte-Este, February 14th, 2003
Ts=87°C
Moles of secondary minerals formed
pH
Reaction progress (mole rock/kg water)
0.1
0.001
1E-005
1E-007
0.001
0.01
0.1
1
12
10
8
6
4
2
0
SiO2 am.
Kaolinite
Magnetite
Illite
Hematite
Anatase
K-alunite
Anhydrite
Pyrite
Diaspore
Pyrite
pH


(a)


(b)


(c)


(d)


(e)


(f)

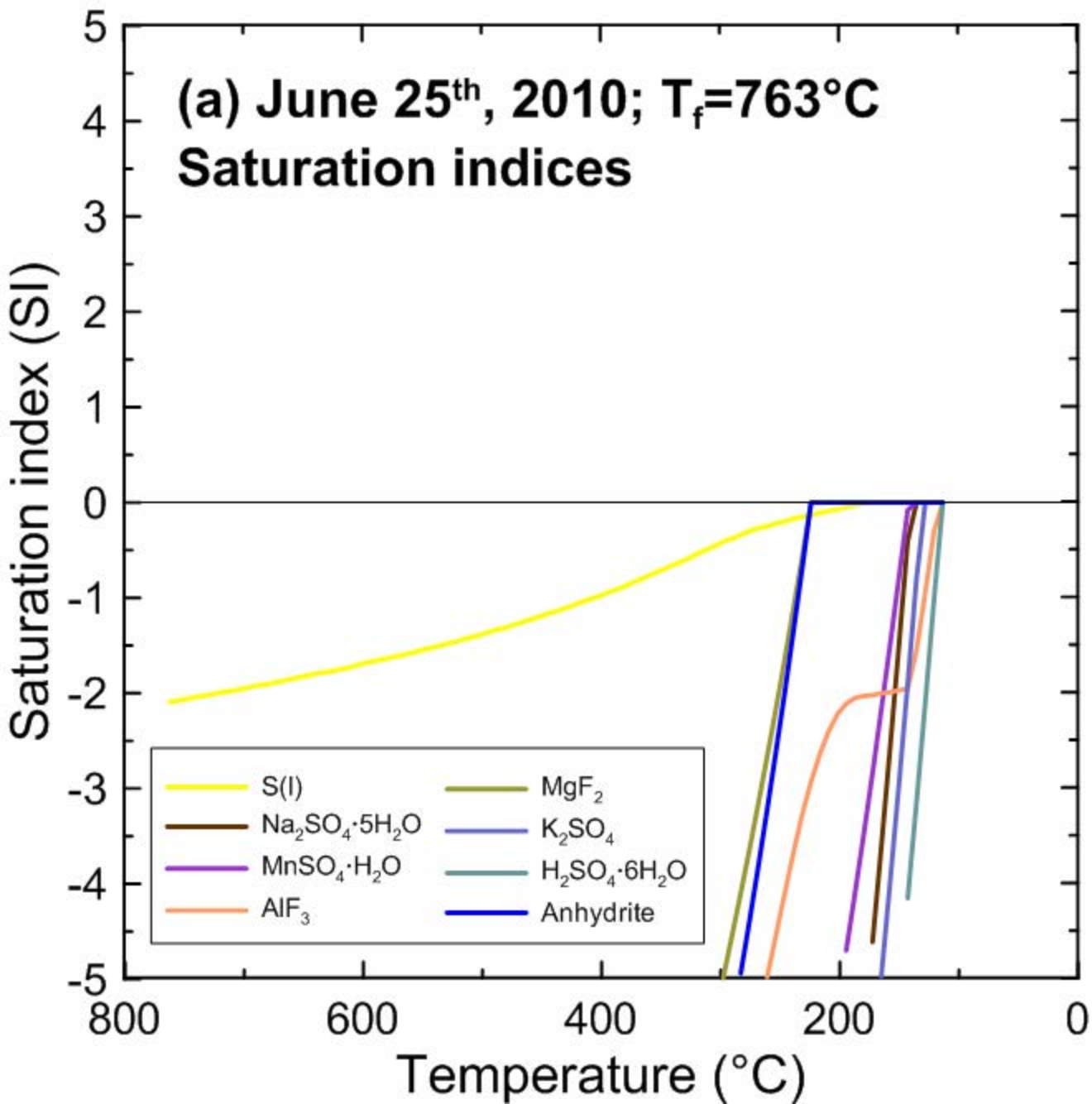
(a) June 25th, 2010; Tf=763°C
Saturation indices
Saturation index (SI)
Temperature (°C)
5
4
3
2
1
0
-1
-2
-3
-4
-5
800
600
400
200
0
S(l)
Na2SO4·5H2O
MnSO4·H2O
AlF3
MgF2
K2SO4
H2SO4·6H2O
Anhydrite

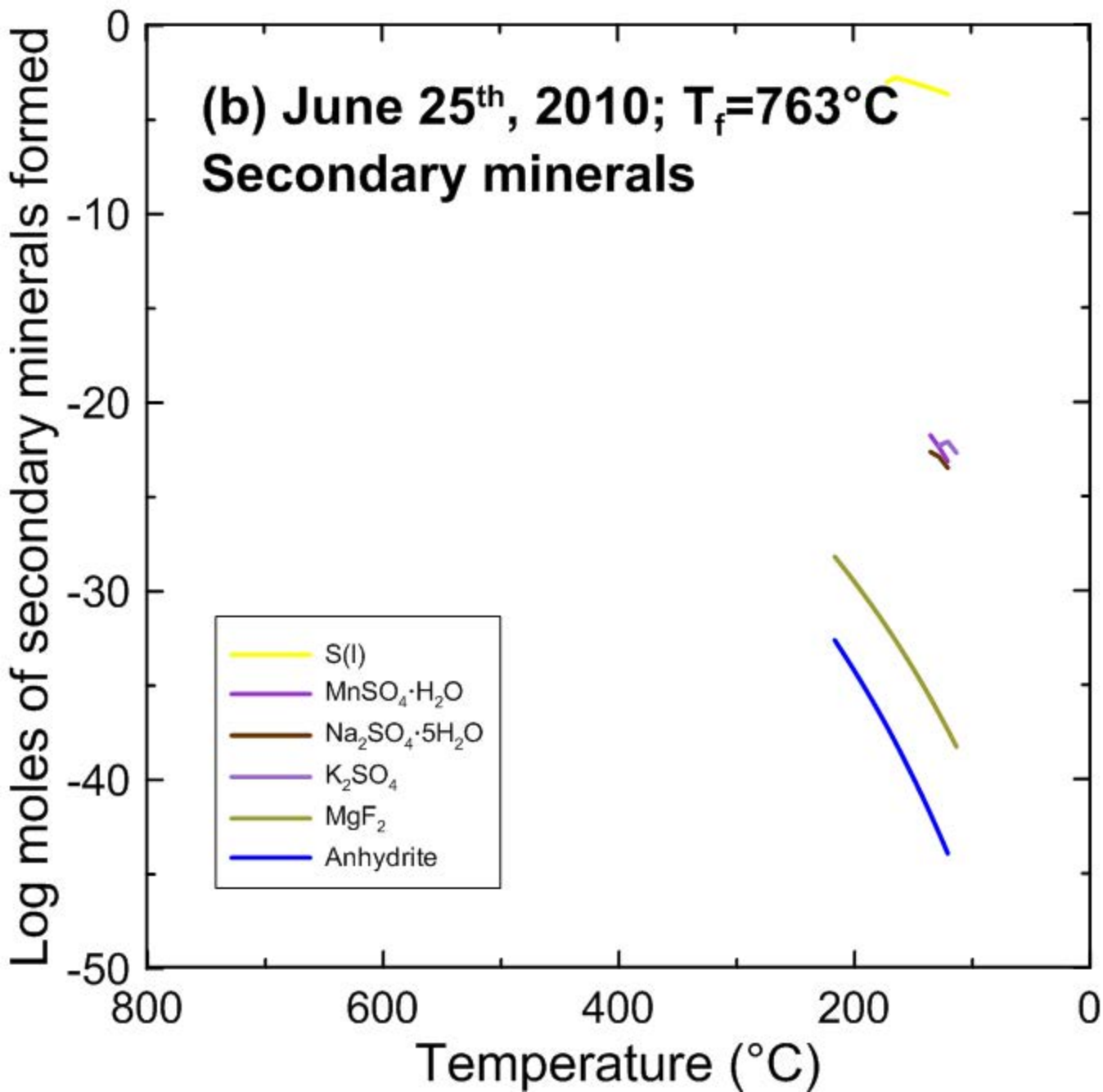
(b) June 25th, 2010; Tf=763°C
Secondary minerals
Log moles of secondary minerals formed
Temperature (°C)
0
-10
-20
-30
-40
-50
800
600
400
200
0
S(l)
MnSO4·H2O
Na2SO4·5H2O
K2SO4
MgF2
Anhydrite

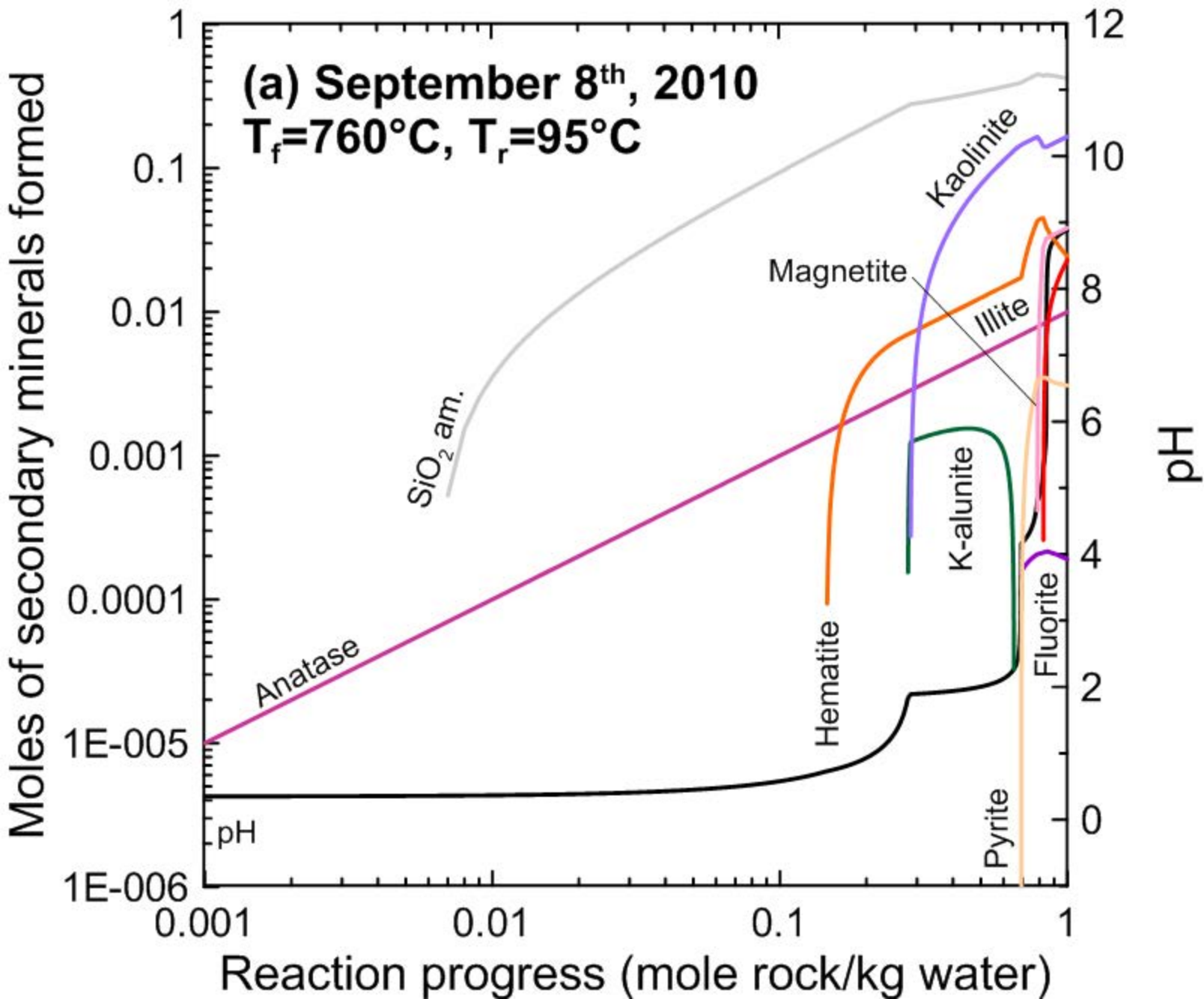
(a) September 8th, 2010
Tf=760°C, Tr=95°C
Moles of secondary minerals formed
pH
Reaction progress (mole rock/kg water)
1
0.1
0.01
0.001
0.0001
1E-005
1E-006
0.001
0.01
0.1
1
12
10
8
6
4
2
0
SiO2 am.
Anatase
Kaolinite
Magnetite
Illite
K-alunite
Hematite
Fluorite
Pyrite
pH

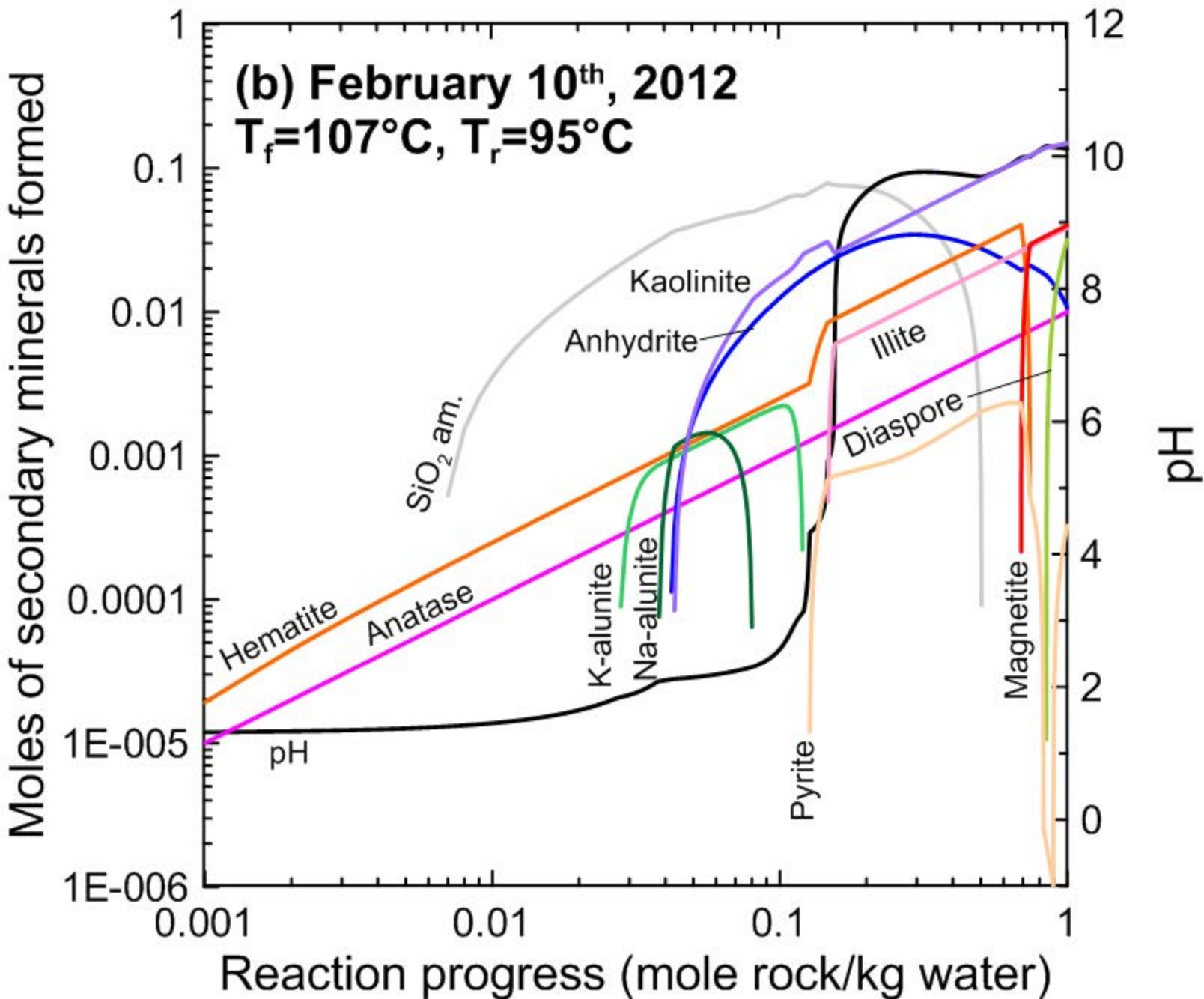
(b) February 10th, 2012
Tf=107°C, Tr=95°C
Moles of secondary minerals formed
pH
Reaction progress (mole rock/kg water)
1
0.1
0.01
0.001
0.0001
1E-005
1E-006
12
10
8
6
4
2
0
0.001
0.01
0.1
1
Kaolinite
Anhydrite
Illite
Diaspore
SiO2 am.
Hematite
Anatase
K-alunite
Na-alunite
Magnetite
Pyrite
pH


(a)
cave


(b)
Canon


(c)


(d)


(e)


(f)

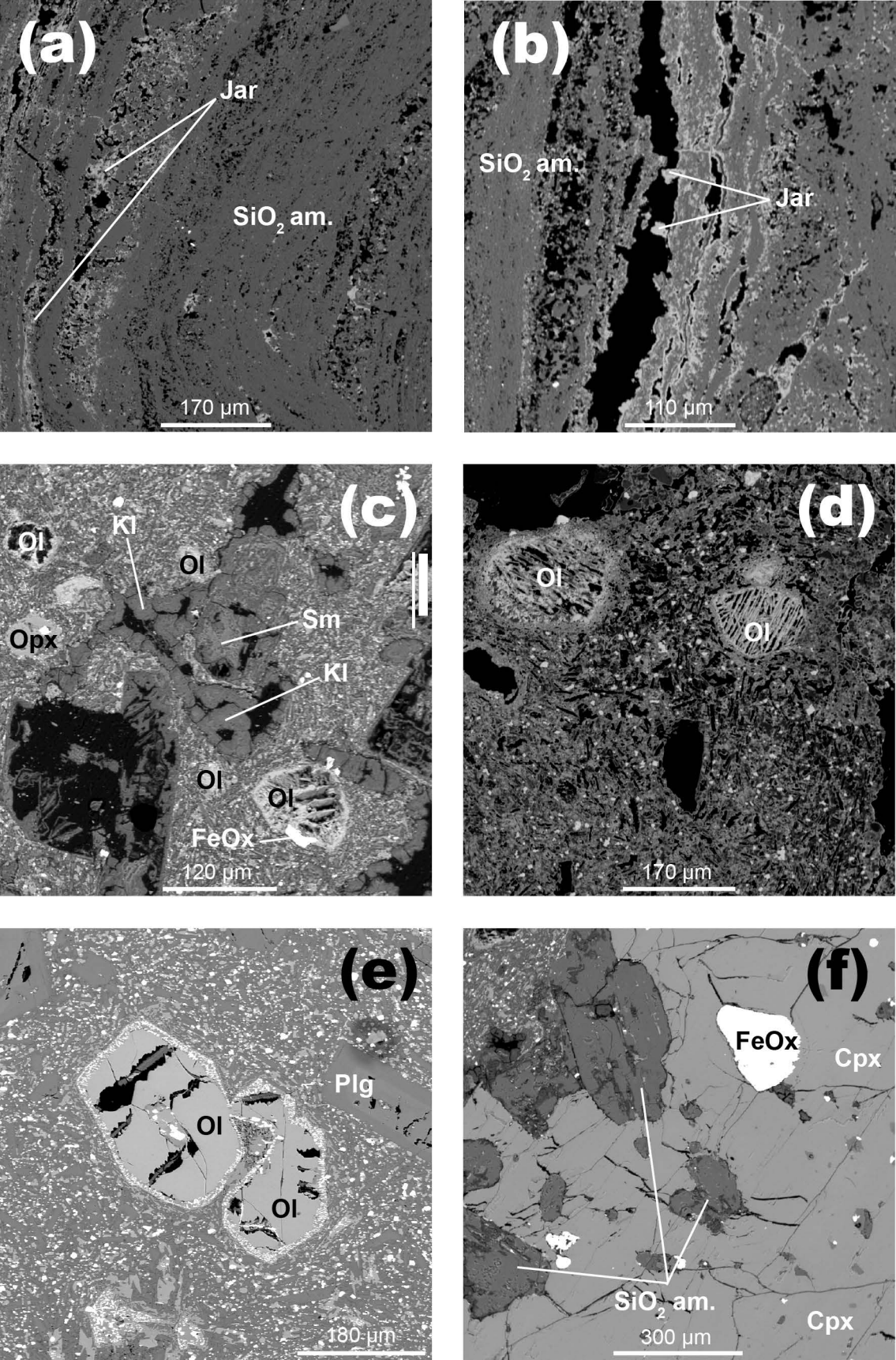
(a)
Jar
SiO2 am.
170 µm
(b)
SiO2 am.
Jar
110 µm
(c)
Ol
Kl
Ol
Sm
Opx
Kl
Ol
Ol
FeOx
120 µm
(d)
Ol
Ol
170 µm
(e)
Plg
Ol
Ol
180 µm
(f)
FeOx
Cpx
SiO2 am.
Cpx
300 µm

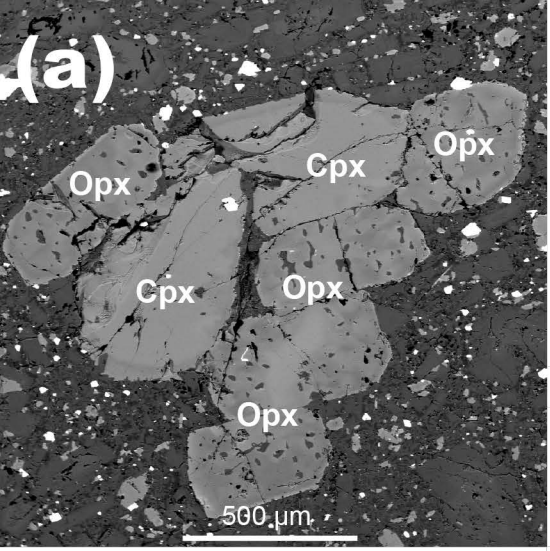
(a)
Opx
Cpx
Opx
Opx
Cpx
Opx
Opx
500 µm

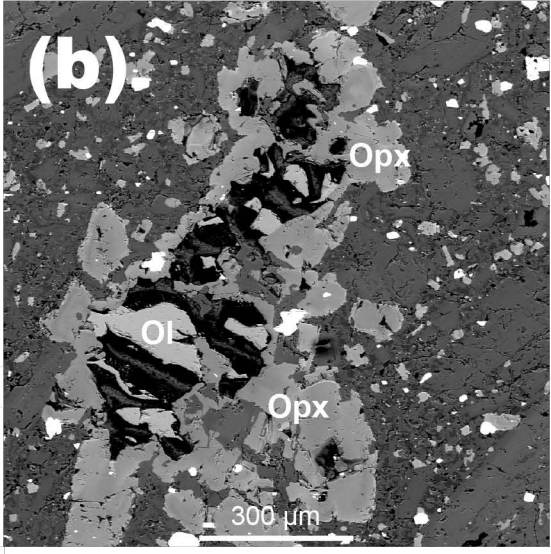
(b)
Opx
Ol
Opx
300 µm

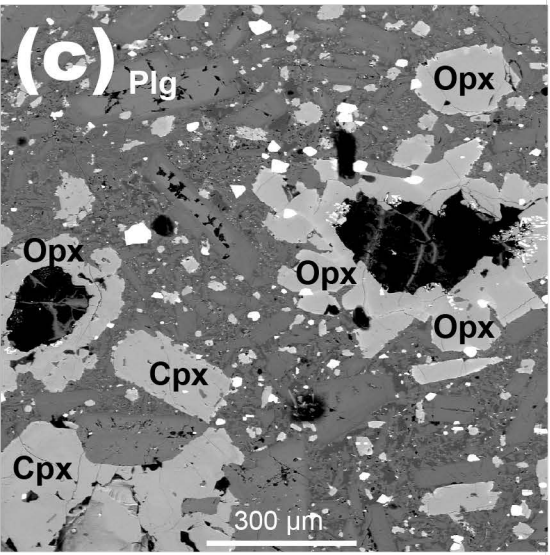
(c)
Plg
Opx
Opx
Opx
Opx
Cpx
Cpx
300 µm

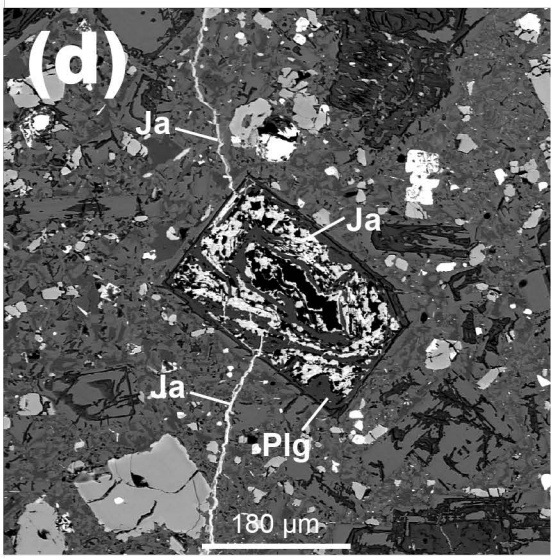
(d)
Ja
Ja
Ja
Plg
180 µm

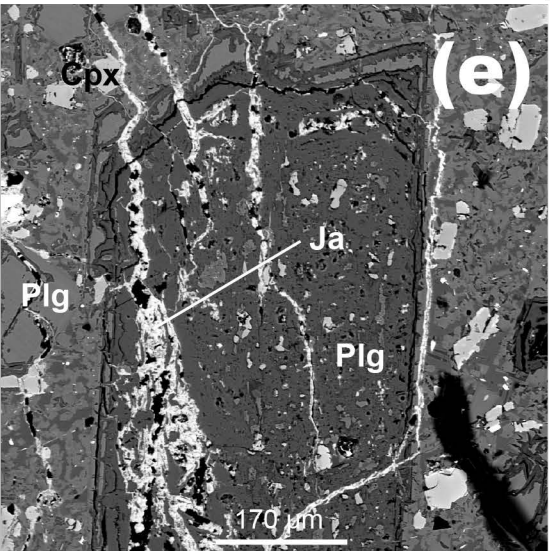
(e)
Cpx
Ja
Plg
Plg
170 µm

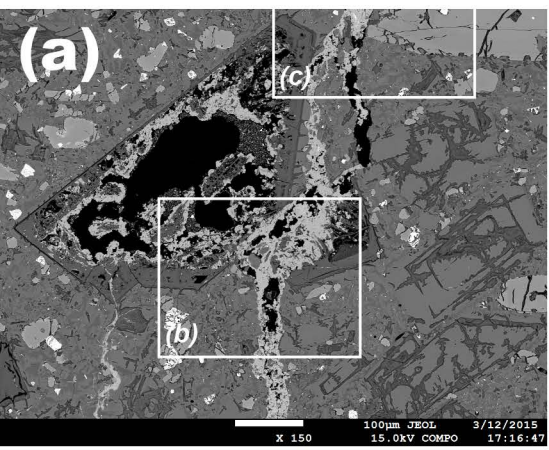
(a)
(c)
(b)
100µm JEOL 3/12/2015
X 150 15.0kV COMPO 17:16:47

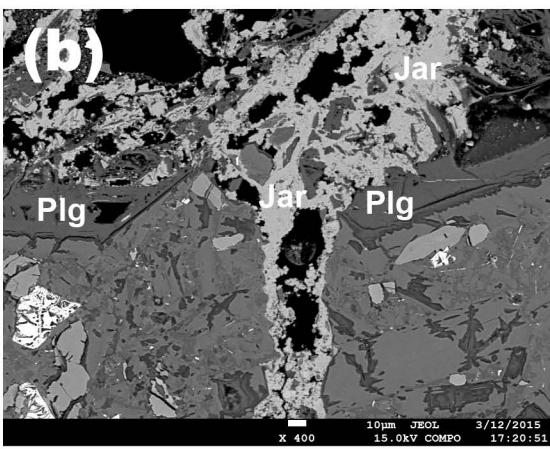
(b)
Jar
Plg
Jar
Plg
10µm JEOL 3/12/2015
X 400 15.0kV COMPO 17:20:51

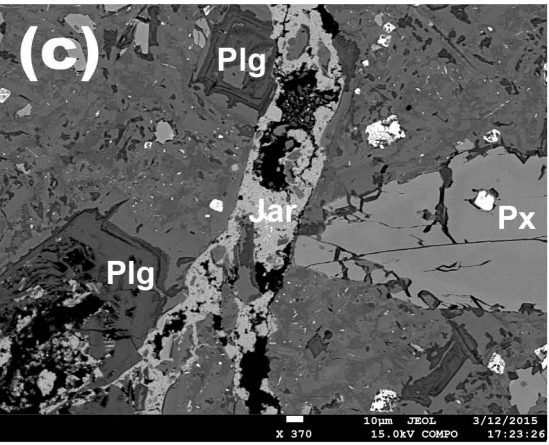
(c)
Plg
Jar
Px
Plg
10µm JEOL 3/12/2015
X 370 15.0kV COMPO 17:23:26

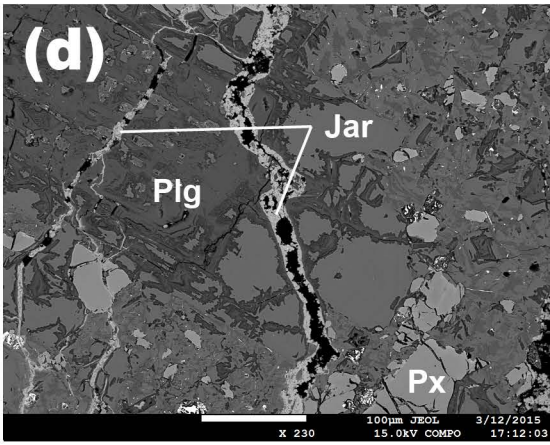
(d)
Jar
Plg
Px
100µm JEOL 3/12/2015
X 230 15.0kV COMPO 17:12:03

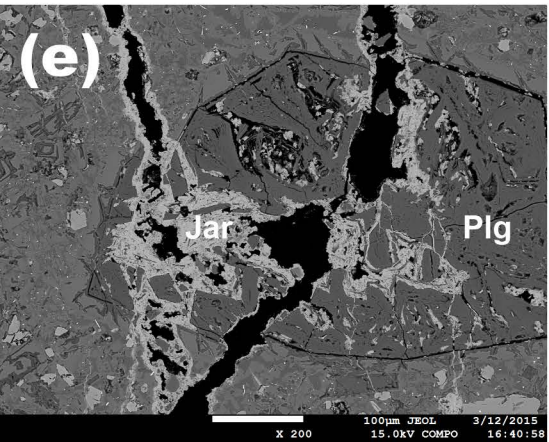
(e)
Jar
Plg
100µm JEOL 3/12/2015
X 200 15.0kV COMPO 16:40:58

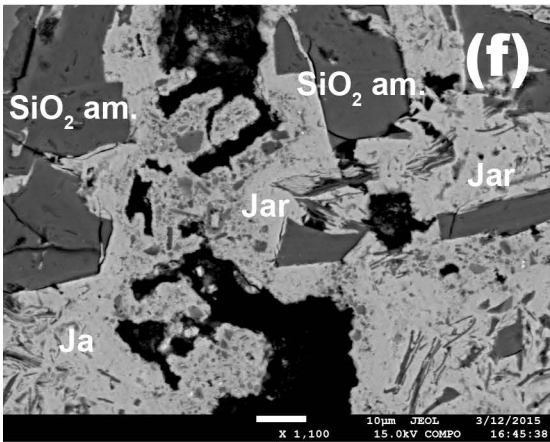
(f)
SiO2 am.
SiO2 am.
Jar
Jar
Ja
10µm JEOL 3/12/2015
X 1,100 15.0kV COMPO 16:45:38

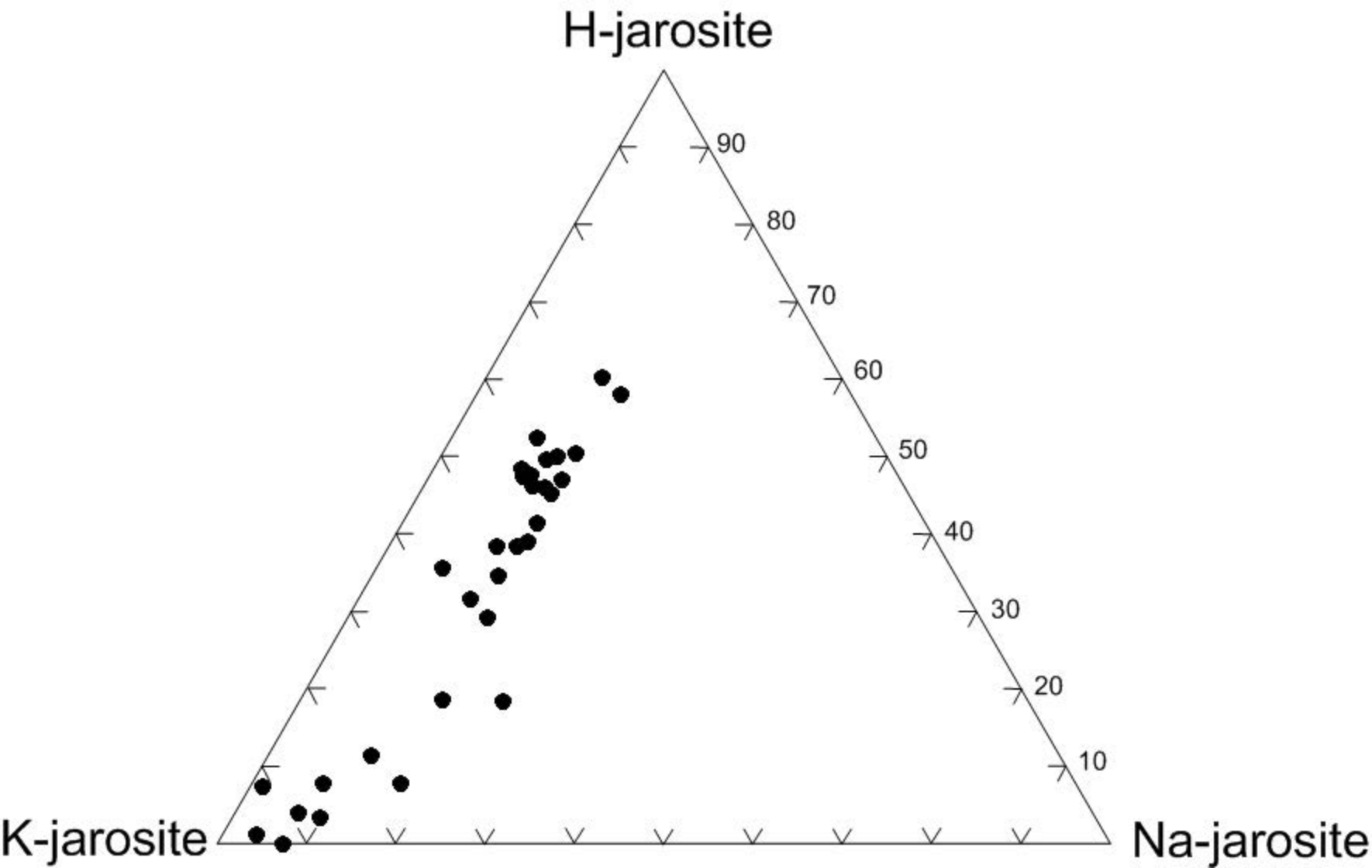
H-jarosite
90
80
70
60
50
40
30
20
10
K-jarosite
Na-jarosite

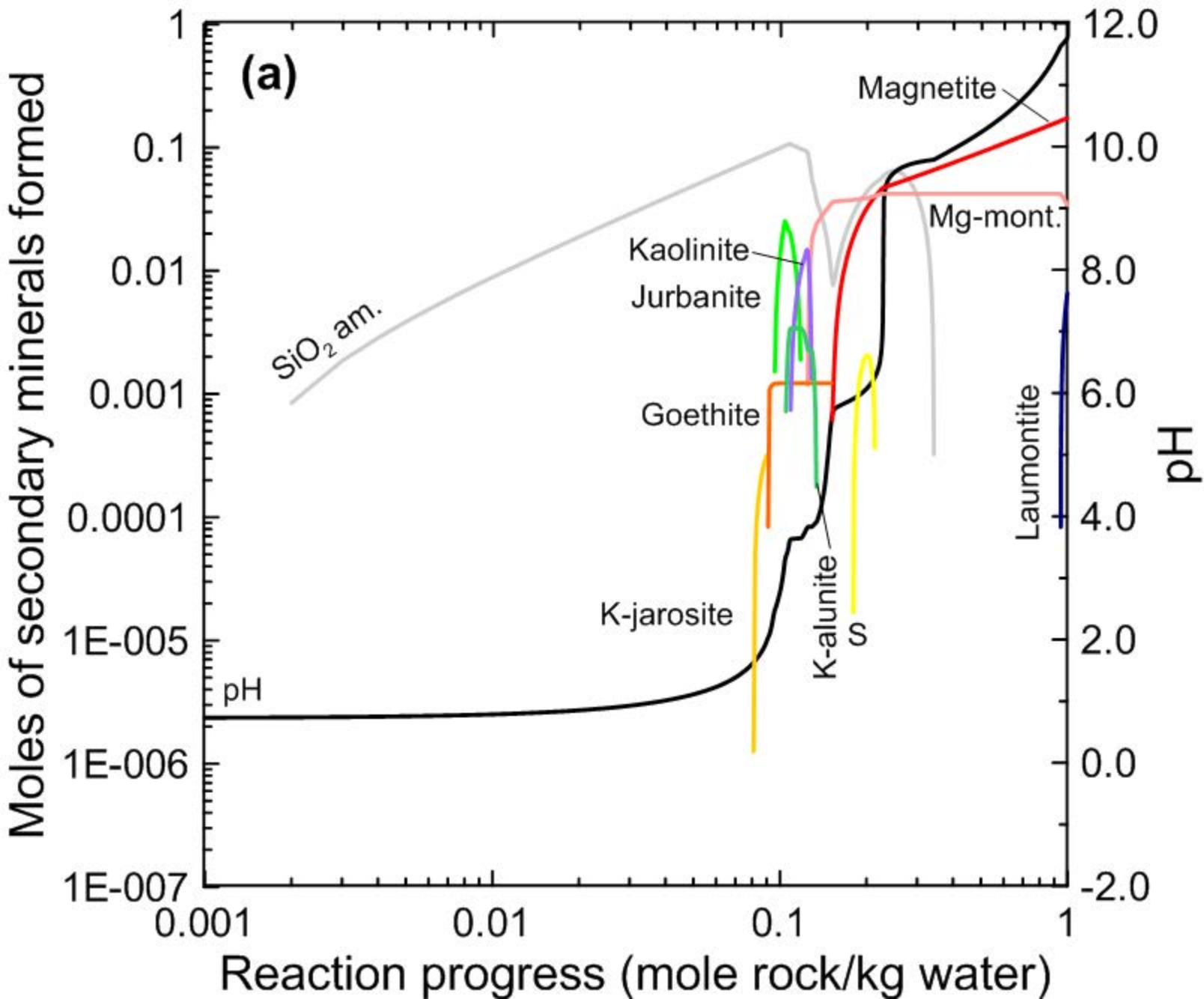
(a)
Magnetite
Mg-mont.
Kaolinite
Jurbanite
SiO_2 am.
Goethite
Laumontite
K-jarosite
K-alunite
S
pH
Moles of secondary minerals formed
pH
Reaction progress (mole rock/kg water)
1
0.1
0.01
0.001
0.0001
1E-005
1E-006
1E-007
12.0
10.0
8.0
6.0
4.0
2.0
0.0
-2.0
0.001
0.01
0.1
1

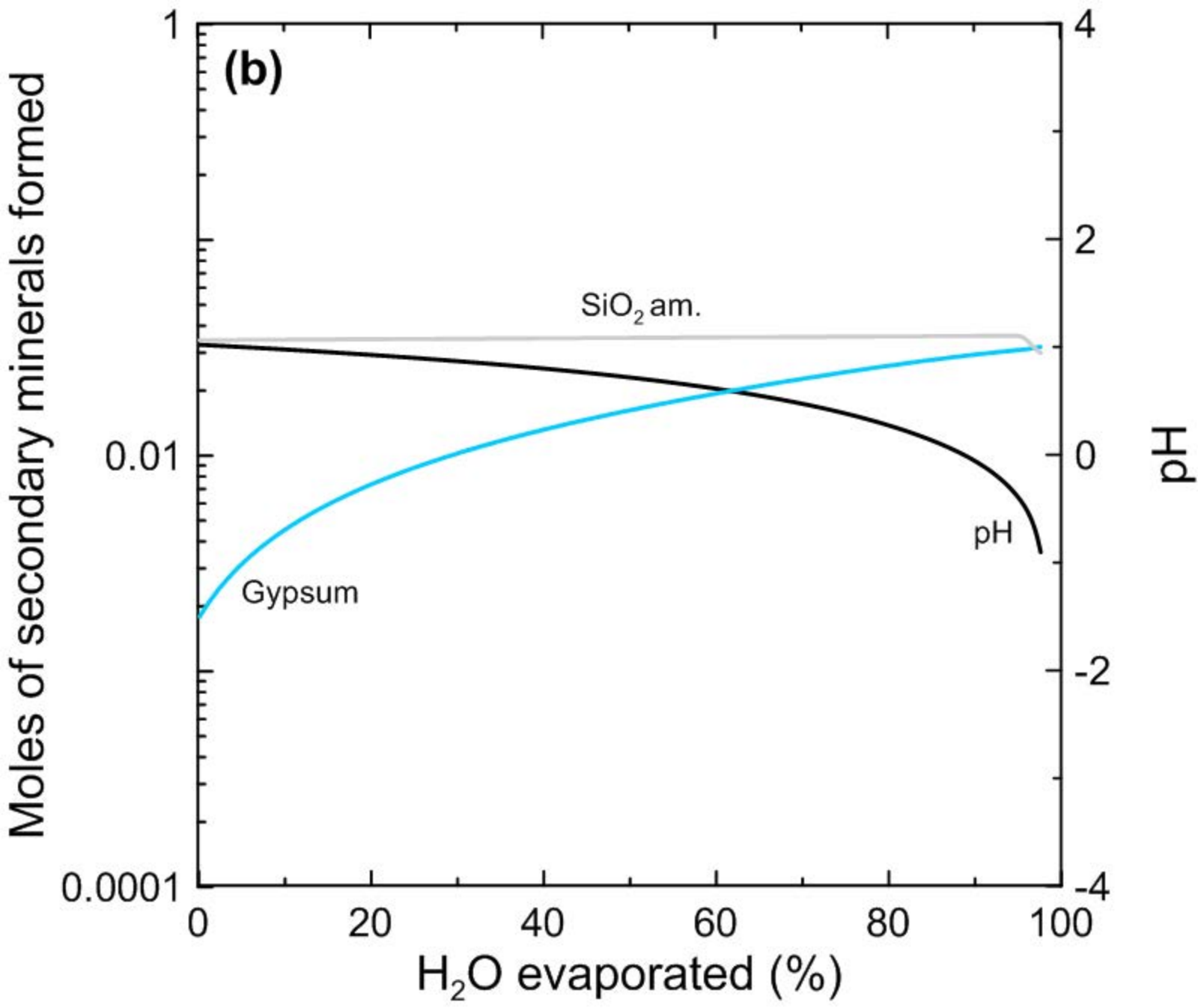
(b)
Moles of secondary minerals formed
pH
H2O evaporated (%)
SiO2 am.
Gypsum
pH
1
0.01
0.0001
4
2
0
-2
-4
0
20
40
60
80
100

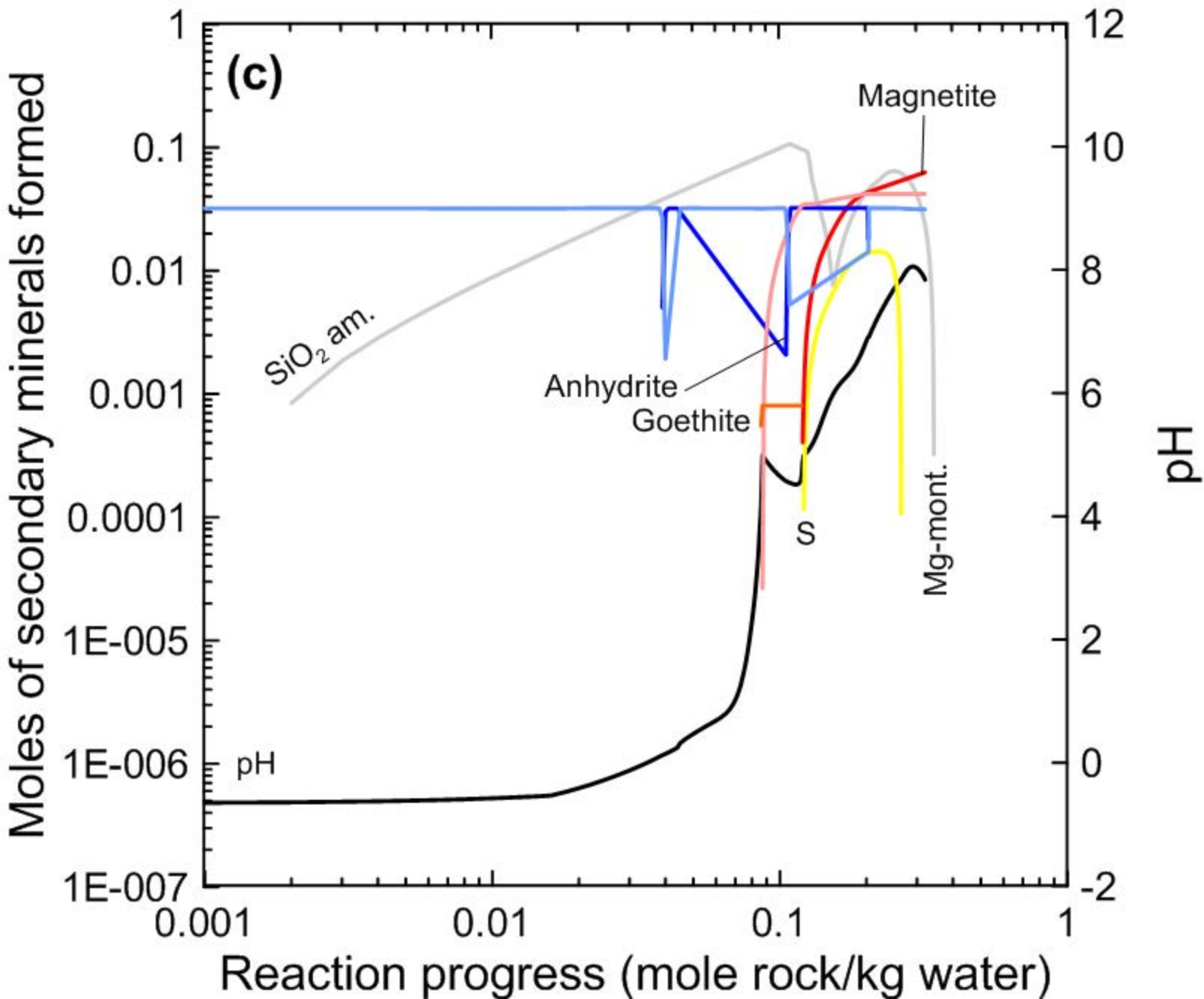
(c)
Magnetite
SiO_2 am.
Anhydrite
Goethite
S
Mg-mont.
pH
Moles of secondary minerals formed
pH
Reaction progress (mole rock/kg water)
1
0.1
0.01
0.001
0.0001
1E-005
1E-006
1E-007
12
10
8
6
4
2
0
-2
0.001
0.01
0.1
1

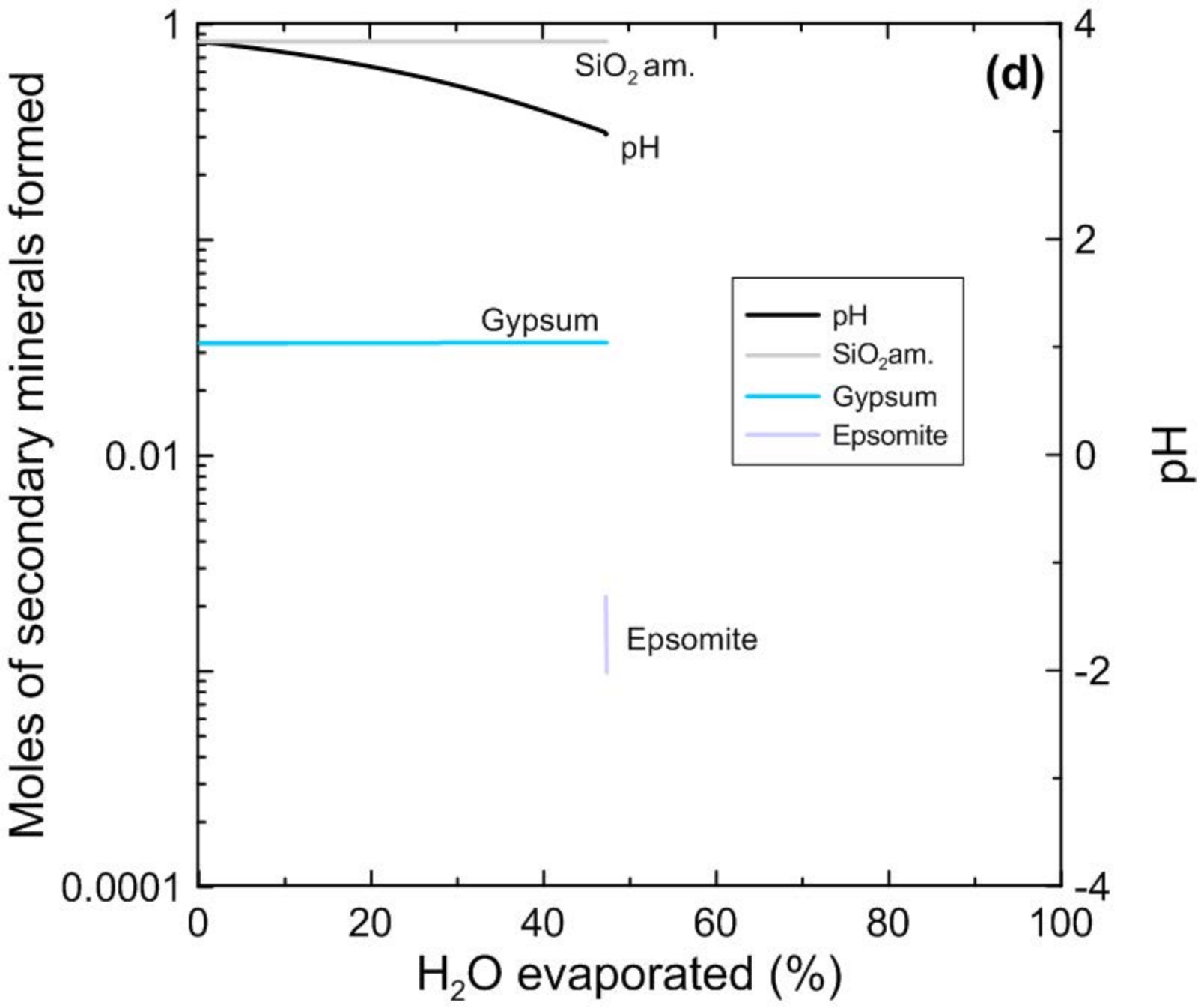
(d)
SiO2 am.
pH
Gypsum
Epsomite
pH
SiO2am.
Gypsum
Epsomite
Moles of secondary minerals formed
pH
H2O evaporated (%)
1
0.01
0.0001
4
2
0
-2
-4
0
20
40
60
80
100

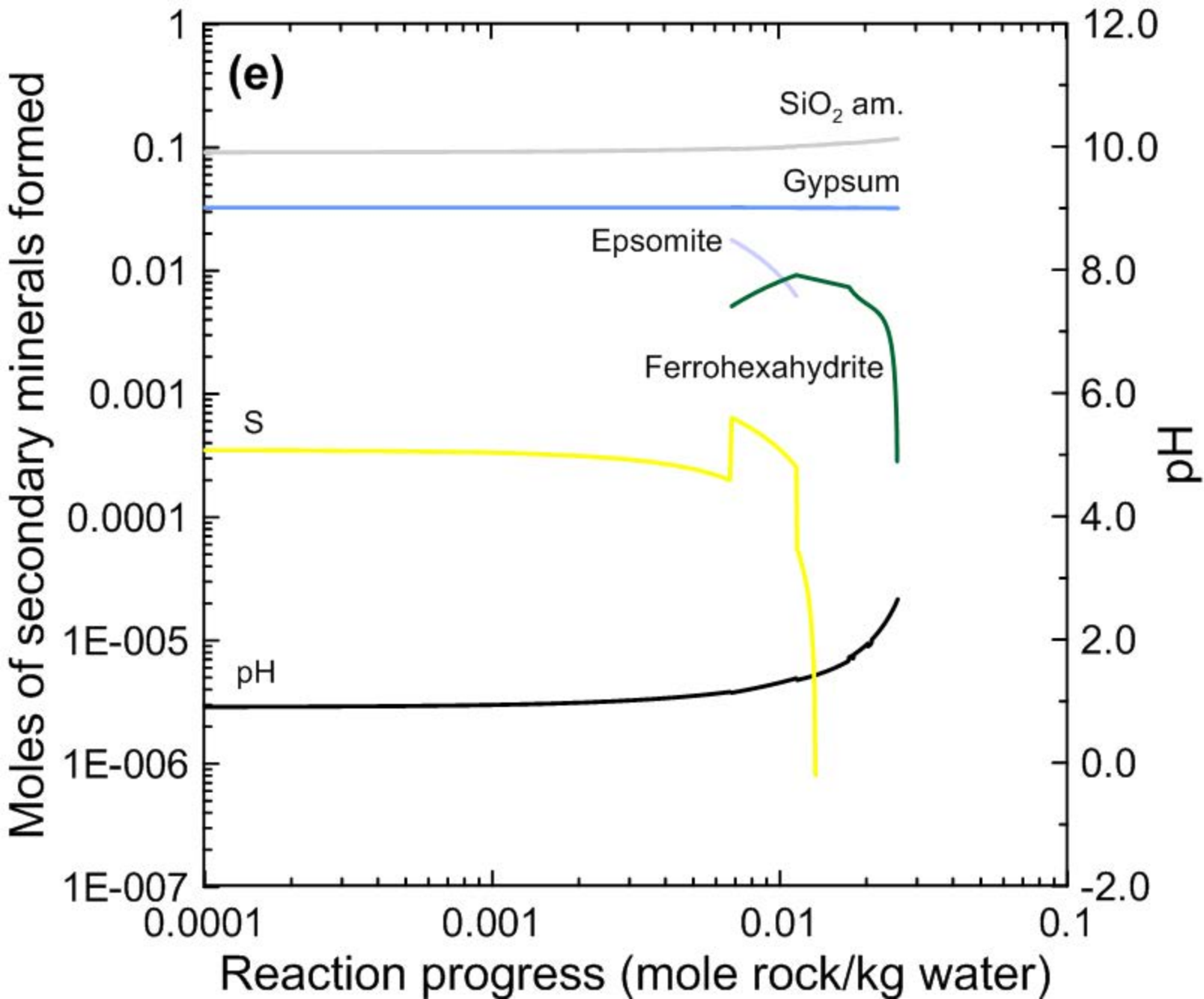
(e)
SiO2 am.
Gypsum
Epsomite
Ferrohexahydrite
S
pH
Moles of secondary minerals formed
pH
Reaction progress (mole rock/kg water)
1
0.1
0.01
0.001
0.0001
1E-005
1E-006
1E-007
12.0
10.0
8.0
6.0
4.0
2.0
0.0
-2.0
0.0001
0.001
0.01
0.1

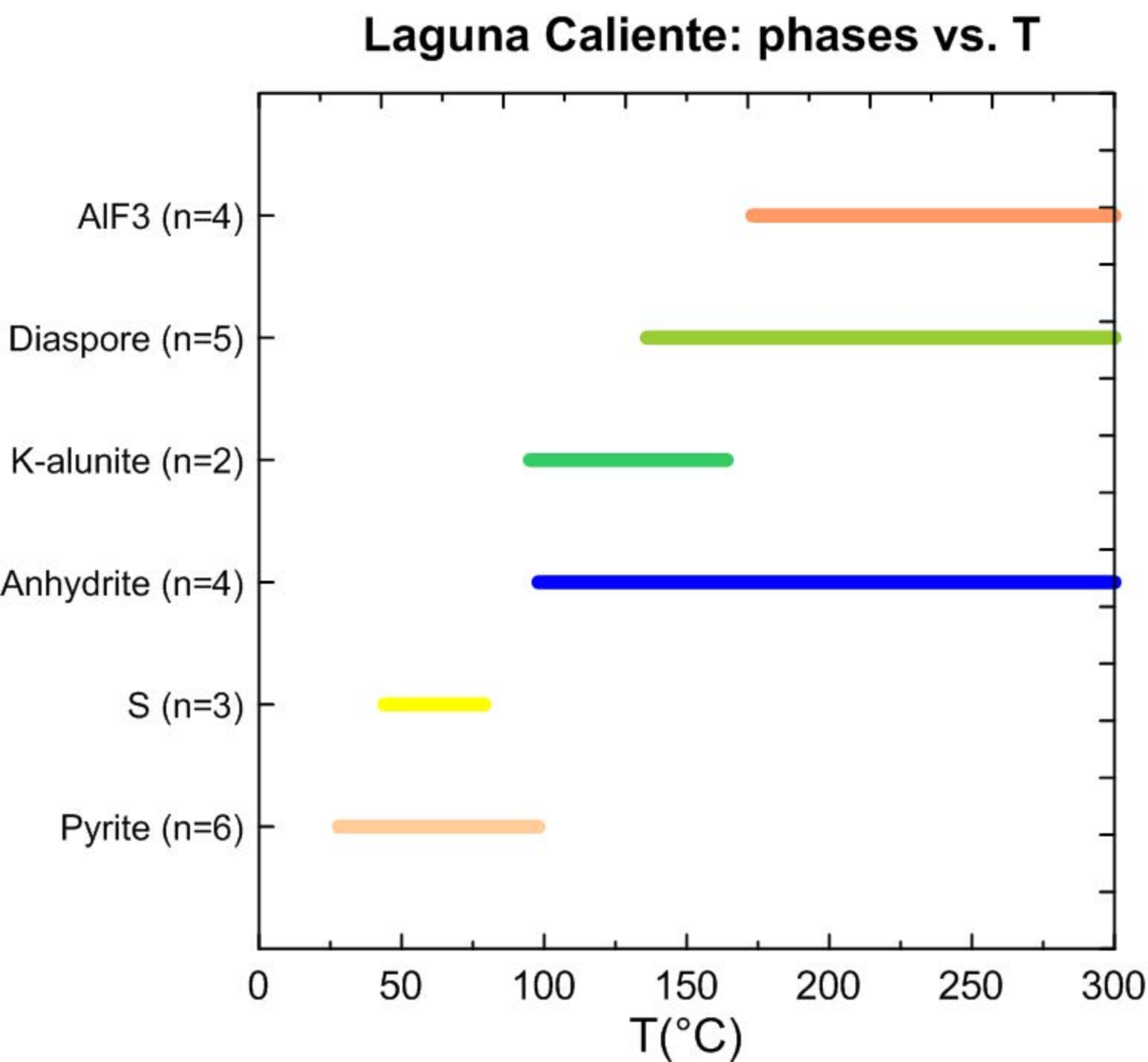
Laguna Caliente: phases vs. T
AlF3 (n=4)
Diaspore (n=5)
K-alunite (n=2)
Anhydrite (n=4)
S (n=3)
Pyrite (n=6)
0
50
100
150
200
250
300
T(°C)

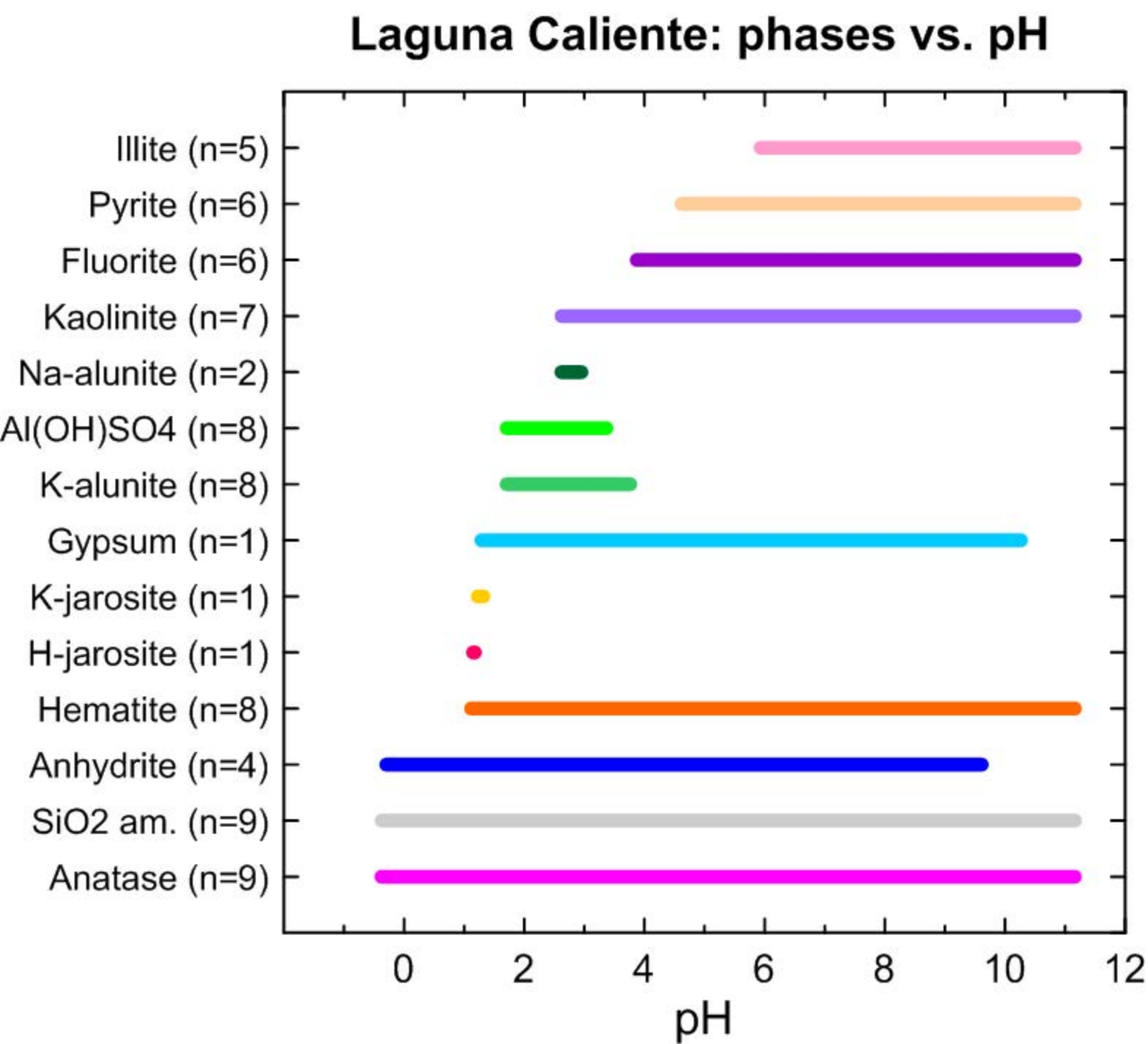
Laguna Caliente: phases vs. pH
Illite (n=5)
Pyrite (n=6)
Fluorite (n=6)
Kaolinite (n=7)
Na-alunite (n=2)
Al(OH)SO4 (n=8)
K-alunite (n=8)
Gypsum (n=1)
K-jarosite (n=1)
H-jarosite (n=1)
Hematite (n=8)
Anhydrite (n=4)
SiO2 am. (n=9)
Anatase (n=9)
0
2
4
6
8
10
12
pH

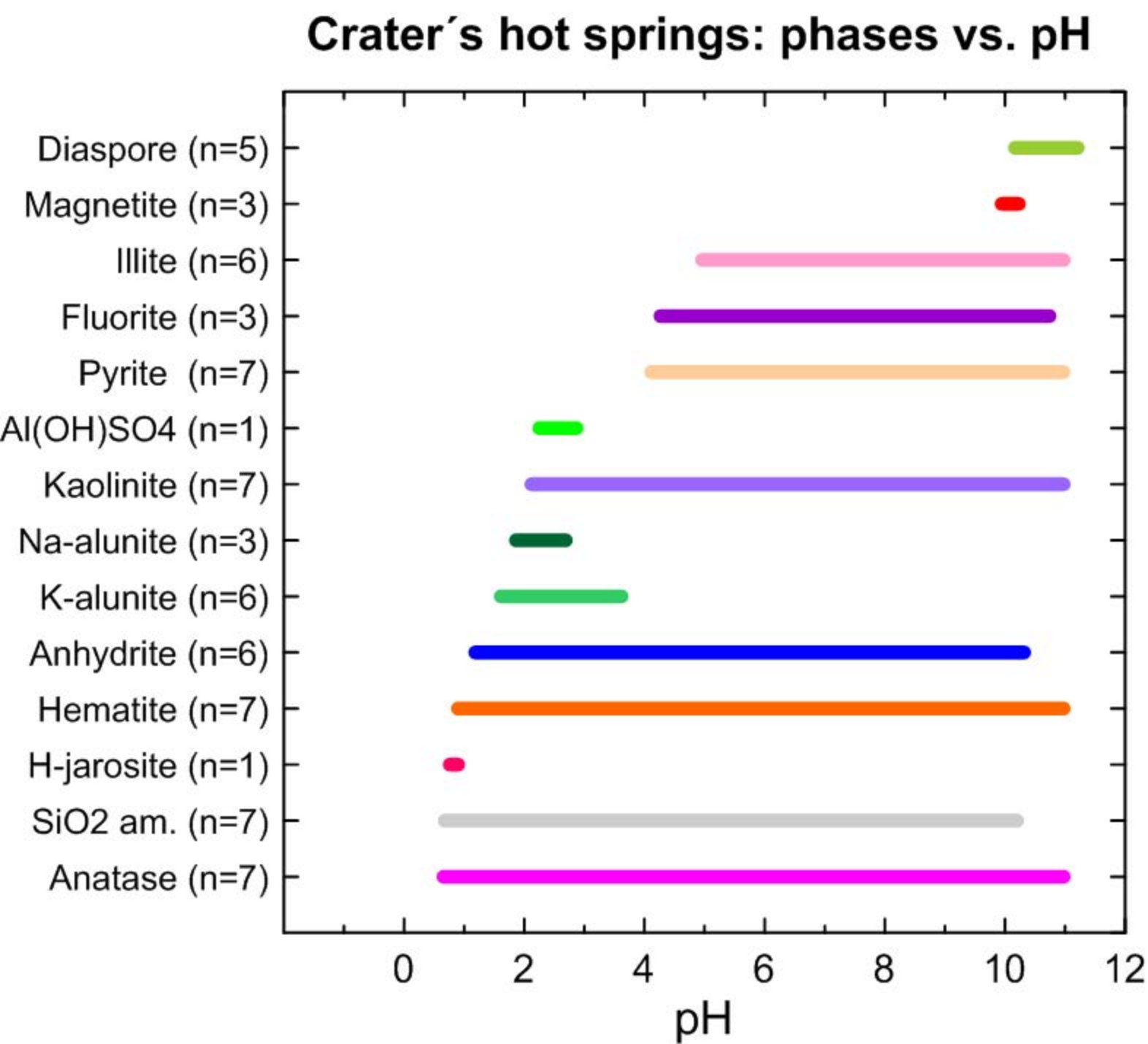
Crater´s hot springs: phases vs. pH
Diaspore (n=5)
Magnetite (n=3)
Illite (n=6)
Fluorite (n=3)
Pyrite (n=7)
Al(OH)SO4 (n=1)
Kaolinite (n=7)
Na-alunite (n=3)
K-alunite (n=6)
Anhydrite (n=6)
Hematite (n=7)
H-jarosite (n=1)
SiO2 am. (n=7)
Anatase (n=7)
0
2
4
6
8
10
12
pH

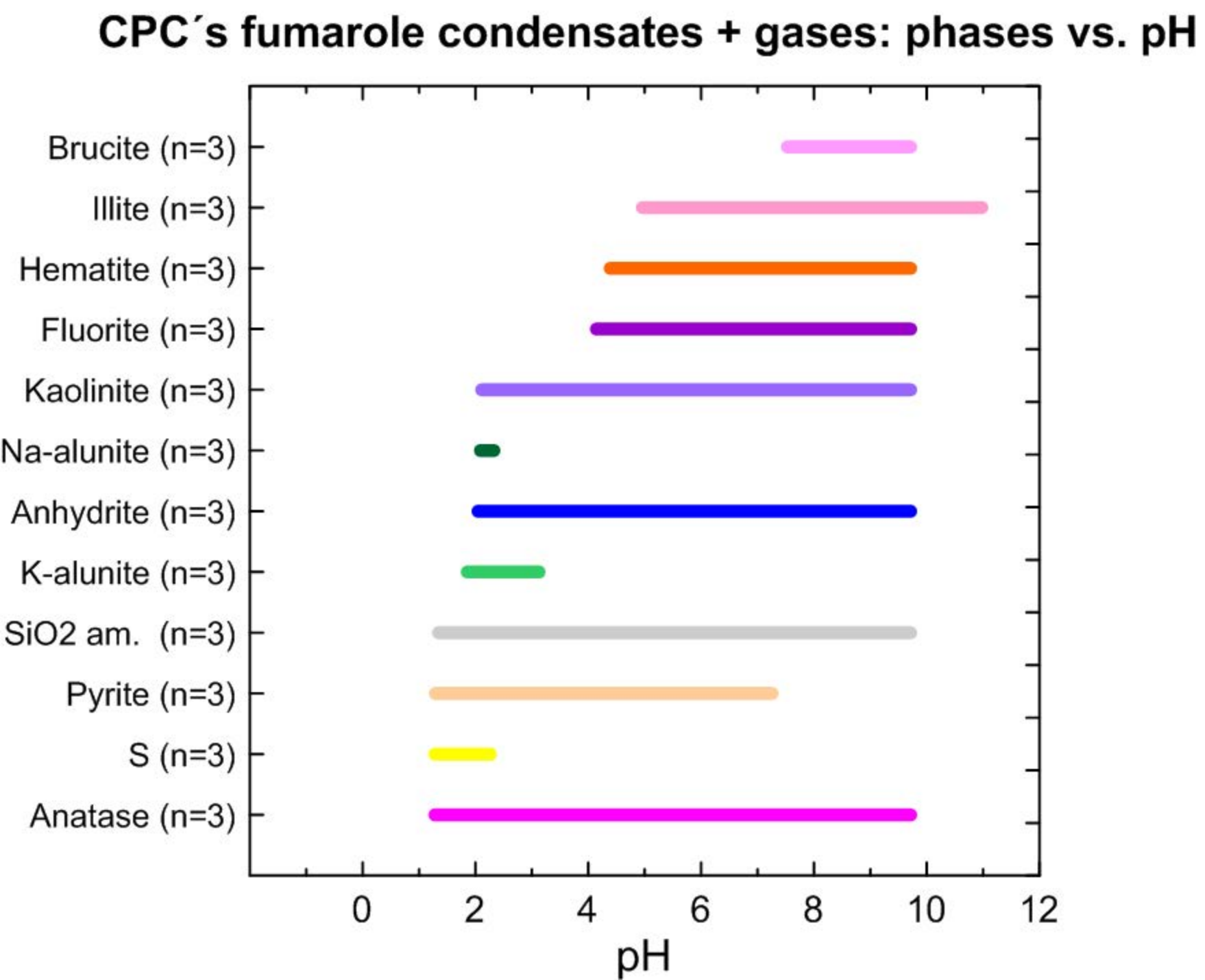
CPC´s fumarole condensates + gases: phases vs. pH
Brucite (n=3)
Illite (n=3)
Hematite (n=3)
Fluorite (n=3)
Kaolinite (n=3)
Na-alunite (n=3)
Anhydrite (n=3)
K-alunite (n=3)
SiO2 am. (n=3)
Pyrite (n=3)
S (n=3)
Anatase (n=3)
0
2
4
6
8
10
12
pH

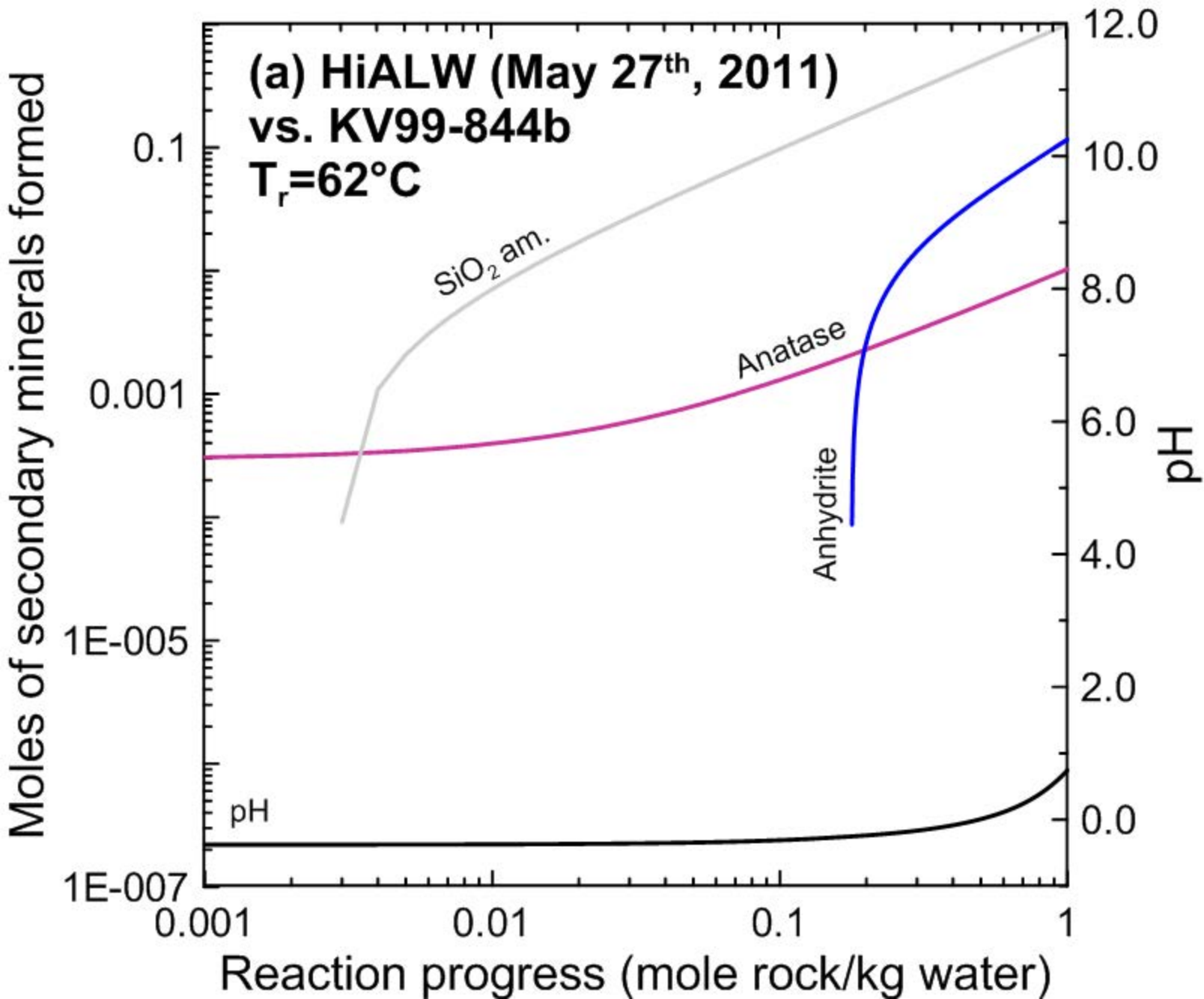
(a) HiALW (May 27th, 2011)
vs. KV99-844b
Tr=62°C
SiO2 am.
Anatase
Anhydrite
pH
Moles of secondary minerals formed
0.1
0.001
1E-005
1E-007
12.0
10.0
8.0
6.0
4.0
2.0
0.0
pH
0.001
0.01
0.1
1
Reaction progress (mole rock/kg water)

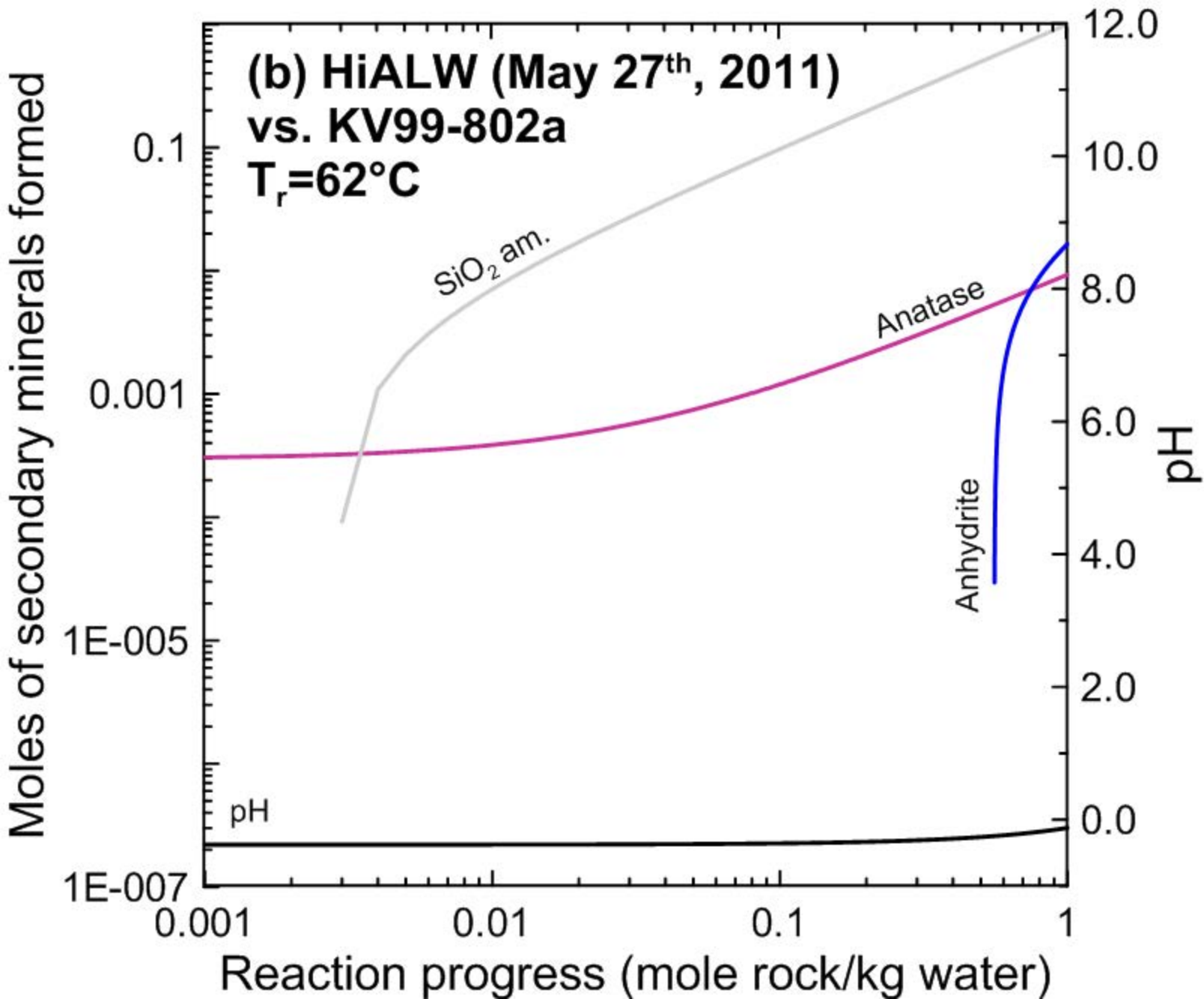
(b) HiALW (May 27th, 2011)
vs. KV99-802a
Tr=62°C
SiO2 am.
Anatase
Anhydrite
pH
Moles of secondary minerals formed
0.1
0.001
1E-005
1E-007
12.0
10.0
8.0
6.0
4.0
2.0
0.0
pH
0.001
0.01
0.1
1
Reaction progress (mole rock/kg water)

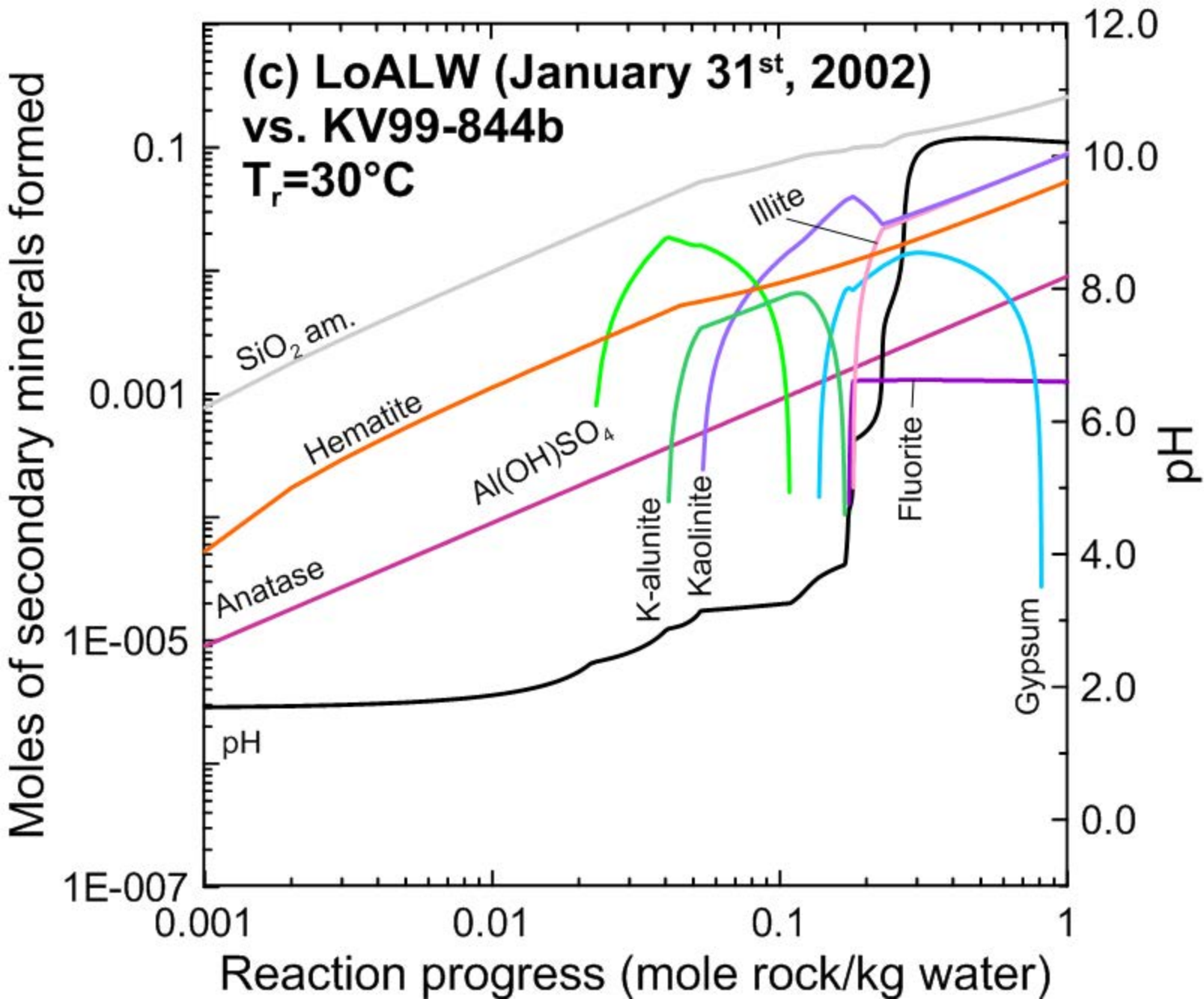
(c) LoALW (January 31st, 2002)
vs. KV99-844b
Tr=30°C
Moles of secondary minerals formed
Reaction progress (mole rock/kg water)
pH
0.1
0.001
1E-005
1E-007
0.001
0.01
0.1
1
12.0
10.0
8.0
6.0
4.0
2.0
0.0
SiO2 am.
Hematite
Anatase
Al(OH)SO4
K-alunite
Kaolinite
Illite
Fluorite
Gypsum
pH

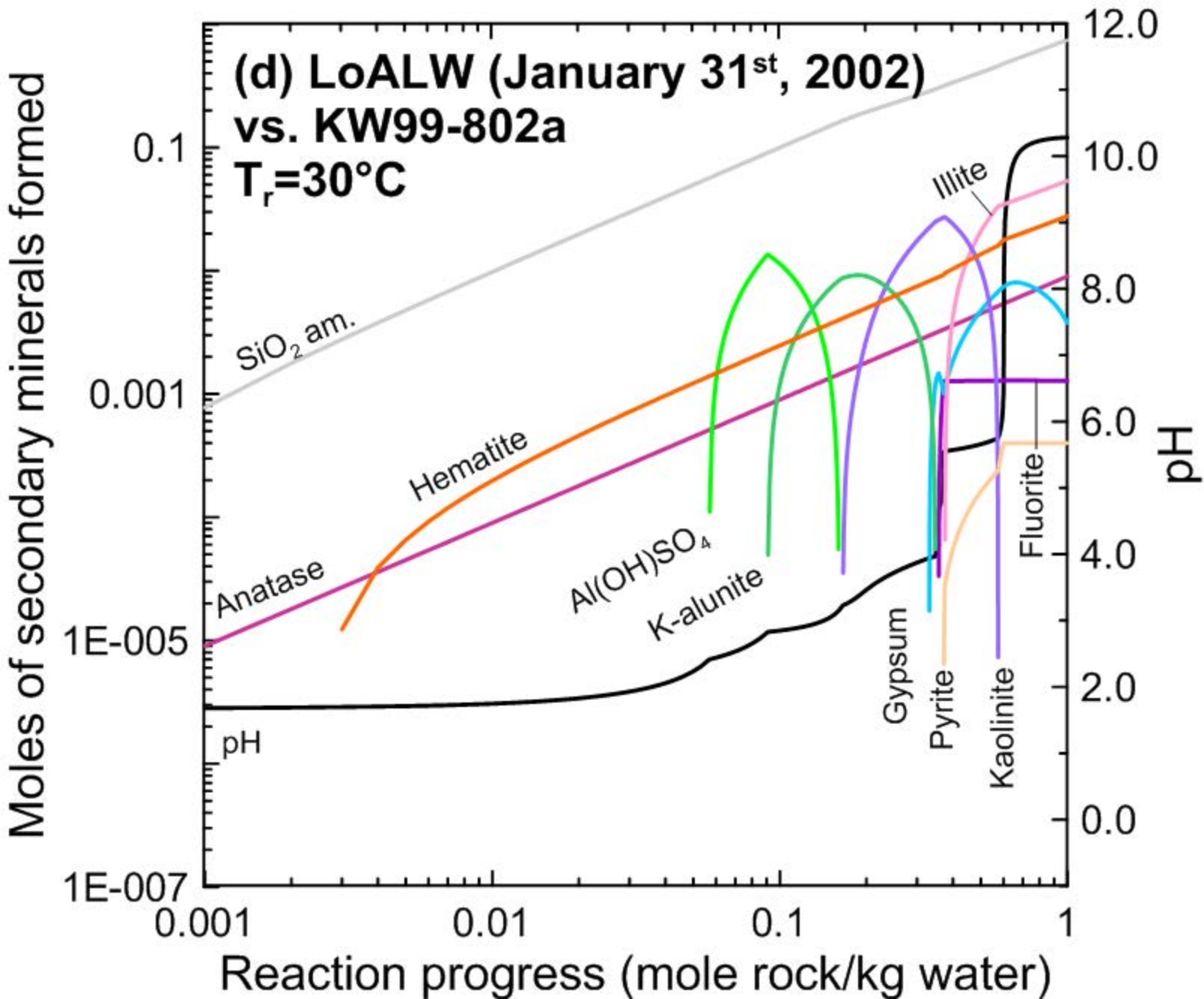
(d) LoALW (January 31st, 2002)
vs. KW99-802a
Tr=30°C
Moles of secondary minerals formed
Reaction progress (mole rock/kg water)
pH
0.1
0.001
1E-005
1E-007
0.001
0.01
0.1
1
12.0
10.0
8.0
6.0
4.0
2.0
0.0
SiO2 am.
Hematite
Anatase
Al(OH)SO4
K-alunite
Illite
Gypsum
Pyrite
Kaolinite
Fluorite
pH